USC-SIPI REPORT #179

A Robust Approach to Linearly-Constrained Adaptive Array Processing

by

George Thomas Zunich

May 1991

Signal and Image Processing Institute
UNIVERSITY OF SOUTHERN CALIFORNIA
Department of Electrical Engineering-Systems
Powell Hall of Engineering
University Park/MC-0272
Los Angeles, CA 90089 U.S.A.

Acknowledgements

I would like to thank Professor Lloyd Griffiths for his guidance during my graduate work at USC. His perspective and good nature made research rewarding and enjoyable. I am also grateful to Professors Richard Leahy, Robert Scholtz, and William Harris, Jr. for their participation on my dissertation committee. Their eagerness to share thoughts and ideas contributed to the breadth of this dissertation. I am also appreciative to the Army Research Office and Rome Air Development Center for supporting this research.

The Signal and Image Processing Institute (SIPI) at USC provided an ideal setting to carry on signal processing research. Its high quality computing facilities were warmly complemented with a comfortable working environment. I am appreciative to Allan Weber for his help with software, hardware, networks, bicycles, and golf equipment. The camaraderie and friendship with fellow researchers Mike Rude, Ching-Yih Tseng, and David Feldman helped solve many problems while maintaining perspective on life and its pursuits. Staff members Gloria Bullock, Delsa Tan, Linda Varilla, and Milly Montenegro all helped me overcome many bureaucratic matters with good humor.

I would like to thank veteran doctoral colleagues Dr. Joe Twicken and Dr. Daniel Weidman for their encouragement. Housemates Mike Bergman and V. W. Liu always brightened my more despondent days at the grindstone. My brother

Butch always gave me perspectives from "the real world" and kept my goals balanced.

Most of all, I would like to thank my parents Alexander and Nada for all the love and encouragement they gave me through this endeavor. This dissertation is dedicated to them.

"There exists a passion for comprehension, just as there exists a passion for music. That passion is rather common in children, but gets lost in most people later on. Without this passion, there would be neither mathematics nor natural science."

Albert Einstein

Contents

Acknowledgements i

List of Tables viii

List of Figures ix

Abstract xi

1 Introduction 1

2 Background 5

2.1 Adaptive Array Processing 5

2.1.1 Preliminaries 6

2.1.2 Array Beamforming 9

2.1.3 Linearly-Constrained Adaptive Beamforming 10

2.1.4 Adaptive Implementations 12

2.2 Phase Perturbation in Arrays 15

2.2.1 Misaligned Desired Signal 16

2.2.2 SINR Degradation 16

2.2.3 Quantitative Analysis of Degradation 18

2.3 Existing Methods of SINR Improvement 20
2.3.1 Steering Derivative Constraint 20
2.3.2 Artificial Noise Injection 21
2.3.3 Quadratic Inequality Constraints 23
2.3.4 Eigenvector and Quadratic Inequality Constraints 24
2.4 Summary 24

3 Robust Technique Development **26**
3.1 Linear Constraints 26
3.2 Output Power Analysis 27
3.3 SINR Degradation 29
3.3.1 Region of Degradation 29
3.3.2 Robust Constraints 31
3.4 Small Phase Error Approximation 32
3.4.1 Simplification of Constraints 34
3.4.2 New Constraint Problem 35
3.4.3 Transformation into Real Domain 35
3.4.4 GSC Implementation 40
3.4.5 Optional Use of Additional Constraints 42
3.5 Summary 43

4 Analysis of New Algorithm **45**
4.1 The Steering Derivative Constraint 45
4.2 Derivative Constraints for Array Elements 48
4.2.1 Development of Derivative Constraints 49
4.2.2 Discussion 50

4.3 Phase Constraints on Weights 51
4.4 Robust Constraints for Magnitude Errors 53
4.5 Degrees of Freedom 54
4.6 Degradation For Large Phase Errors 55
4.6.1 Single Error Sources 56
4.6.2 Multiple Error Sources 57
4.7 SINR Improvement 59
4.8 Partially Adaptive Beamforming 61
4.9 Summary 62

5 Simulations and Experimental Results **63**
5.1 Small Phase Errors 64
5.1.1 Channel Phase Errors 65
5.1.2 Element Placement Errors 70
5.1.3 Steering Errors 72
5.1.4 Frequency Errors 75
5.2 Effects of Numerous Jammers 77
5.3 Robust Generalized Sidelobe Canceller 79
5.4 Experimental Data Results 84
5.5 Summary 88

6 Conclusion **90**
6.1 Review 90
6.2 Areas for Future Research 92

Appendices 94

A Subspace Result with Small Phase Perturbations 94

B Biasing the Error Term 98

C Complex to Real Restructuring 100

C.1 Linearly Constrained Power Minimization Equivalence 100

C.2 Transformed GSC 103

D Error Variance Expressions 106

D.1 Uniform Phase Perturbation 106

D.1.1 Variance without Robust Constraints 106

D.1.2 Variance with Robust Constraints 107

D.2 Array Placement Errors 109

D.2.1 Variance without Robust Constraints 109

D.2.2 Variance with Robust Constraints 110

References **112**

List of Tables

5.1 Signal Parameters for Simulation in Fig. 5.2 67

5.2 Signal Parameters for Simulation in Fig. 5.3 68

5.3 Signal Parameters for Simulation in Fig. 5.4 71

5.4 Signal Parameters for Simulation in Fig. 5.5 72

5.5 Signal Parameters for Simulation in Fig. 5.6 75

5.6 Signal Parameters for Simulation in Fig. 5.7 76

5.7 Signal Parameters for Simulation in Fig. 5.9 80

5.8 Signal Parameters for Simulation in Fig. 5.11 82

5.9 Comparative Performances for Different Weight Vectors 87

List of Figures

2.1 Narrowband Array Environment 6

2.2 Output Power Contours with a Linear Constraint 11

2.3 The Generalized Sidelobe Canceller (GSC) Structure 14

2.4 Misaligned Signal Being Nulled by Adaptive Constrained Weight . 16

2.5 SINR for Adaptive Arrays with Various Perturbations 17

2.6 Elements of 36 Element Circular Array Used for Perturbation Simulations: (a) 36 elements, (b) 18 elements, (c) 12 elements, (d) 6 elements 18

3.1 Signal Degradation Region for $\mathbf{w}^\dagger\mathbf{\Delta}$ 30

3.2 $\mathbf{w}^\dagger\mathbf{\Delta}$ Tradeoff Region Disjoint From Constraint Region 31

3.3 Small Phase Perturbations Create Approximately Constant Phase of Error Vector Elements 33

3.4 Real Form of the GSC With Robust Constraints 41

4.1 Phase Constraint on Weight Vector Elements 52

5.1 Geometry of 36 Element Circular Array 65

5.2 SINR Performance for Uniformly Distributed Phase Perturbations 66

5.3 SINR Performance for Large Phase Error without Jammers Present 69

5.4 SINR Performance for the Ten Element Linear Array 70
5.5 SINR Performance for Array Placement Errors 73
5.6 SINR Performance for Steering Errors 74
5.7 SINR Performance for Frequency Errors 77
5.8 SINR as Function of Physical Element Perturbation 78
5.9 SINR Performance Comparison Between the Original GSC and the Modified GSC with Robust Constraints 80
5.10 Noise Performance Comparison Between the Original GSC and the Modified GSC with Robust Constraints 81
5.11 SINR Performance Comparison Between the Original GSC and the Modified GSC with Robust Constraints and One Jammer 83
5.12 Noise Performance Comparison Between the Original GSC and the Modified GSC with Robust Constraints and One Jammer 84
5.13 Jammer Performance Comparison Between the Original GSC and the Modified GSC with Robust Constraints 85
5.14 DFT of Output of Traditional Minimum Variance Beamformer with a Single Steering Constraint 87
5.15 DFT of Output of Traditional Minimum Variance Beamformer with the Addition of Robust Constraints 88

Abstract

Minimum variance beamforming is a powerful technique in adaptive array processing that allows the reception of a signal of interest while nulling unwanted interfering signals. In the presence of a high input signal-to-noise ratio (SNR), however, the technique is very sensitive to amplitude and phase perturbations of the array processing system and the processor may attempt to null the signal of interest as if it were an interfering signal. The result is a substantial degradation of the output SNR of the beamformer over that achieved for the error-free system.

This dissertation presents and analyzes robust constraints that protect a minimum variance beamformer from the effects of small phase anomalies resulting from factors such as random channel phase errors, array placement errors, steering errors, and/or frequency miscalibration. The use of robust constraints is shown to eliminate the need for precise phase calibration of the array. This is an important contribution because, in most practical applications, precise phase calibration is more difficult than is accurate amplitude calibration.

The approach taken in this thesis is to first demonstrate that the robust constraints can be derived directly from an analysis of the beamformer output power. A critical parameter which depends on both the beamformer weighting coefficients and the phase errors is identified. It is shown that performance degradation will only occur when this parameter lies within a circular region in the complex plane.

Robust constraints for the array weights are then identified which force the parameter value to be external to the circular region, regardless of the specific values of sufficiently small phase errors. An identical set of robust constraints is shown to arise when derivative constraints are placed on individual array elements.

A closed-form solution for the weight coefficients achieved with robust constraints is derived for the specific case of a narrowband adaptive array processor. Equations are developed that predict SNR performance resulting from the use of the robust constraints. An adaptive processor for the robust system is developed using a modified Generalized Sidelobe Canceller structure. Performance of the robust system is illustrated using both simulation experiments with synthesized input data and computations on actual array data. The results obtained confirm the effectiveness of the constraints in phase-perturbed environments.

Chapter 1

Introduction

Adaptive processing is a method that allows systems to track time-varying signal environments. It has been used in conjunction with arrays of multiple sensors as well as with single-channel communication systems. The term *adaptive array processing* refers to the case of multiple sensor systems.

Sensors which are placed at differing spatial locations provide valuable time delay information that can be exploited to enhance desired signals while simultaneously minimizing the effect of unwanted interference signals. This allows, for example, the reception of a desired signal in an environment consisting of other signals which have the same carrier frequency. Practical applications range from underwater acoustic hydrophone arrays to antenna arrays that receive radio frequency information.

Adaptive array techniques are frequently used in unknown environments to reduce the effect of unwanted signals [1,2]. Unfortunately, at high input signal-to-noise ratio (SNR) levels, slight phase perturbations can cause substantial performance degradation [3]. Vural [4] has observed that adaptive algorithms are

less sensitive to perturbations in low SNR environments. Many researchers have offered techniques to make adaptive algorithms more robust to these perturbation effects. Zahm [5] originally proposed artificially adding white noise into the input signal during parameter calculations. This artificial noise injection approach has the effect of lowering the apparent SNR and thus lessening the adaptive processor's sensitivity to errors. Unfortunately, this method also reduces the ability of the adaptive algorithm to reject unwanted signals (jammers) from the processor output. Jablon [6] further analyzed the single jammer case and suggested an implementation scheme for artificial noise injection. For the case of a single desired signal and one jammer with known power levels, he derived a closed-form expression for the optimal noise injection level. Unfortunately, the *a priori* power level information required for this method is not always available. Jablon [7] also studied the reduction in effective beamwidth which results with the use of an adaptive beamformer in the presence of perturbations. Cox *et al.* [8] studied the concept of bounding the norm of the weight vector using quadratic inequality constraints to provide robust performance. This approach is similar to artificial white noise injection, however, and consequently it also requires *a priori* knowledge of the signal environment to determine the optimal weight bound.

Other authors have studied combinations of existing robust techniques. Er and Cantoni [9] supplemented the approach of quadratic inequality constraints with eigenvector null constraints which are designed to span the space of all possible perturbed signals. Hoffman and Buckley [10] used linear hyperslab constraints (also known as *soft linear constraints*) in addition to quadratic inequality constraints on the weight vector.

Although these methods provide improved performance in the presence of general array perturbations, they do not take advantage of the special structure that exists for the case of small phase perturbations. In fact, it is shown in this dissertation that eigenvector null constraints cannot be used with such perturbations. Small phase perturbations arise due to such common problems as array element placement error, non-isotropic propagation mediums, misalignment of the array relative to the signal of interest (steering errors), and frequency calibration errors. Under conditions of high input SNR, array designers have found it difficult, if not impossible, to design phase calibration methods which prevent severe performance degradation when traditional adaptive array algorithms are employed. As will be shown, errors as small as one thousandth of a wavelength at each array element can cause significant degradation of the adaptive array output SNR. This dissertation examines the small phase perturbation case in detail and presents a new approach for this important class of problems.

The remainder of this dissertation is divided into five chapters. Chapter 2 reviews adaptive array processing, signal models, and an adaptive implementation scheme known as the Generalized Sidelobe Canceller. Closed-form equations are presented that predict output SNR performance in the presence of phase perturbations. Existing techniques that combat performance degradation are explained and examined.

Chapter 3 develops an analysis of the perturbation problem and presents new robust constraints that exploit the special structure of small phase errors within an adaptive array. These constraints are transformed into a new structure that provides a closed-form weight vector solution and allows a modified Generalized Sidelobe Canceller to be used for adaptive implementation of the robust system.

Chapter 4 analyzes the new robust constraints and shows their equivalence to derivative constraints placed at individual array elements. Closed-form expressions for robust SNR performance are developed and compared to non-robust performance.

Chapter 5 presents simulation results for the new technique and includes performance measurements using actual data from a radio frequency linear array. Predicted performance is compared to simulated performance to verify the analysis of the previous chapter.

Chapter 6 summarizes the work and describes areas for future research.

Chapter 2

Background

2.1 Adaptive Array Processing

Adaptive array processing provides advantages over conventional processing in many practical applications. Traditionally, non-adaptive array techniques direct the mainlobe of the array response toward the signal of interest [11]. The array response in such systems is susceptible to sidelobe *leakage*. If a strong interference signal (jammer) is incident on the array from a direction corresponding to one of the sidelobes of the array response, for example, the output of the conventional processor may contain more power from the jammer than from the signal of interest. Adaptive techniques have an advantage over non-adaptive beamforming in that they are capable of changing the array response in order to effectively null any jammer that appears in the sidelobes. A well researched and powerful area in adaptive array processing that achieves this desired effect is *linearly-constrained minimum variance beamforming.*

2.1.1 Preliminaries

Array processing uses several sensors located in different positions to receive signal energy from the surrounding environment. By selectively combining the output of these sensors, the processor can constructively sum a desired incoming signal and simultaneously reduce the power of unwanted interfering signals to enhance the signal-to-interference-plus-noise ratio (SINR) observed at the processor output. A typical sensor array is shown in Fig. 2.1. Each of N array elements is located

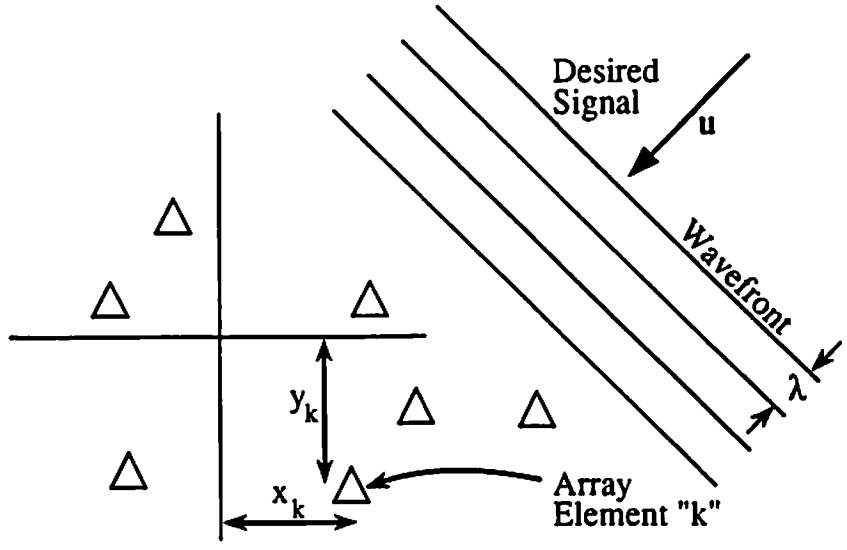

Figure 2.1: Narrowband Array Environment

in 3-dimensional space with Cartesian coordinates given by a position vector $\mathbf{a}_k$,

$$\mathbf{a}_k \triangleq \begin{bmatrix} x_k \\ y_k \\ z_k \end{bmatrix}, \qquad k = 1, 2, \ldots, N \ . \tag{2.1}$$

In an ideal system, each sensor is assumed to be omni-directional and the medium of propagation is assumed to be isotropic. The signal of interest is assumed to

be narrowband and located in the far-field of the array (i.e. to produce planer propagation wavefronts at the array). The unit magnitude directional vector $\mathbf{u}$ for a particular propagating signal is given by,

$$\mathbf{u} = \begin{bmatrix} -\sin(\Theta)\cos(\Phi) \\ -\cos(\Theta)\cos(\Phi) \\ -\sin(\Phi) \end{bmatrix}, \tag{2.2}$$

where Θ and Φ represent polar coordinate angles. The symbol Θ denotes the azimuth angle measured clockwise from the positive y-axis within the x-y plane, and Φ is the elevation angle above the x-y plane. The output response of the k^{th} element at time t is $x_k(t)$. This continuous-time output signal is sampled at uniform time intervals spaced by T seconds to create a sampled signal denoted as $x_k(n)$,

$$x_k(t) = x_k(nT) = x_k(n), \qquad n = 1, 2, \ldots \ . \tag{2.3}$$

The output for each array element is assumed to consist of a desired signal $s_k(n)$ and a background noise-plus-interference term $n_k(n)$,

$$x_k(n) = s_k(n) + n_k(n). \tag{2.4}$$

For the narrowband case, the signal is further assumed to be an unmodulated complex exponential of the form,

$$s_k(n) = \sigma_s e^{j\xi} e^{j\frac{2\pi}{\lambda}\mathbf{a}_k^{\dagger}\mathbf{u}} e^{j\omega nT}, \tag{2.5}$$

where σ_s is the signal magnitude term, ξ is the signal phase, $\frac{2\pi}{\lambda}\mathbf{a}_k^{\dagger}\mathbf{u}$ is the phase delay of the k^{th} array element relative to the coordinate origin, λ is the spatial wavelength, ω is the temporal frequency, and $\dagger$ represents complex conjugate transpose. Note that the only element-dependent component in this expression is

the phase term $e^{j\frac{2\pi}{\lambda}\mathbf{a}_k^\dagger\mathbf{u}}$. The N-dimensional vector containing these phase terms is called *the steering vector* and is given by,

$$\mathbf{d} \triangleq \begin{bmatrix} d_1 \\ d_2 \\ \vdots \\ d_N \end{bmatrix} \triangleq \begin{bmatrix} e^{j\frac{2\pi}{\lambda}\mathbf{a}_1^\dagger\mathbf{u}} \\ e^{j\frac{2\pi}{\lambda}\mathbf{a}_2^\dagger\mathbf{u}} \\ \vdots \\ e^{j\frac{2\pi}{\lambda}\mathbf{a}_N^\dagger\mathbf{u}} \end{bmatrix}. \tag{2.6}$$

In a similar manner, the individual output responses $x_k(n)$, signal responses $s_k(n)$, and noise responses $n_k(n)$ are elements of the vectors $\mathbf{x}$, $\mathbf{s}$, $\mathbf{n}$, respectively. Note that the time sample index "n" has been dropped for notational convenience. It is used only when needed to differentiate between different time samples. The relevant spatial sample vectors are then,

$$\mathbf{x} \triangleq \begin{bmatrix} x_1 \\ x_2 \\ x_3 \\ \vdots \\ x_N \end{bmatrix}, \quad \mathbf{s} \triangleq \begin{bmatrix} s_1 \\ s_2 \\ s_3 \\ \vdots \\ s_N \end{bmatrix}, \text{ and } \quad \mathbf{n} \triangleq \begin{bmatrix} n_1 \\ n_2 \\ n_3 \\ \vdots \\ n_N \end{bmatrix}, \tag{2.7}$$

where,

$$\mathbf{x} = \mathbf{s} + \mathbf{n}. \tag{2.8}$$

The signal vector can be written as a complex-scaled version of the steering vector $\mathbf{d}$,

$$\mathbf{s} = \sigma_s e^{j\xi}\mathbf{d}. \tag{2.9}$$

2.1.2 Array Beamforming

The output y of a narrowband array beamformer is defined as the inner product of the complex data vector $\mathbf{x}$ with a complex weight vector $\mathbf{w}$,

$$y = \mathbf{w}^\dagger \mathbf{x}, \tag{2.10}$$

where the weight vector $\mathbf{w}$ contains a single complex coefficient for each array element,

$$\mathbf{w} \triangleq \begin{bmatrix} w_1 \\ w_2 \\ w_3 \\ \vdots \\ w_N \end{bmatrix}. \tag{2.11}$$

The output power of the beamformer is the expected value of the output magnitude squared. Thus, for a fixed weight vector $\mathbf{w}$,

$$\begin{aligned} E\left[|y|^2\right] &= E\left[\left|\mathbf{w}^\dagger \mathbf{x}\right|^2\right], & (2.12)\\ &= E\left[\mathbf{w}^\dagger \mathbf{x}\mathbf{x}^\dagger \mathbf{w}\right], & (2.13)\\ &= \mathbf{w}^\dagger E\left[\mathbf{x}\mathbf{x}^\dagger\right] \mathbf{w}, & (2.14) \end{aligned}$$

and the term $E\left[\mathbf{x}\mathbf{x}^\dagger\right]$ is the *correlation matrix* and is denoted by $\mathbf{R}_{xx}$. The beamformer output power can then be expressed as,

$$E\left[|y|^2\right] = \mathbf{w}^\dagger \mathbf{R}_{xx} \mathbf{w}. \tag{2.15}$$

2.1.3 Linearly-Constrained Adaptive Beamforming

Multiple Constraints

The object in linearly-constrained adaptive beamforming is to minimize the output power of the beamformer while maintaining one or more linear constraints on the weight vector. Thus, the equation which defines w is,

$$\min_{\mathbf{w}} \mathbf{w}^{\dagger}\mathbf{R}_{xx}\mathbf{w} \quad \textit{subject to} \quad \mathbf{C}^{\dagger}\mathbf{w} = \mathbf{f}. \tag{2.16}$$

The constraint matrix C contains M column vectors that define the constraints, while f is a vector whose M elements contain the constraint value for each column of C. Thus,

$$\mathbf{C} \triangleq \begin{bmatrix} | & | & \cdots & | \\ \mathbf{c}_1 & \mathbf{c}_2 & \cdots & \mathbf{c}_M \\ | & | & \cdots & | \end{bmatrix}, \quad \text{and} \quad \mathbf{f} \triangleq \begin{bmatrix} f_1 \\ f_2 \\ \vdots \\ f_M \end{bmatrix}. \tag{2.17}$$

Figure 2.2 illustrates the geometry for a 2-dimensional real example which employs one constraint. The concentric rings represent contours of constant value of the quadratic power output function in Eq. (2.15). The upper diagonal line represents the constraint that the weight vector must satisfy and any weight vector which satisfies the constraint must terminate on this line. The optimal weight solution $\mathbf{w}_{opt}$ is defined by the point where the constraint line is tangent to the lowest contour level. At this point, the output power is minimized and the constraints are satisfied. Linearly-constrained adaptive beamforming is also termed *minimum variance beamforming* (MVB) [11].

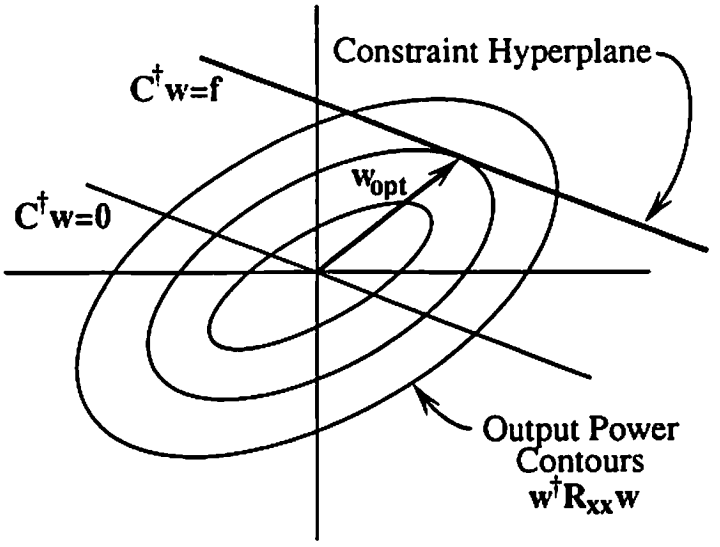

Figure 2.2: Output Power Contours with a Linear Constraint

The solution to the constrained minimization problem in Eq. (2.16) is well known [12] and given by,

$$\mathbf{w}_{opt} = \mathbf{R}_{xx}^{-1}\mathbf{C}\left(\mathbf{C}^{\dagger}\mathbf{R}_{xx}^{-1}\mathbf{C}\right)^{-1}\mathbf{f}. \tag{2.18}$$

When the environment consists of independent and equal variance noise at each sensor, the system operates in *spatially white noise* and $\mathbf{R}_{xx} = \mathbf{I}$. The optimal weight vector in this case is termed the *quiescent weight vector* $\mathbf{w}_q$,

$$\mathbf{w}_q = \mathbf{C}\left(\mathbf{C}^{\dagger}\mathbf{C}\right)^{-1}\mathbf{f}. \tag{2.19}$$

Single Constraint Case

When only one constraint is employed, Eq. (2.16) simplifies to,

$$\min_{\mathbf{w}} \mathbf{w}^{\dagger}\mathbf{R}_{xx}\mathbf{w} \quad \textit{subject to} \quad \mathbf{c}^{\dagger}\mathbf{w} = f. \tag{2.20}$$

An important special case occurs when the steering vector $\mathbf{d}$ for the signal of interest is used as the single constraint vector and the array is constrained to have unity gain, i.e.,

$$\mathbf{c} \triangleq \mathbf{d} \quad \textit{and} \quad f \triangleq 1. \tag{2.21}$$

The defining equation for this case is then,

$$\min_{\mathbf{w}} \mathbf{w}^{\dagger}\mathbf{R}_{xx}\mathbf{w} \quad \textit{subject to} \quad \mathbf{d}^{\dagger}\mathbf{w} = 1, \tag{2.22}$$

and the quiescent weight vector $\mathbf{w}_q$ is given by,

$$\begin{aligned} \mathbf{w}_q &= \mathbf{C}\left(\mathbf{C}^{\dagger}\mathbf{C}\right)^{-1}\mathbf{f}, & (2.23)\\ &= \mathbf{d}\left(\mathbf{d}^{\dagger}\mathbf{d}\right)^{-1}, & (2.24)\\ &= \frac{\mathbf{d}}{\|\mathbf{d}\|^2}. & (2.25) \end{aligned}$$

Equivalently, $\mathbf{w}_q$ is a scaled version of the desired steering vector $\mathbf{d}$. In this system, the output is constrained to pass any signal which is incident on the array from a direction defined by the steering vector $\mathbf{d}$ while simultaneously minimizing the total output power. Incident waveforms that do not have the same steering vector as the signal of interest are then susceptible to nulling.

2.1.4 Adaptive Implementations

In many practical array applications, the correlation matrix $\mathbf{R}_{xx}$ is not known *a priori*. In these cases, direct application of Eq. (2.18) to calculate the weight vector requires an estimate of the correlation matrix. Alternatively, methods exist that iteratively converge to the optimal weight vector $\mathbf{w}_{opt}$ without estimating and inverting the correlation matrix $\mathbf{R}_{xx}$. The following sections describe these adaptive techniques.

The Least-Mean-Square Algorithm

The Least-Mean-Square (LMS) method is an adaptive algorithm that uses an estimate for the gradient of a quadratic function. When a reference signal $r(n)$ is available, the LMS algorithm is given by,

$$\mathbf{w}(n+1) = \mathbf{w}(n) + 2\mu\mathbf{x}(n)\left[r(n) - y(n)\right]^*, \tag{2.26}$$

where μ is the adaptive step size parameter. Widrow [13] has shown that this procedure results in a weight vector which converges in the mean to a value which minimizes mean-square error (mse) where,

$$mse = E\left[\left|r(n) - y(n)\right|^2\right]. \tag{2.27}$$

In many array applications, however, no reference signal is available and alternative adaptive methods must be applied.

The Generalized Sidelobe Canceller (GSC)

Griffiths and Jim [14] have described an adaptive structure for the power minimization problem defined in Eq. (2.16). In their approach, the constrained problem is decomposed so that it can be solved in an unconstrained fashion. The resulting structure is known as the Generalized Sidelobe Canceller (GSC) and is depicted in Fig. 2.3. Tseng [15] offers an excellent proof that the GSC solves the same problem as stated in Eq. (2.16).

In the GSC, the weight vector is expressed as the difference of two orthogonal components,

$$\mathbf{w} = \mathbf{w}_q - \mathbf{W}_s\mathbf{w}_a, \tag{2.28}$$

where both the quiescent weight vector $\mathbf{w}_q$ and the matrix $\mathbf{W}_s$ are non-adaptive. The adaptive portion of the processor, $\mathbf{w}_a$, is used to minimize the output power

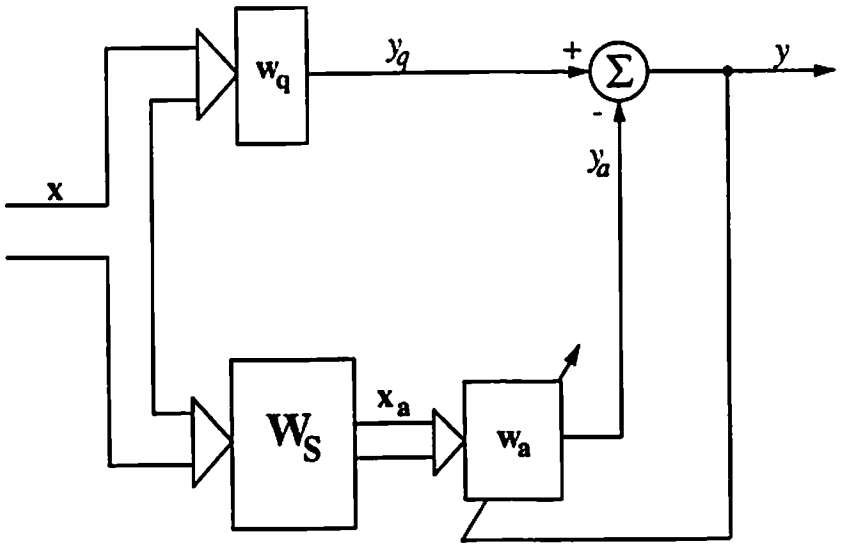

Figure 2.3: The Generalized Sidelobe Canceller (GSC) Structure

$E\left[|y|^2\right]$. The columns of $\mathbf{W}_s$ are chosen to be any linearly independent set of vectors that span the orthogonal space of the columns of the constraint matrix C. Equivalently,

$$\mathbf{C}^\dagger \mathbf{W}_s = 0, \tag{2.29}$$

where 0 is a matrix containing all zeros. As a result of this condition, the vector $\mathbf{x}_a$ has dimension $N - M$ or, equivalently, contains a number of elements equal to the number of degrees of freedom (DOF) in the constrained system.

With the GSC structure, an unconstrained LMS algorithm can be implemented to update the reduced-dimensional adaptive weight vector $\mathbf{w}_a$. The output $y_q(n)$ produced by the quiescent weight vector $\mathbf{w}_q$ is used as the reference signal $r(n)$ in the LMS algorithm. The final output $y(n)$ is treated as the LMS error $e(n)$. The GSC vectors $\mathbf{x}_a(n)$ and $\mathbf{w}_a(n)$ are used as the LMS data and weight vectors, respectively.

The upper path of the GSC can be viewed as a fixed filter (defined by the constraint equations) for the desired signal. Since the columns of $\mathbf{W}_s$ are orthogonal to the desired signal constraint, signals that meet the constraints are blocked in the lower path. Thus, $\mathbf{W}_s$ is referred to as the *blocking matrix*. Minimum output power is achieved when the adaptive weights $\mathbf{w}_a$ cancel signals in the upper path which are correlated with those in the lower path. Since the desired signal is blocked in the lower path, it cannot be cancelled by the adaptive weights. Hence, the desired signal always passes through the system. Other signals that appear in both upper and lower paths are reduced in power at the system output.

2.2 Phase Perturbation in Arrays

Although adaptive array processing is a very powerful technique for the reception of a desired signal in the presence of jammers, its performance may be sensitive to sensor phase errors. Phase errors (perturbations) can result from several sources. One such common source is element placement error. Differences in propagation delay from those expected for ideal placement cause inaccuracies between the assumed and actual steering vectors. Since *a priori* knowledge of the desired signal frequency is necessary when designing the constraint vector, frequency errors can also cause problems. Anticipated arrival direction information is also needed to calculate the desired signal steering vector, hence, such errors may cause perturbation. In addition, when the environment is not isotropic, channel phase errors can cause misaligned steering vectors. Whenever the actual steering vector differs from the computed steering vector, SINR degradation may occur.

2.2.1 Misaligned Desired Signal

When phase anomalies occur, the actual steering vector $\tilde{\mathbf{d}}$ is perturbed from the theoretical steering vector $\mathbf{d}$. Even when this difference is small, adaptive beamformers may interpret the misaligned signal as a jammer [16] and attempt to null it, as illustrated in Fig. 2.4. The constraint ensures that the projection of $\mathbf{w}$ on $\mathbf{d}$ is constant. However, as the perturbed steering vector $\tilde{\mathbf{d}}$ deviates from its nominal value, the constrained adaptive beamformer reduces the signal output $\mathbf{w}^{\dagger}\tilde{\mathbf{d}}$.

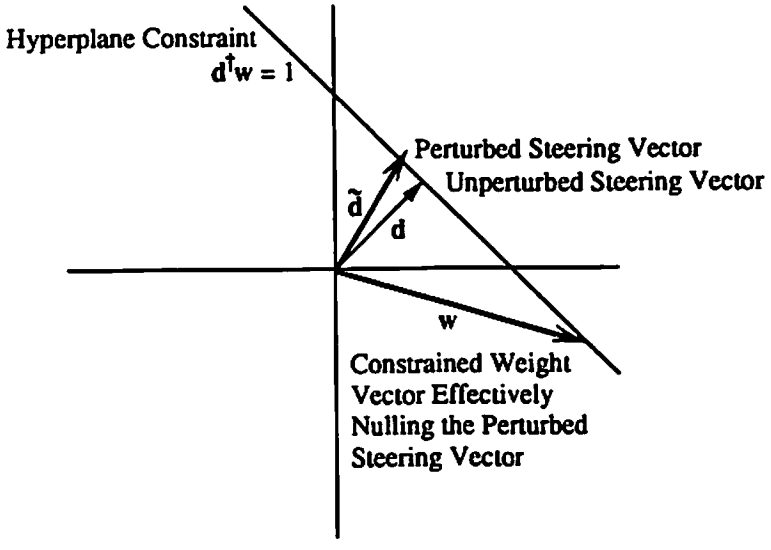

Figure 2.4: Misaligned Signal Being Nulled by Adaptive Constrained Weight

2.2.2 SINR Degradation

To demonstrate the effects of phase errors, the output SINR of a minimum variance beamformer was computed as a function of array element placement perturbation values. The results are shown in Fig. 2.5. For these computations, a

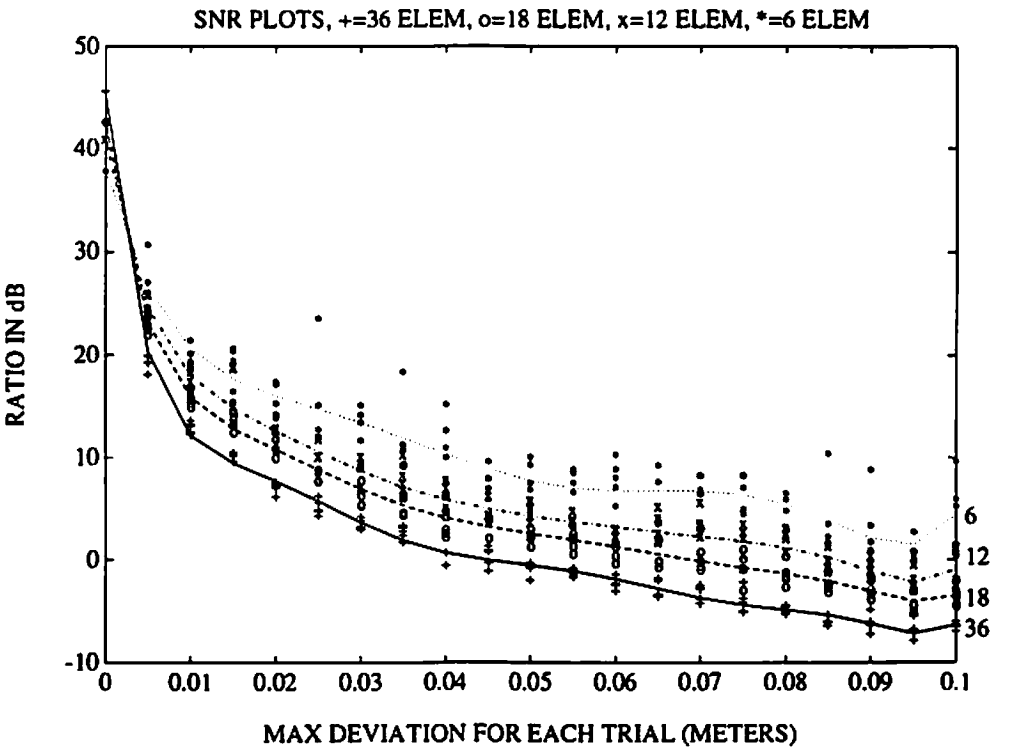

Figure 2.5: SINR for Adaptive Arrays with Various Perturbations

30 dB narrowband signal in spatially white noise was used as the signal environment. A single linear constraint consisting of the non-perturbed steering vector was employed. A 36 element array was used that consisted of 3 circular rings with radii $\frac{5}{6}\lambda$, $\frac{10}{6}\lambda$, and $\frac{15}{6}\lambda$. Each ring contained 12 uniformly spaced elements. Three smaller subarrays containing 18, 12, and 6 elements, respectively, were drawn from this array as shown in Fig. 2.6.

Five random trials were performed for each perturbation value for each array size. Each trial consisted of independent uniform random displacements of each array element in the X, Y, and Z directions. The maximum value of the uniform distribution is given on the abscissa of the plot. The continuous lines represent

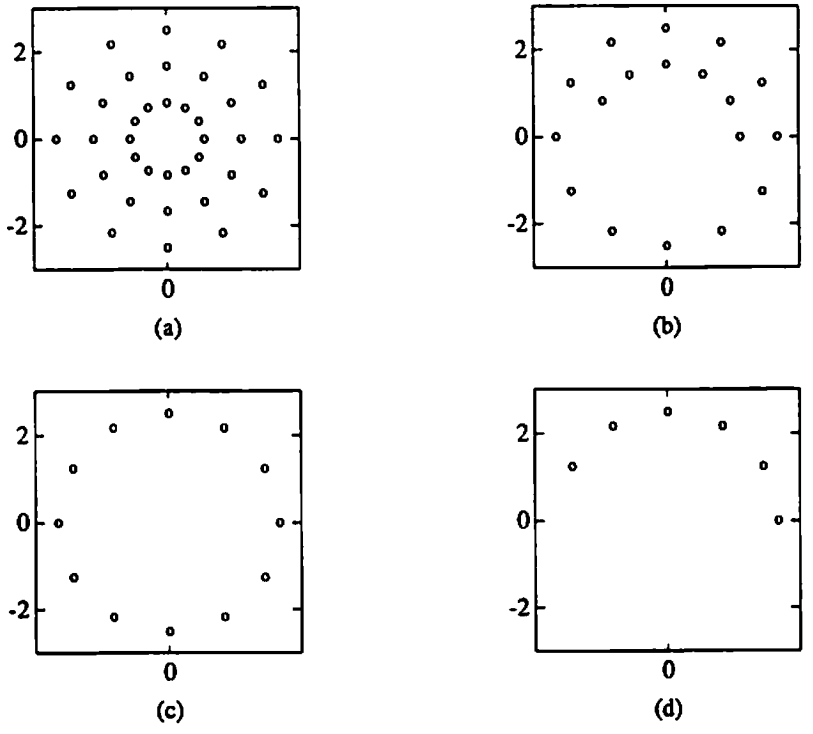

Figure 2.6: Elements of 36 Element Circular Array Used for Perturbation Simulations: (a) 36 elements, (b) 18 elements, (c) 12 elements, (d) 6 elements

polynomial best-fit curves for the trials. These results demonstrate that the output SINR for each perturbation value was reduced as more elements were used in the array. This effect has also been observed by Compton [17].

2.2.3 Quantitative Analysis of Degradation

Hudson [18] has derived a formula for the output SNR performance of a single-constraint narrowband adaptive array for a desired signal (with steering vector $\mathbf{d}$) in spatially white noise. For a particular value of the perturbed steering vector

$\tilde{\mathbf{d}}$, the output SNR is,

$$SNR_o = \frac{(N \cdot SNR_i)\,\Omega}{1 + N \cdot SNR_i\,(2 + N \cdot SNR_i)\,(1 - \Omega)}, \tag{2.30}$$

where SNR_i is the input SNR at each sensor and,

$$\Omega \triangleq \left| \frac{\mathbf{d}^\dagger \tilde{\mathbf{d}}}{N} \right|^2. \tag{2.31}$$

In this expression, the perturbed steering vector $\tilde{\mathbf{d}}$ has been assumed to be scaled so that $\|\tilde{\mathbf{d}}\|^2 = N$.

Jablon [16] extended the analysis to cases in which the perturbed steering vector $\tilde{\mathbf{d}}$ is unknown, but the statistics of the perturbation are known. His equation for the mean output signal-to-interference-plus-noise ratio is,

$$SINR_o = \frac{(SNR_i)\,N}{1 + (SNR_i)^2\,N\,(N-1)\,\sigma_\Delta^2}, \tag{2.32}$$

where σ_Δ^2 is the variance of the random perturbation at each element. Although, the SINR compares signal power to noise plus interference power [16]. Jablon argues that the output SNR depends little on the presence of additional jammers, and thus, $SNR_o \approx SINR_o$. Equation (2.32) is valid under certain assumptions, one of which is that the jammer power is greater than the signal power.

One measurement of performance degradation is defined by the value of the random perturbation variance σ_Δ^2 which produces a 3 dB reduction in performance. From Eq. (2.32), this value is given by,

$$\sigma_\Delta^2 = \frac{1}{(SNR_i)^2\,N\,(N-1)}. \tag{2.33}$$

2.3 Existing Methods of SINR Improvement

Many methods have been developed that attempt to combat perturbation effects in adaptive processors. The following sections summarize some of these techniques.

2.3.1 Steering Derivative Constraint

A special case of perturbation error results when phase error is caused by a steering error. This occurs when the constraint steering vector $\mathbf{d}$ is calculated for a signal with azimuth of Θ_0 and the actual steering vector $\bar{\mathbf{d}}$ corresponds to an arrival azimuth of Θ_1. Under these conditions, a phase mismatch exists and SINR performance degrades. One approach taken in such cases is to add a derivative constraint [19,20,21] to the steering vector constraint so as to protect the system.

The steering derivative constraint approach consists of adding a constraint that forces the first derivative with respect to azimuth of the array beampattern to be zero at the desired signal azimuth Θ_0. With this constraint, the adaptive beamformer is unable to place a null which is close in azimuth to the desired signal direction. Hence, if the desired signal strays slightly from its nominal direction, degradation does not occur.

The beampattern response in direction Θ is real function defined as the square of the magnitude of the output response, $|y|^2$, when the input consists only of the steering vector $\mathbf{d}(\Theta)$ for that direction. In general, the beampattern response is computed as a continuous function of Θ over the range of azimuthal angles of interest. It can also be defined over a range of elevation angles Φ or as a function of both azimuth and elevation.

Er and Cantoni [19] derived the first partial derivative of the beampattern with respect to azimuth evaluated at $\Theta = \Theta_0$ for the broadband case. The narrowband version of their constraint reduces to,

$$\frac{\partial y}{\partial \Theta}\Big|_{\Theta=\Theta_0} = \mathbf{w}^\dagger \dot{\mathbf{d}} = \dot{\mathbf{d}}^\dagger \mathbf{w} = 0, \tag{2.34}$$

where the elements of the vector $\dot{\mathbf{d}}$ are given by,

$$\dot{d}_k \triangleq j\frac{2\pi}{\lambda}\left[\frac{\partial}{\partial \Theta}\left(\mathbf{a}_k^\dagger \mathbf{u}\right)\right] e^{j\frac{2\pi}{\lambda}\mathbf{a}_k^\dagger \mathbf{u}}\Big|_{\Theta=\Theta_0} \qquad k = 1, 2, \ldots, N. \tag{2.35}$$

It should be noted that these expressions represent a sufficient (but not necessary) condition to ensure that the first derivative of the beampattern is zero. Since this result is in the form of a linear equality constraint, it can be added to the original steering constraint $\mathbf{d}^\dagger \mathbf{w} = 1$ to form an expanded constraint matrix $\mathbf{C}$ and constraint value vector $\mathbf{f}$ as,

$$\mathbf{C} = \begin{bmatrix} | & | \\ \mathbf{d} & \dot{\mathbf{d}} \\ | & | \end{bmatrix}, \quad \text{and} \quad \mathbf{f} = \begin{bmatrix} 1 \\ 0 \end{bmatrix}. \tag{2.36}$$

This new adaptive beamformer still meets the steering constraint but is now robust to steering errors. The optimal weight vector $\mathbf{w}_{opt}$ can be found by substituting $\mathbf{C}$ and $\mathbf{f}$ in the closed-form solution given in Eq. (2.18) or adaptively by using the GSC.

2.3.2 Artificial Noise Injection

The technique of artificial noise injection has been well studied [16] and is acknowledged as being effective in combatting perturbation effects. The method decreases the apparent output SINR ratio of a perturbed array by artificially

adding spatially white noise to the signal for the purposes of calculation of the optimal weights. These weights are then used on the signal *without* the additional noise (i.e. noise is not added to the actual input data). The benefits of noise injection can be shown by analyzing the output power of the minimum variance beamformer with a desired signal in spatially white noise. Assuming that the signal and noise are uncorrelated, the correlation matrix for the input data vector becomes,

$$\mathbf{R}_{xx} = \mathbf{s}\mathbf{s}^\dagger + \sigma_n^2\mathbf{I}, \tag{2.37}$$

where σ_n^2 is the input spatial white noise power. Substitution of Eq. (2.9) yields an equation in terms of the steering vector $\mathbf{d}$,

$$\mathbf{R}_{xx} = \sigma_s^2\mathbf{d}\mathbf{d}^\dagger + \sigma_n^2\mathbf{I}. \tag{2.38}$$

The output power is given by,

$$\mathbf{w}^\dagger\mathbf{R}_{xx}\mathbf{w} = \sigma_s^2\mathbf{w}^\dagger\mathbf{d}\mathbf{d}^\dagger\mathbf{w} + \sigma_n^2\|\mathbf{w}\|^2, \tag{2.39}$$

$$= \sigma_s^2 + \sigma_n^2\|\mathbf{w}\|^2, \tag{2.40}$$

where the constraint $\mathbf{d}^\dagger\mathbf{w} = 1$ has been used to simplify the expression.

When the adaptive beamformer results in reduced power for the perturbed signal of interest, the magnitude of the weight vector increases significantly (refer to Fig. 2.4). Increasing the magnitude of the weight vector increases the total output power, as shown by Eq. (2.40). Since adaptive beamforming minimizes output power subject to the linear constraint, there is a self-governing effect that keeps the adaptive beamformer from completely nulling a perturbed signal. Increases in spatial white noise power (caused by increasing the magnitude of the weight vector $\mathbf{w}$) will eventually offset any power savings accrued by nulling the signal of

interest. As a result, by artificially "penalizing" the beamformer for an increased magnitude of the weight vector, the adaptive process is less able to null the perturbed signal. This "penalty" to improve SINR performance is implemented by artificially increasing the noise power σ_n^2 during calculation of the optimal weight vector.

Jablon [16] has derived an equation which specifies the amount of noise injection power required to produce maximal output SINR. The equation for the case of one narrowband signal of interest and one narrowband jammer is,

$$\frac{\sigma_{i,opt}^2}{\sigma_n^2} = \left(\frac{(SNR_i)^2 (INR_i) N^2 (N-1) \sigma_\Delta^2}{|\nu_j|^2} \right)^{\frac{1}{4}}, \tag{2.41}$$

where $\frac{\sigma_{i,opt}^2}{\sigma_n^2}$ is the optimal added noise-to-noise injection ratio, INR_i is the input interference-to-noise ratio at each element, σ_Δ^2 is the variance of random perturbation, 1 is a vector containing all ones, and,

$$\nu_j \triangleq \frac{1}{N} 1^\dagger \mathbf{d}_j, \tag{2.42}$$

where $\mathbf{d}_j$ is the steering vector for the single jammer. In many practical applications, it is not realistic to assume that both signal and jammer powers are known *a priori* and, as a result, this method cannot be applied.

2.3.3 Quadratic Inequality Constraints

Another method of achieving robust performance is the imposition of a quadratic inequality constraint on the weight vector. The new set of constraints is given by,

$$\mathbf{C}^\dagger \mathbf{w} = \mathbf{f} \quad and \quad \mathbf{w}^\dagger \mathbf{w} \leq \gamma, \tag{2.43}$$

where γ is real valued scalar used to bound the norm of the weight vector. Cox *et al.* [8] have implemented this method in an iterative adaptive array that requires

little additional computation. Hudson [18] showed that applying this bound is equivalent to the method of noise injection. Hence, the analysis and discussion of the previous section are applicable to this method.

2.3.4 Eigenvector and Quadratic Inequality Constraints

Er and Cantoni [9] suggested supplementing the inequality constraint technique with additional linear constraints. Their approach was to minimize the effects of error in the adaptive array response. The linear constraints were expressed as,

$$\mathbf{e}_i^{\dagger}\mathbf{w} = 0 \qquad i = 1, 2, \ldots, m, \tag{2.44}$$

where $\mathbf{e}_i$ is one of m non-zero eigenvectors of the correlation matrix formed over all possible perturbed signal steering vectors.

This algorithm uses two techniques to obtain robust performance. The first is weight bounding while the second takes advantage of a preferred steering vector subspace that includes all perturbed steering vectors. The linear constraints ensure that this subspace is nulled. However, it is shown in Chapter 3 that small random phase perturbations do not create a preferred complex subspace. As a result, this approach is not applicable to the small phase perturbation problem.

2.4 Summary

Linearly-constrained adaptive beamforming provides flexibility by allowing the use of multiple linear constraints in addition to a steering constraint. When the input SINR of these systems is high, the output SINR is very sensitive to phase perturbations that occur at individual array elements. A relatively small amount

of phase error can create a dramatic loss in output SINR. Closed-form expressions have been derived to predict the loss in SINR performance for both known and stochastic perturbation models.

Previous methods which have been proposed to protect the array processor output from perturbation effects include derivative constraints, noise injection, a quadratic inequality constraint, and subspace nulling constraints. Each of these methods has a drawback that prevents it from being widely used. The derivative constraint method only provides robust performance for steering errors and other types of phase perturbation are not necessarily protected. The techniques based on noise injection and the quadratic inequality constraint require that a parameter be set for optimal performance. Unfortunately, this parameter can only be determined *a priori* for special cases. Subspace nulling constraints are not appropriate for small random phase errors at individual elements because these error do not span a preferred complex subspace.

The next chapter develops a method that provides robust protection in the presence of small random phase errors. One advantage of the new technique is that it can be implemented without *a priori* knowledge of signal and interference powers. As a result, it has application to many practical problems.

Chapter 3

Robust Technique Development

In this chapter, a technique is developed that prevents the output signal power loss that occurs in phase-perturbed, minimum-variance beamformers. Additionally, a modified form of the GSC is developed to implement the technique adaptively.

3.1 Linear Constraints

The addition of linear constraints is one technique that has been used to provide robust performance in adaptive arrays. By further constraining the subspace for the weight vector, this method prevents the adaptive array processor from trying to null signals arriving from slightly perturbed directions. For example, the combination of a derivative constraint on the array response (which is in the form of a linear constraint) and the steering vector constraint forces a given point in the array response to have both a specified gain value and a zero derivative with respect to arrival angle. This method indirectly constrains the array gain in the neighborhood of this point to have a near constant value.

Appendix A presents an analysis which shows that the space of all complex steering vectors formed from all combinations of small phase errors of independent and identically distributed (i.i.d.), zero-mean symmetrically distributed random variables has no preferred subspace. Er and Cantoni's method [9] exploits situations in which the perturbed steering vectors have a favored subspace. Since this is not the case for small phase perturbations, their approach does not apply.

3.2 Output Power Analysis

In this section, the perturbation problem is examined from a new point of view. Instead of taking a subspace approach, the beamformer output power is analyzed directly. This approach offers insight as to the cause of the severe SINR degradation observed in perturbed system..

Under conditions of element perturbations, the steering vector $\tilde{\mathbf{d}}$ for the signal of interest differs from the desired vector $\mathbf{d}$. The difference is represented by the error vector $\boldsymbol{\Delta}$,

$$\tilde{\mathbf{d}} \triangleq \mathbf{d} + \boldsymbol{\Delta}, \tag{3.1}$$

and the perturbed signal vector $\tilde{\mathbf{s}}$ is then,

$$\tilde{\mathbf{s}} = \sigma_s e^{j\xi} (\mathbf{d} + \boldsymbol{\Delta}). \tag{3.2}$$

This leads to an expression for the modified correlation matrix,

$$\mathbf{R}_{xx} = \tilde{\mathbf{s}}\tilde{\mathbf{s}}^\dagger + \sigma_n^2 \mathbf{I}, \tag{3.3}$$

$$= \sigma_s^2 (\mathbf{d} + \boldsymbol{\Delta})(\mathbf{d} + \boldsymbol{\Delta})^\dagger + \sigma_n^2 \mathbf{I}. \tag{3.4}$$

Under these conditions, the output power is computed as,

$$\mathbf{w}^\dagger \mathbf{R}_{xx} \mathbf{w} = \sigma_s^2 \mathbf{w}^\dagger (\mathbf{d} + \boldsymbol{\Delta})(\mathbf{d} + \boldsymbol{\Delta})^\dagger \mathbf{w} + \sigma_n^2 \mathbf{w}^\dagger \mathbf{I} \mathbf{w}, \tag{3.5}$$

$$= \sigma_s^2 \left(\mathbf{w}^\dagger \mathbf{d} + \mathbf{w}^\dagger \boldsymbol{\Delta}\right)\left(\mathbf{d}^\dagger \mathbf{w} + \boldsymbol{\Delta}^\dagger \mathbf{w}\right) + \sigma_n^2 \|\mathbf{w}\|^2. \tag{3.6}$$

Substitution of the linear constraint $\mathbf{d}^\dagger \mathbf{w} = 1$ yields,

$$\mathbf{w}^\dagger \mathbf{R}_{xx} \mathbf{w} = \sigma_s^2 \left(1 + \mathbf{w}^\dagger \boldsymbol{\Delta}\right)\left(1 + \boldsymbol{\Delta}^\dagger \mathbf{w}\right) + \sigma_n^2 \|\mathbf{w}\|^2, \tag{3.7}$$

$$= \sigma_s^2 \left(1 + \mathbf{w}^\dagger \boldsymbol{\Delta}\right)\left(1 + \mathbf{w}^\dagger \boldsymbol{\Delta}\right)^* + \sigma_n^2 \|\mathbf{w}\|^2, \tag{3.8}$$

and the final form for the output power under perturbed conditions becomes,

$$\mathbf{w}^\dagger \mathbf{R}_{xx} \mathbf{w} = \sigma_s^2 |1 + \mathbf{w}^\dagger \boldsymbol{\Delta}|^2 + \sigma_n^2 \|\mathbf{w}\|^2. \tag{3.9}$$

The minimization of power in Eq. (3.9) is a trade-off between minimizing the power term $|1 + \mathbf{w}^\dagger \boldsymbol{\Delta}|^2$ and the noise term $\|\mathbf{w}\|^2$. The degree to which each term is minimized depends on the relative powers of σ_s^2 and σ_n^2. To reduce the signal power significantly in a slightly perturbed environment (i.e. when the norm of $\boldsymbol{\Delta}$ is small), the weight vector norm would have to increase dramatically. In low SNR environments, the resulting increase in the noise power term inhibits such an increase. However, in large SNR situations, $\sigma_n^2 << \sigma_s^2$ and the penalty for increasing the weight vector norm is diminished. The result is a decrease in output signal power and a relatively small increase in output noise power. Hence, error-induced output SNR degradation is more severe at higher values of input SNR.

Noise injection may be viewed as a technique whereby the weight vector is optimized under simulated low SNR conditions. Equivalently, the object of noise injection is to artificially cause the output power to become large when the norm of $\mathbf{w}$ is increased. This is accomplished by artificially increasing σ_n^2. Restricting the norm of $\mathbf{w}$ also restricts the term $\mathbf{w}^\dagger \boldsymbol{\Delta}$ and the SINR remains high. The extreme case would be to inject a near-infinite amount of noise. Under this condition, the

autocorrelation matrix is dominated by its diagonal and the weight vector is equal to the quiescent value.

There are two main problems with the artificial noise injection method. First, the proper amount of noise to add cannot be calculated without *a priori* information regarding the input signal and interference power levels. Secondly, optimal values for the level of noise injection have only be calculated for the case of one narrowband signal and one narrowband jammer.

3.3 SINR Degradation

A preventative measure against SINR degradation is now presented. If the signal output power for a perturbed array is inhibited from being attenuated (i.e. by forcing $|1 + \mathbf{w}^\dagger\boldsymbol{\Delta}|^2 > 1$ in Eq. (3.9)), then the adaptive beamformer is not able to use the error term $\boldsymbol{\Delta}$ to cause a drop in output signal power. If output signal power cannot be reduced, the noise power cannot increase because of the the minimum output power criteria. Hence, a new constraint is proposed for the adaptive beamformer in addition to its previous linear constraint,

$$|1 + \mathbf{w}^\dagger\boldsymbol{\Delta}|^2 \geq 1. \tag{3.10}$$

3.3.1 Region of Degradation

After some algebra, Eq. (3.10) can be rewritten as,

$$\left(1 + \mathbf{w}^\dagger\boldsymbol{\Delta}\right)\left(1 + \mathbf{w}^\dagger\boldsymbol{\Delta}\right)^\dagger \geq 1, \tag{3.11}$$

$$1 + \mathbf{w}^\dagger\boldsymbol{\Delta} + \boldsymbol{\Delta}^\dagger\mathbf{w} + \mathbf{w}^\dagger\boldsymbol{\Delta}\boldsymbol{\Delta}^\dagger\mathbf{w} \geq 1, \tag{3.12}$$

$$2\Re\left(\mathbf{w}^\dagger\boldsymbol{\Delta}\right) \geq -\mathbf{w}^\dagger\boldsymbol{\Delta}\boldsymbol{\Delta}^\dagger\mathbf{w}, \tag{3.13}$$

$$2\Re\left(\mathbf{w}^{\dagger}\Delta\right) \geq -|\mathbf{w}^{\dagger}\Delta|^2, \tag{3.14}$$

$$\Re\left(\mathbf{w}^{\dagger}\Delta\right) \geq \frac{-|\mathbf{w}^{\dagger}\Delta|^2}{2}, \tag{3.15}$$

where $\Re(\cdot)$ denotes real part. A generic representation of this constraint in the complex plane is shown in Fig. 3.1. If $\mathbf{w}^{\dagger}\Delta$ is kept exterior to the signal-noise

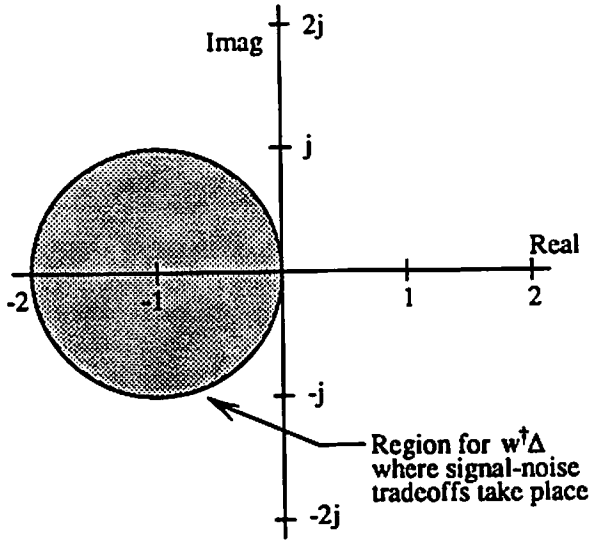

Figure 3.1: Signal Degradation Region for $\mathbf{w}^{\dagger}\Delta$

trade-off circle shown in the figure, the adaptive beamformer will be prevented from cancelling signal power. However, constraints which force $\mathbf{w}^{\dagger}\Delta$ to lie outside the circle cannot be imposed without knowledge of the error vector Δ. Such knowledge is an impractical requirement. In fact, if Δ is known, it can be used to correct the desired signal steering vector and the array will then operate as an error free (unperturbed) system.

3.3.2 Robust Constraints

To achieve the goal of avoiding the signal-noise trade-off zone in Fig. 3.1, each term of the inner product $\mathbf{w}^\dagger \Delta$ is constrained to have a non-negative real part,

$$\Re\left(w_k^* \Delta_k\right) \geq 0 \qquad k = 1, 2, \ldots, N. \tag{3.16}$$

Since each term of $\mathbf{w}^\dagger \Delta$ has a non-negative real component, the sum forming the inner product will also have a non-negative real component,

$$\Re\left(\mathbf{w}^\dagger \Delta\right) \geq 0. \tag{3.17}$$

This inequality represents a sufficient constraint to prevent signal-noise trade off (see Fig. 3.2). Hence, by construction, signal-noise power trade-off cannot

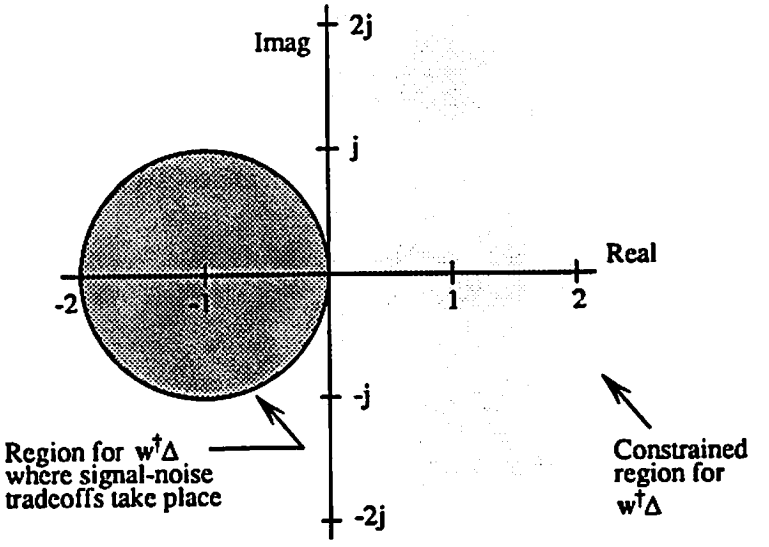

Figure 3.2: $\mathbf{w}^\dagger \Delta$ Tradeoff Region Disjoint From Constraint Region

occur.

3.4 Small Phase Error Approximation

The robust method proposed adds constraints to the original single constraint system of Eq. (2.22),

$$\min_{\mathbf{w}} \mathbf{w}^{\dagger}\mathbf{R}_{xx}\mathbf{w} \quad \textit{such that} \quad \mathbf{d}^{\dagger}\mathbf{w} = 1,$$
$$\textit{and} \qquad \Re\left(w_k^{*}\Delta_k\right) \geq 0, \qquad k = 1, 2, \ldots, N. \tag{3.18}$$

These inequalities cannot be evaluated without knowledge of each error vector element Δ_k. Fortunately, such knowledge can be obtained by assuming that the the error vector elements contain only small phase errors. The definition of "small" in this context is defined below.

Each element $\tilde{d}_k$ of the perturbed steering vector can be written as a phase shifted version of the unperturbed steering vector element d_k,

$$\tilde{d}_k = d_k e^{j\Delta p_k}, \tag{3.19}$$

where Δp_k is the random real-valued phase error variable for element k in radians. Expanding the exponential term using the Maclaurin series yields,

$$e^{j\Delta p_k} = 1 + j\Delta p_k - \frac{{\Delta p_k}^2}{2!} - j\frac{{\Delta p_k}^3}{3!} + \ldots. \tag{3.20}$$

Equation (3.19) then becomes,

$$\tilde{d}_k = d_k\left(1 + j\Delta p_k - \frac{{\Delta p_k}^2}{2!} - j\frac{{\Delta p_k}^3}{3!} + \ldots\right), \tag{3.21}$$
$$= d_k + d_k\left(j\Delta p_k - \frac{{\Delta p_k}^2}{2!} - j\frac{{\Delta p_k}^3}{3!} + \ldots\right), \tag{3.22}$$

and use of Eq. (3.1) yields the expansion form for the error vector element Δ_k,

$$\Delta_k = d_k\left(j\Delta p_k - \frac{{\Delta p_k}^2}{2!} - j\frac{{\Delta p_k}^3}{3!} + \ldots\right). \tag{3.23}$$

For small errors (i.e. $\frac{\Delta p_k{}^2}{2!} << 1$), the error vector element Δ_k retains only its first order term,

$$\Delta_k \approx d_k (j\Delta p_k), \tag{3.24}$$

$$\approx \Delta p_k e^{j\frac{\pi}{2}} d_k. \tag{3.25}$$

Under these conditions, the error vector element Δ_k has a $\frac{\pi}{2}$ phase shift relative to the steering vector element d_k. Small fluctuations in the phase error Δp_k only affect the magnitude of the error vector element Δ_k (i.e. the phase component of the error vector element Δ_k is not significantly altered). The small phase error situation is depicted in Fig. 3.3.

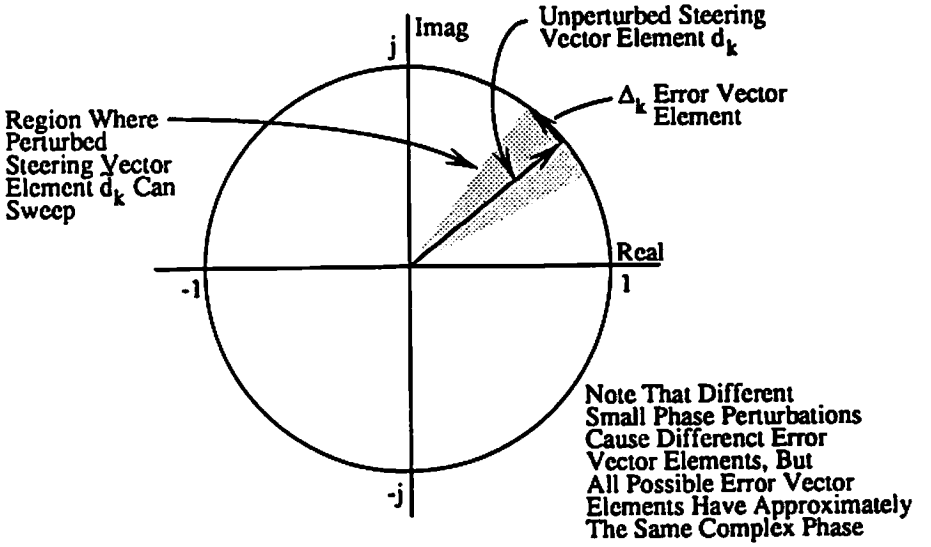

Figure 3.3: Small Phase Perturbations Create Approximately Constant Phase of Error Vector Elements

3.4.1 Simplification of Constraints

With the small phase approximation, it will be shown that the inequality constraints in Eq. (3.16) can be reduced to equality constraints. Substituting the small error approximation from Eq. (3.25) into the the inequality constraint of Eq. (3.18) and noting that $\Im$ represents the complex imaginary part yields,

$$\Re\left(w_k^* \Delta_k\right) \geq 0, \tag{3.26}$$

$$\Re\left(w_k^* \Delta p_k d_k e^{j\frac{\pi}{2}}\right) \geq 0, \tag{3.27}$$

$$\Delta p_k \Im\left(w_k^* d_k\right) \leq 0. \tag{3.28}$$

Since the phase error Δp_k is assumed to be a random variable that can take on positive, zero, or negative values, the inequality in Eq. (3.28) can only be met if $\Im\left(w_k^* d_k\right) = 0$. As a result, the inequality constraints in Eq. (3.16) can be satisfied with either of the following two equivalent sets of equality constraints:

$$\Re\left(w_k^* \Delta_k\right) = 0 \qquad k = 1, 2, \ldots, N, \tag{3.29}$$

$$\Im\left(d_k^* w_k\right) = 0 \qquad k = 1, 2, \ldots, N. \tag{3.30}$$

The inequality constraints in Eq. (3.16) are preferred over the equality constraints in Eqs. (3.29) and (3.30) due to the fact that they provide a larger feasible region for the weight vector $\mathbf{w}$. A discussion of this approach is given in Appendix B where the error term is biased in an attempt to force $\Delta p_k > 0$. This approach is shown to reduce the inequality constraints to the same equality constraints of Eqs. (3.29) and (3.30).

3.4.2 New Constraint Problem

The analysis in the last section transformed the inequality constraints of Eq. (3.16) into equality constraints. This allows Eq. (3.18) to be rewritten as,

$$\min_{\mathbf{w}} \mathbf{w}^\dagger \mathbf{R}_{xx} \mathbf{w} \quad \textit{such that} \quad \mathbf{d}^\dagger \mathbf{w} = 1,$$
$$\textit{and} \qquad \Im\left(d_k^* w_k\right) = 0, \qquad k = 1, 2, \ldots, N. \tag{3.31}$$

These additional constraints imply that,

$$\Re\left(\mathbf{w}^\dagger \mathbf{\Delta}\right) = 0, \tag{3.32}$$

and ensure that $\mathbf{w}^\dagger \mathbf{\Delta}$ is outside the signal power trade-off circle in Fig. 3.1. In fact, the equality constraints force $\mathbf{w}^\dagger \mathbf{\Delta}$ to lie on the imaginary axis in Fig. 3.1. Hence, these constraints are sufficient to provide robust SINR performance. Although it is might be desirable to achieve Eq. (3.32) without the very restrictive equality constraints on individual weight elements shown in Eq. (3.31), the random and independent nature of the elements of the error vector $\mathbf{\Delta}$ require the use of such restrictive constraints on the individual weight elements.

3.4.3 Transformation into Real Domain

Except for the imaginary-part operator $\Im(\cdot)$ in Eq. (3.31), the formulation appears to be a traditional power minimization problem with multiple linear constraints. If they were linear constraints, the problem could be solved by placing all the constraints in the matrix $\mathbf{C}$ and then using the closed-form solution for the optimal weight vector $\mathbf{w}_{opt}$ in Eq. (2.18), or by adaptively converging to the optimal weight vector with the GSC as described in Chapter 2. Unfortunately, the $\Im(\cdot)$ operator makes the problem a non-linear one in the complex domain.

Real Formulation of the Problem

The nonlinearly-constrained power minimization problem in Eq. (3.31) can be converted to a linearly-constrained problem by converting the complex valued problem to a real valued problem. Details of the restructuring are given in Appendix C. Each complex matrix or vector can be broken down as the sum of two real matrices:

$$\mathbf{w} = \mathbf{w}_r + j\mathbf{w}_i, \tag{3.33}$$

$$\mathbf{d} = \mathbf{d}_r + j\mathbf{d}_i, \tag{3.34}$$

$$\mathbf{R}_{xx} = \mathbf{R}_{xxr} + j\mathbf{R}_{xxi}, \tag{3.35}$$

$$f = f_r + jf_i, \tag{3.36}$$

where the subscripts "r" and "i" represent the real and imaginary components of each matrix. Applying the restructuring shown in Appendix C yields a new format for each matrix, each with all real components,

$$\mathbf{w}_R \triangleq \begin{bmatrix} \mathbf{w}_r \\ \mathbf{w}_i \end{bmatrix}, \tag{3.37}$$

$$\mathbf{D}_R \triangleq \begin{bmatrix} \mathbf{d}_r & -\mathbf{d}_i \\ \mathbf{d}_i & \mathbf{d}_r \end{bmatrix}, \tag{3.38}$$

$$\mathbf{R}_{xxR} \triangleq \begin{bmatrix} \mathbf{R}_{xxr} & -\mathbf{R}_{xxi} \\ \mathbf{R}_{xxi} & \mathbf{R}_{xxr} \end{bmatrix}, \tag{3.39}$$

$$\mathbf{f}_R \triangleq \begin{bmatrix} f_r \\ f_i \end{bmatrix}. \tag{3.40}$$

For the case of a single steering constraint, $f = 1$, Eq. (3.40) reduces to,

$$\mathbf{f}_R = \begin{bmatrix} 1 \\ 0 \end{bmatrix}. \tag{3.41}$$

For notational convenience, the two columns of the transformed matrix $\mathbf{D}_R$ in Eq. (3.38) are denoted by $\mathbf{d}_{R1}$ and $\mathbf{d}_{R2}$,

$$\mathbf{D}_R \triangleq \begin{bmatrix} | & | \\ \mathbf{d}_{R1} & \mathbf{d}_{R2} \\ | & | \end{bmatrix}, \tag{3.42}$$

where,

$$\mathbf{d}_{R1} \triangleq \begin{bmatrix} \mathbf{d}_r \\ \mathbf{d}_i \end{bmatrix} \quad \text{, and} \quad \mathbf{d}_{R2} \triangleq \begin{bmatrix} -\mathbf{d}_i \\ \mathbf{d}_r \end{bmatrix}. \tag{3.43}$$

With these transformed matrices, the transformed problem for the original minimum variance beamformer from Eq. (2.22) (i.e. without the additional robust constraints) becomes,

$$\min_{\mathbf{w}_R} \mathbf{w}_R^T \mathbf{R}_{xx\,R} \mathbf{w}_R \quad \textit{subject to} \quad \mathbf{D}_R^T \mathbf{w}_R = \mathbf{f}_R, \tag{3.44}$$

where "T" represents real transpose. The optimal weight vector in the real structure format $\mathbf{w}_{opt,R}$ can be calculated using the closed-form solution given by Eq. (2.18),

$$\mathbf{w}_{opt,R} = \mathbf{R}_{xx\,R}^{-1} \mathbf{D}_R \left(\mathbf{D}_R^T \mathbf{R}_{xx\,R}^{-1} \mathbf{D}_R \right)^{-1} \mathbf{f}_R. \tag{3.45}$$

This real formulation of the original problem utilizes the following two real constraints:

$$\mathbf{d}_{R1}^T \mathbf{w}_R = 1, \tag{3.46}$$

$$\mathbf{d}_{R2}^T \mathbf{w}_R = 0. \tag{3.47}$$

By using Eq. (3.43) it can be shown that these two real constraints can be written as,

$$\Re\left(\mathbf{d}^{\dagger}\mathbf{w}\right) = 1, \tag{3.48}$$

$$\Im\left(\mathbf{d}^{\dagger}\mathbf{w}\right) = 0. \tag{3.49}$$

This form is equivalent to the original single complex constraint $\mathbf{d}^{\dagger}\mathbf{w} = 1$. The advantages of this new real structure are apparent: the non-linear $\Re(\cdot)$ and $\Im(\cdot)$ constraints in the complex domain have been written as real linear constraints. with the new real structure. Any additional $\Im(\cdot)$ constraints can then be added as simple linear constraints.

Addition of Robust Real Constraints

In the transformed representation, the previous $\Re(w_k^*\Delta_k) = 0$ constraints on the weight vector $\mathbf{w}$ from Eq. (3.31) can be added as real linear constraints to the problem stated in Eq. (3.44). To illustrate, the robust constraints are expanded as follows:

$$\Im(d_k^* w_k) = 0, \tag{3.50}$$

$$\Im\left((d_{k,r} - jd_{k,i})(w_{k,r} + jw_{k,i})\right) = 0, \tag{3.51}$$

$$-d_{k,i}w_{k,r} + d_{k,r}w_{k,i} = 0, \qquad k = 1, 2, \ldots, N, \tag{3.52}$$

where the "r" and "i" subscripts represent the real and imaginary parts of d_k and w_k. Eq. (3.52) can then be written as,

$$\Delta_{R,k}^T \mathbf{w}_R = 0, \qquad k = 1, 2, \ldots, N, \tag{3.53}$$

where the vector $\Delta_{R,k}$ of length $2N$ contains all zeros except in positions k and $k+N$,

$$\Delta_{R,k} = \begin{bmatrix} 0 \\ \vdots \\ 0 \\ -d_{k,i} \\ 0 \\ \vdots \\ 0 \\ d_{k,r} \\ 0 \\ \vdots \\ 0 \end{bmatrix}. \tag{3.54}$$

In summary, the steering and robust constraints in the real structured format from Eqs. (3.46), (3.47), and (3.53) can be written as,

$$\mathbf{d}_{R1}{}^T \mathbf{w}_R = 1, \tag{3.55}$$

$$\mathbf{d}_{R2}{}^T \mathbf{w}_R = 0, \tag{3.56}$$

$$\Delta_{R,k}^T \mathbf{w}_R = 0, \qquad k = 1, 2, \ldots, N. \tag{3.57}$$

It can be shown, however, that the constraint in Eq. (3.56) is a linear combination of the mutually independent constraints in Eq. (3.57),

$$\sum_{k=1}^{N} \Delta_{R,k} = \begin{bmatrix} -\mathbf{d}_i \\ \mathbf{d}_r \end{bmatrix} = \mathbf{d}_{R2}. \tag{3.58}$$

As a result, Eq. (3.56) is a redundant constraint. The remaining constraints of Eqs. (3.55) and (3.57) can be placed into a real constraint matrix $\mathbf{C}_R$ of size

$(2N)$x$(N+1)$ with the real constraint values in the vector $\mathbf{f}_R$ of size $(N+1)$x1,

$$\mathbf{C}_R \triangleq \begin{bmatrix} | & | & \cdots & | \\ \mathbf{d}_{Rl} & \Delta_{R,1} & \cdots & \Delta_{R,N} \\ | & | & \cdots & | \end{bmatrix}, \quad \text{and} \quad \mathbf{f}_R \triangleq \begin{bmatrix} 1 \\ 0 \\ \vdots \\ 0 \end{bmatrix}. \tag{3.59}$$

The final matrix form of the real constraint equation is then,

$$\mathbf{C}_R^T \mathbf{w}_R = \mathbf{f}_R. \tag{3.60}$$

The real transformed problem has a closed-form solution given by Eq. (2.18) with appropriate substitutions, i.e.,

$$\mathbf{w}_{opt_R} = \mathbf{R}_{xx}^{-1}{}_R \mathbf{C}_R \left(\mathbf{C}^\dagger{}_R \mathbf{R}_{xx}^{-1}{}_R \mathbf{C}_R \right)^{-1} \mathbf{f}_R. \tag{3.61}$$

The complex optimal weight vector $\mathbf{w}_{opt}$ can be obtained from real version $\mathbf{w}_{opt_R}$ by selecting the real and imaginary components from $\mathbf{w}_{opt_R}$ as defined in Eq. (3.37).

3.4.4 GSC Implementation

Since implementation of robust constraints can be achieved through power minimization with real linear constraints, a real domain form of the Generalized Sidelobe Canceller can be used to iteratively solve for the optimal weights. The real domain form of the GSC is shown in Fig. 3.4. In a manner analogous to the complex form of the GSC in Eq. (2.28), the real form of the weight vector $\mathbf{w}_R$ is divided into orthogonal components,

$$\mathbf{w}_R = \mathbf{w}_{q,R} - \mathbf{W}_{s,R} \mathbf{w}_{a,R}, \tag{3.62}$$

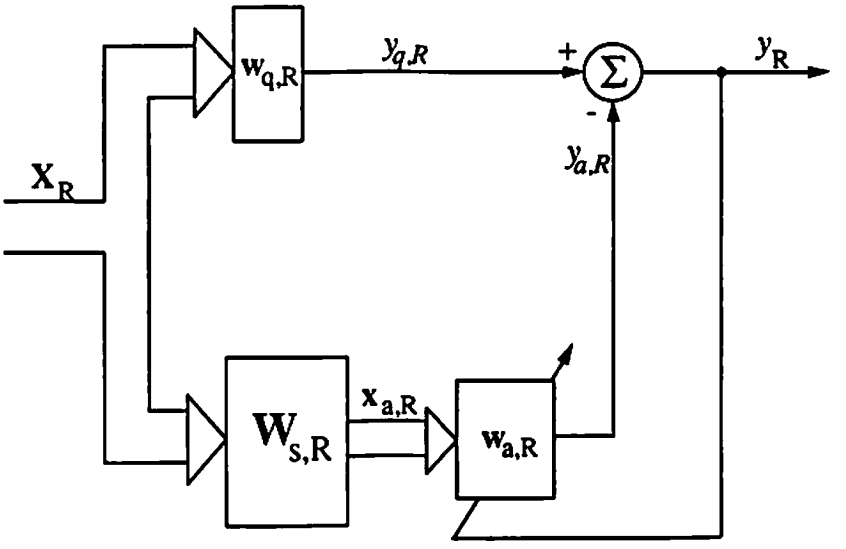

Figure 3.4: Real Form of the GSC With Robust Constraints

where the columns of the matrix $\mathbf{W}_{s,R}$ are linearly independent vectors that span the orthogonal space of the real constraint matrix $\mathbf{C}_R$. Thus,

$$\mathbf{C}_R^T \mathbf{W}_{s,R} = 0. \tag{3.63}$$

The complex data vector $\mathbf{x}$ is transformed in a similar fashion as,

$$\mathbf{X}_R \triangleq \begin{bmatrix} \mathbf{x}_r & -\mathbf{x}_i \\ \mathbf{x}_i & \mathbf{x}_r \end{bmatrix} \triangleq \begin{bmatrix} | & | \\ \mathbf{x}_{R1} & \mathbf{x}_{R2} \\ | & | \end{bmatrix}. \tag{3.64}$$

The lower path data matrix $\mathbf{X}_{a,R}$ is defined as,

$$\mathbf{X}_{a,R} \triangleq \mathbf{W}_{s,R}^T \mathbf{X}_R \triangleq \begin{bmatrix} | & | \\ \mathbf{x}_{a,R1} & \mathbf{x}_{a,R2} \\ | & | \end{bmatrix}, \tag{3.65}$$

where $\mathbf{x}_{a,R1}$ and $\mathbf{x}_{a,R2}$ are the two real columns of $\mathbf{X}_{a,R}$. Note that $\mathbf{X}_{a,R}$ does not share the block symmetry properties of the previously defined matrices (e.g.

$\mathbf{D}_R$, $\mathbf{X}_R$, etc.). The particular method for organizing the computations is shown in Appendix C. The real output $\mathbf{y}_R$ is a row vector which contains the real and imaginary components of the complex version of the output y,

$$\mathbf{y}_R \triangleq [y_r, -y_i]. \tag{3.66}$$

The LMS adaptive algorithm for this system is derived in Appendix C and involves minimizing the output power using an instantaneous gradient. The resulting adaptive weight update $\mathbf{w}_{a,R}(n+1)$,

$$\mathbf{w}_{a,R}(n+1) = \mathbf{w}_{a,R}(n) + 2\mu\mathbf{X}_{a,R}(n)\mathbf{y}_R^T(n), \tag{3.67}$$

where the time sample index has been included to denote the iteration number. Thus, the GSC format can be used with the transformed structure with only slight modifications. The choice for μ must be small enough to ensure convergence. A sufficient condition on μ [13] is,

$$0 < \mu < Trace\left(\mathbf{W}_{s,R}^T \mathbf{R}_{xxR} \mathbf{W}_{s,R}\right), \tag{3.68}$$

or, equivalently,

$$\mu = \frac{\alpha}{Trace\left(\mathbf{W}_{s,R}^T \mathbf{R}_{xxR} \mathbf{W}_{s,R}\right)}, \tag{3.69}$$

where $0 < \alpha < 1$.

3.4.5 Optional Use of Additional Constraints

In many practical applications of interest, additional linear constraints are used to supplement the steering and robust constraints to enhance performance. Each additional complex constraint for the form $\mathbf{c}^\dagger{}_k\mathbf{w} = f_k$ can be restructured into the

real domain and added to the constraint matrix $\mathbf{C}_R$ and constraint value vector $\mathbf{f}_R$. The transformed constraints becomes,

$$\mathbf{C}_{k,R} \triangleq \begin{bmatrix} \mathbf{c}_{k,r} & -\mathbf{c}_{k,i} \\ \mathbf{c}_{k,i} & \mathbf{c}_{k,r} \end{bmatrix} \triangleq \begin{bmatrix} | & | \\ \mathbf{c}_{k,R1} & \mathbf{c}_{k,R2} \\ | & | \end{bmatrix}, \tag{3.70}$$

and,

$$\mathbf{f}_{k,R} \triangleq \begin{bmatrix} f_{k,r} \\ f_{k,i} \end{bmatrix}, \tag{3.71}$$

which yields two real constraints,

$$\mathbf{c}_{k,R1}^T \mathbf{w}_k = f_{k,r}, \tag{3.72}$$

$$\mathbf{c}_{k,R2}^T \mathbf{w}_k = f_{k,i}. \tag{3.73}$$

These constraints can then be appended to $\mathbf{C}_R$ and $\mathbf{f}_R$ to form the newly constrained problem.

3.5 Summary

In this chapter, a new approach was presented to prevent the output SINR degradation that occurs in phase-perturbed minimum variance beamformers. An output signal power degradation region was defined and constraints developed to remain in its exterior. A consequence of preventing output signal power degradation is the inhibition of an increase in output noise power. Hence, SINR performance is preserved. These constraints were arranged in linear form by restructuring the complex-valued problem into a real-valued problem. Consequently, a closed-form solution was developed for the optimal weight vector. The Generalized Sidelobe

Canceller was modified to implement the restructured constraints and provide an iterative means for implementation.

Chapter 4

Analysis of New Algorithm

The robust constraints developed in Chapter 3 were specifically chosen to protect the output power of the desired signal in an adaptive array processor under conditions of small uncorrelated phase errors. This chapter shows that these robust constraints can also be derived from the application of derivative constraints to individual array elements.

Although the robust constraints protect the output SINR under small phase perturbations, larger phase errors may cause degradation. In this chapter, analytic expressions are derived to predict SINR performance as a function of phase error.

4.1 The Steering Derivative Constraint

Before deriving the robust constraints as individual derivative constraints, it is useful to observe that the steering derivative constraint described in Chapter 2 is actually a special case of the robust constraints, i.e., adding a steering derivative constraint to the robust constraint system is redundant.

Following the analysis by Tseng [22], the approach taken in applying a steering derivative constraint uses the partial derivative of the output magnitude squared,

$$\left.\frac{\partial |y|^2}{\partial \Theta}\right|_{\Theta=\Theta_0} = 0, \tag{4.1}$$

where Θ_0 is the arrival angle of the desired signal. Application of the chain rule yields,

$$\begin{aligned}
\frac{\partial |y|^2}{\partial \Theta} &= \frac{\partial y}{\partial \Theta} y^* + \frac{\partial y^*}{\partial \Theta} y, && (4.2)\\
&= \frac{\partial y}{\partial \Theta} y^* + \left(\frac{\partial y}{\partial \Theta}\right)^* y, && (4.3)\\
&= \frac{\partial y}{\partial \Theta} y^* + \left(\frac{\partial y}{\partial \Theta} y^*\right)^*, && (4.4)\\
&= 2\Re\left(\frac{\partial y}{\partial \Theta} y^*\right), && (4.5)
\end{aligned}$$

and substitution into Eq. (4.1) then yields,

$$\Re\left(\frac{\partial y}{\partial \Theta} y^*\right)\Big|_{\Theta=\Theta_0} = 0. \tag{4.6}$$

As shown in Eq. (2.34), this operation is applied when y is the output due to an input which consists of only the desired signal. The partial $\left.\frac{\partial y}{\partial \Theta}\right|_{\Theta=\Theta_0}$ then has a linear form,

$$\left.\frac{\partial y}{\partial \Theta}\right|_{\Theta=\Theta_0} = \mathbf{w}^\dagger \dot{\mathbf{d}}, \tag{4.7}$$

where $\dot{\mathbf{d}}$ is a vector with elements determined by the partial derivative operation. The steering constraint $\mathbf{d}^\dagger \mathbf{w} = 1$ ensures that the output is unity under signal-only conditions. As a result,

$$\begin{aligned}
\Re\left(\frac{\partial y}{\partial \Theta} y^*\right)\Big|_{\Theta=\Theta_0} &= 0, && (4.8)\\
\Re\left(\left(\mathbf{w}^\dagger \dot{\mathbf{d}}\right)\left(\mathbf{w}^\dagger \mathbf{d}\right)^*\right) &= 0, && (4.9)\\
\Re\left(\dot{\mathbf{d}}^\dagger \mathbf{w}\right) &= 0. && (4.10)
\end{aligned}$$

This approach ensures that any weight vector w meeting the derivative constraint in Eq. (4.10) is robust to small steering errors between the actual and designed directions. It will be shown that the steering derivative constraint is already satisfied with the robust constraints of Eq. (3.29).

In order to demonstrate that this is, in fact, the case, each element of the steering vector d is expressed in terms of the angle of arrival of the signal,

$$d_k = e^{jf_k(\Theta)}, \tag{4.11}$$

where $f_k(\Theta)$ represents a real function of the angle of arrival Θ. Each element $\dot{d}_k$ of the derivative vector $\dot{\mathbf{d}}$ can be expressed as the partial derivative of the steering vector element with respect to the arrival angle,

$$\begin{aligned} \dot{d}_k &= \frac{\partial d_k}{\partial \Theta}, & (4.12)\\ &= j\frac{\partial f_k(\Theta)}{\partial \Theta} e^{jf_k(\Theta)}, & (4.13)\\ &= j\frac{\partial f_k(\Theta)}{\partial \Theta} d_k. & (4.14) \end{aligned}$$

In this expression, $f_k(\Theta)$ is real and thus $\frac{\partial f_k(\Theta)}{\partial \Theta}$ is also a real quantity. Therefore, the elements of the derivative vector $\dot{\mathbf{d}}$ are magnitude scaled and $\frac{\pi}{2}$ shifted versions of the elements of the steering vector. This is identical to the relationship described in Eq. (3.25) for use in the robust constraints of Eq. (3.29), i.e.,

$$\Delta_k \approx \Delta p_k e^{j\frac{\pi}{2}} d_k = j\Delta p_k d_k. \tag{4.15}$$

Thus, the robust constraints $\Re(w_k^* \Delta_k) = 0$ are sufficient to ensure that the real part of each term of $\dot{\mathbf{d}}^\dagger \mathbf{w}$ is zero. Hence, the derivative constraint $\Re\left(\dot{\mathbf{d}}^\dagger \mathbf{w}\right) = 0$ is satisfied with the robust constraints.

The steering derivative constraint has been shown to be a special form of the robust error constraints. The difference is that only one constraint is needed to

protect against azimuth steering errors compared to the N constraints needed to protect against random phase perturbations at each element. This is because there is only one parameter that is assumed in error: the azimuth arrival angle Θ. With random phase perturbations at each element, there is an independent phase error at each element, therefore, each element needs a separate constraint equation (totaling N constraints). The phase errors due to steering errors are perfectly correlated between elements, and so they only span one degree of freedom in the real structured transformed space described in Chapter 3. Thus, only one constraint is needed to protect against azimuth steering errors.

The next section will show how the derivative constraint technique can be applied to each element phase error instead of the steering error. The resulting constraints will be shown to be equivalent to the robust constraints.

4.2 Derivative Constraints for Array Elements

This section illustrates that robust constraints can be developed from derivative constraints on individual array elements. The previous derivative constraint, $\Re\left(\dot{\mathbf{d}}^{\dagger}\mathbf{w}\right) = 0$, is generalized from that of a single steering constraint on the arrival angle to include a constraint on the random phase term on each array element. This approach ensures that he output power of the desired signal is insensitive to small changes in the phase of each element.

4.2.1 Development of Derivative Constraints

A phase-perturbed steering vector element can be expressed as a function of its random phase error term Δp_k,

$$\tilde{d}_k = d_k e^{j\Delta p_k}. \tag{4.16}$$

The phase error term Δp_k is induced by steering error, frequency error, and/or random perturbation phase effects at each array element.

As in Eq. (4.1), the partial derivative with respect to each individual array element phase error term Δp_k is set to zero,

$$\left.\frac{\partial |y|^2}{\partial \Delta p_k}\right|_{\Delta p_k = 0} = 0, \qquad k = 1, 2, \ldots, N. \tag{4.17}$$

In a derivation that is analogous to that used in Eq. (4.2) to Eq. (4.5), this derivative can be expressed as,

$$\begin{aligned} \frac{\partial |y|^2}{\partial \Delta p_k} &= \frac{\partial y}{\partial \Delta p_k} y^* + \frac{\partial y^*}{\partial \Delta p_k} y, & (4.18)\\ &= 2\Re\left(\frac{\partial y}{\partial \Delta p_k} y^*\right). & (4.19) \end{aligned}$$

Substitution of Eq. (4.19) into Eq. (4.17) yields,

$$\left.2\Re\left(\frac{\partial y}{\partial \Delta p_k} y^*\right)\right|_{\Delta p_k = 0} = 0, \qquad k = 1, 2, \ldots, N. \tag{4.20}$$

The partial derivative is then evaluated by substituting the beamformer output $y = \mathbf{w}^\dagger \tilde{\mathbf{d}}$ corresponding to the perturbed desired signal vector $\tilde{\mathbf{d}}$,

$$\begin{aligned} \frac{\partial y}{\partial \Delta p_k} &= \frac{\partial\left(\mathbf{w}^\dagger \tilde{\mathbf{d}}\right)}{\partial \Delta p_k}, & (4.21)\\ &= \frac{\partial\left(\sum_{k=1}^{N} w_k^* d_k e^{j\Delta p_k}\right)}{\partial \Delta p_k}, & (4.22)\\ &= j w_k^* d_k e^{j\Delta p_k}. & (4.23) \end{aligned}$$

Since $y^* = 1$ at the nominal unperturbed phase error value of $\Delta p_k = 0$, the substitution of Eq. (4.23) into Eq. (4.20) yields,

$$\Re\left(\frac{\partial y}{\partial \Delta p_k} y^*\right)\Big|_{\Delta p_k = 0} = 0, \tag{4.24}$$

$$\Re\left(\frac{\partial y}{\partial \Delta p_k}\right)\Big|_{\Delta p_k = 0} = 0, \tag{4.25}$$

$$\Re\left(j w_k^* d_k e^{j\Delta p_k}\right)\Big|_{\Delta p_k = 0} = 0, \tag{4.26}$$

$$\Re\left(e^{j\frac{\pi}{2}} w_k^* d_k\right) = 0, \tag{4.27}$$

$$\Im\left(d_k^* w_k\right) = 0, \qquad k = 1, 2, \ldots, N. \tag{4.28}$$

This latter expression is identical to the robust constraints in Eq. (3.31). Thus, application of derivative constraints to each individual element produces the same power protection constraints that were developed in Chapter 3.

4.2.2 Discussion

Application of a derivative constraint to each individual element provides protection against independent phase errors at these elements. It is a natural extension of the use of a single derivative constraint to protect against steering errors. The form of the original derivative constraint described in Chapter 2, $\dot{\mathbf{d}}^\dagger \mathbf{w} = 0$, uses a single complex degree of freedom. Application of an analogous derivative constraint to each individual element would require N degrees of freedom. Since there are only $N - 1$ degrees of freedom available in the system, the set of equations would be overdetermined and inconsistent. Use of the derivative constraint $\Re\left(\dot{\mathbf{d}}^\dagger \mathbf{w}\right) = 0$ developed by Tseng [22], however, requires only *half* of a complex

degree of freedom. Application of an analogous derivative constraint to each individual element therefore requires only $\frac{N}{2}$ complex degrees of freedom and yields a set of equations that is underdetermined and consistent.

The individual derivative constraints require more degrees of freedom than a single steering derivative constraint, but the resulting system is more robust to random phase perturbations. A steering error produces correlated phase errors between array elements. When interelement phase perturbations are uncorrelated, the steering constraint does not provide protection. Since the multiple individual derivative constraints do not assume a correlation between element phase errors, they protect the system output for this important class of problems.

4.3 Phase Constraints on Weights

Examination of the robust constraints yields an interesting interpretation. The elements of the weight vector w and steering vector d can be expressed in magnitude and phase notation as,

$$d_k = e^{j\theta_k}, \tag{4.29}$$

$$w_k = v_k e^{j\phi_k}. \tag{4.30}$$

With this notation, the robust constraints of Eq. (3.31) become,

$$\Im\left(d_k^* w_k\right) = 0, \tag{4.31}$$

$$\Im\left(e^{-j\theta_k} v_k e^{j\phi_k}\right) = 0, \tag{4.32}$$

$$v_k \sin\left(\phi_k - \theta_k\right) = 0. \tag{4.33}$$

Except for the trivial cases when $v_k = 0$, the $\sin\left(\phi_k - \theta_k\right)$ term in this equation implies that each weight vector element must be colinear with its corresponding

steering vector element, as illustrated in Fig. 4.1. Equivalently, the robust

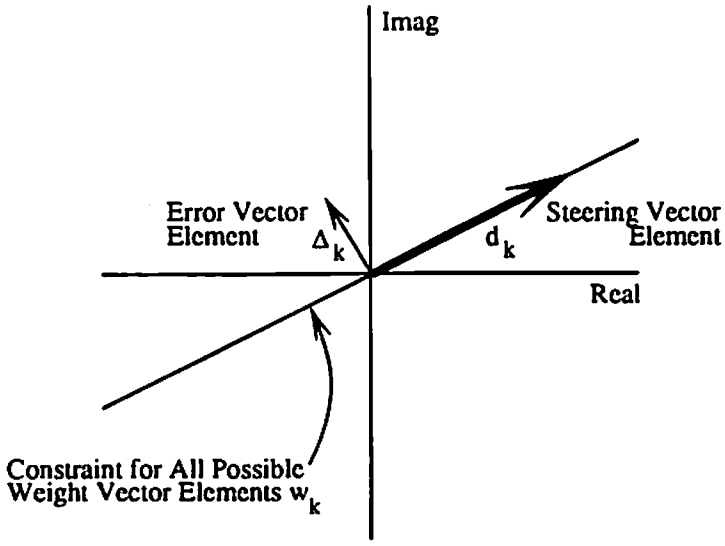

Figure 4.1: Phase Constraint on Weight Vector Elements

constraints can be interpreted as *phase constraints* on the weight vector elements.

Wang [23] suggested the use of *real* weights on complex data generated from a linear array that was steered to the broadside. His approach was equivalent to the application of phase constraints described above for the special case of broadside steering. Wang's intent was to simplify computation by removing half of the weight coefficients (i.e. remove the imaginary portion of each weight vector element). Hudson [18] analyzed this real weight concept and noted that it provides robust performance to steering errors. What this chapter has shown is that the N robust constraints are not necessary to provide robust performance for steering errors. Although the N robust constraints are sufficient to provide protection for steering errors, only a single constraint is necessary for steering protection. Thus, the analysis presented in this chapter extends Hudson's analysis to show

that the real weight concept is not only applicable for random steering errors, but to individual phase errors at each element as well.

4.4 Robust Constraints for Magnitude Errors

It was shown in the last section that restricting the phase of the weight vector elements provides robust performance due to small phase errors. A natural question that arises is the possibility of restricting the magnitude of the weight vector elements to provide robust performance due to small magnitude errors. This is impossible, however, due to simple contradictions in the problem statement.

As shown in Eq. (3.29), the general form for the robust constraints is,

$$\Re\left(w_k^* \Delta_k\right) = 0, \qquad k = 1, 2, \ldots, N. \tag{4.34}$$

In the presence of magnitude errors, the model for the error vector element Δ_k is,

$$\Delta_k = \Delta m_k d_k, \tag{4.35}$$

where Δm_k is the real valued amplitude error. The primary difference between the magnitude only error model in Eq. (4.35) and the small phase error in Eq. (3.25) is the absence of the $\frac{\pi}{2}$ phase shift term. Substituting Eq. (4.35) into Eq. (4.34) yields,

$$\Re\left(w_k^* \Delta m_k d_k\right) = 0, \tag{4.36}$$

$$\Re\left(w_k^* d_k\right) = 0, \qquad k = 1, 2, \ldots, N. \tag{4.37}$$

This result implies that the real part of each term of the inner product $\mathbf{w}^\dagger \mathbf{d}$ must equal zero, hence the real part of the entire inner product must also equal zero,

$$\Re\left(\mathbf{w}^\dagger \mathbf{d}\right) = \Re\left(\mathbf{d}^\dagger \mathbf{w}\right) = 0. \tag{4.38}$$

However, this result is in direct contradiction with the steering constraint in Eq. (2.22) which requires $\mathbf{d}^\dagger\mathbf{w} = 1$. An analogous robust form for protection due to magnitude errors is therefore not possible.

It may seem that the original steering constraint could be modified to have a $\frac{\pi}{2}$ phase shift resulting in $\mathbf{d}^\dagger\mathbf{w} = e^{j\frac{\pi}{2}}$ and still satisfy Eq. (4.38). However, Eq. (4.38) is a direct result of using the steering constraint $\mathbf{d}^\dagger\mathbf{w} = 1$. Adding a phase shift to the constraint value results in an equal phase shift in Eq. (4.38) and the result is still in contradiction.

4.5 Degrees of Freedom

An important concept in linearly-constrained minimum variance beamforming is the number of independent narrowband jammers that can be nulled. As Compton [24] noted, the number of complex degrees of freedom can be calculated as the number of array elements N minus the number of complex constraints employed. For the case of a single steering constraint, the number of available complex degrees of freedom is,

$$DOF_{ORIGINAL} = N - 1. \tag{4.39}$$

With the constrained beamformer in the *real* domain, there are $2N$ real weights. Use of the robust constraints leads to a real domain constraint matrix $\mathbf{C}_R$, Eq. (3.59), which contains $N+1$ linearly independent real constraints. Of these, one is the steering vector constraint $\mathbf{d}_{R1}$ and N are robust real linear vector constraints $\Delta_{R,k}$ for $k = 1, 2, \ldots, N$. Therefore, there are $2N - (N+1) = N - 1$ real degrees of freedom. The number of complex degrees of freedom is one half of the number of real degrees of freedom. Thus, the robust constraints results in $(N-1)/2$

complex degrees of freedom.. The greatest integer value less than or equal to this number then represents the available degrees of freedom with respect to complex signals,

$$DOF_{ROBUST} = \lfloor \frac{N-1}{2} \rfloor. \tag{4.40}$$

4.6 Degradation For Large Phase Errors

When the phase error at each array element increases, the small phase assumption is violated and the output SINR decreases even when the robust constraints are employed. This section develops an analytic expression for the SINR performance as a function of phase error which will be achieved while using the robust constraints.

As mentioned previously, the phase errors at each element can be due to several types of perturbations. Steering errors and frequency errors fall into a group called *single error sources* since each error is defined by a single parameter (Θ for steering and ω for frequency). Random phase errors and random placement errors fall into the category of *multiple error sources* since many parameters contribute to the total error (i.e. the N independent random phases at each element). Two types of SINR performance equations are developed: one for single error sources and one for multiple error sources. The single error source equation assumes that the perturbed steering vector $\tilde{\mathbf{d}}$ is known. The multiple error source equation assumes that only certain statistics of the error are known.

4.6.1 Single Error Sources

The equation developed in this section assumes that the perturbed steering vector $\bar{\mathrm{d}}$ is known as a function of a single error parameter. Hence, it is appropriate for SINR evaluation under conditions of steering or frequency error.

The SINR equation for use with the robust constraints is a modified version of the result obtained without robust constraints shown in Eq. (2.30) and repeated here (remembering that SNR and SINR can be used interchangeable due to the minor difference in performance output),

$$SNR_o = \frac{(N \cdot SNR_i)\,\Omega}{1 + N \cdot SNR_i\,(2 + N \cdot SNR_i)\,(1 - \Omega)}. \tag{4.41}$$

The approach used here alters the perturbed steering vector $\bar{\mathrm{d}}$ to reflect the effects induced by the use of the robust constraints.

Each element of the phase perturbed steering vector $\tilde{d}_k$ can be written as a function of the unperturbed steering vector element d_k with an error phase shift of Δp_k,

$$\tilde{d}_k = d_k e^{j\Delta p_k}, \tag{4.42}$$

$$= d_k\left[\cos\left(\Delta p_k\right) + j\sin\left(\Delta p_k\right)\right], \qquad k = 1, 2, \ldots, N. \tag{4.43}$$

The robust constraints result in the nulling of signal vector components which have been phase shifted by $\frac{\pi}{2}$ radians. It is this property that allows the robust constraints to prevent SINR degradation under the conditions of small phase errors. The phase shift in Eq. (4.43) is contained in the $j\sin\left(\Delta p_k\right)$ term and is eliminated from the perturbed signal when the robust constraints are employed. The robust form of the actual steering vector element then becomes,

$$\tilde{d}_{k,ROBUST} = d_k\cos\left(\Delta p_k\right) \qquad k = 1, 2, \ldots, N. \tag{4.44}$$

The steering vector $\tilde{\mathbf{d}}$ in Eq. (4.41) is required to have a norm of $\sqrt{N}$. The normalized version of robust steering vector is denoted by $\tilde{\mathbf{d}}_{ROBUST,NORM}$ and is given by,

$$\tilde{\mathbf{d}}_{ROBUST,NORM} = \frac{\sqrt{N}\tilde{\mathbf{d}}_{ROBUST}}{\|\tilde{\mathbf{d}}_{ROBUST}\|}. \tag{4.45}$$

The resulting SINR for use with the robust constraints then becomes,

$$SINR_{o,ROBUST} = \frac{(N \cdot SNR_i)\,\Omega_{ROBUST}}{1 + N \cdot SNR_i\,(2 + N \cdot SNR_i)\,(1 - \Omega_{ROBUST})}, \tag{4.46}$$

where,

$$\Omega_{ROBUST} \triangleq \left| \frac{\mathbf{d}^{\dagger}\tilde{\mathbf{d}}_{ROBUST,NORM}}{N} \right|^2. \tag{4.47}$$

4.6.2 Multiple Error Sources

The output SINR performance for multiple error sources using the robust constraints can be calculated by using a modified form of the original SINR performance equation given in Eq. (2.32),

$$SINR_o = \frac{(SNR_i)\,N}{1 + (SNR_i)^2\,N\,(N-1)\,\sigma_\Delta^2}. \tag{4.48}$$

The term σ_Δ^2 represents the variance of each independent and identically distributed (i.i.d) error vector element Δ_k. Thus,

$$\sigma_\Delta^2 = E\left[|\Delta_k - m_\Delta|^2\right], \tag{4.49}$$

$$= E\left[|\Delta_k|^2\right] - |m_\Delta|^2, \tag{4.50}$$

where m_Δ is the probability mean of Δ_k. The remainder of this section presents a derivation for σ_Δ^2.

As shown in Eq. (3.19), each phase perturbed steering vector element $\tilde{d}_k$ can be written as a phase shifted version of the unperturbed steering vector element

d_k,

$$\tilde{d}_k = d_k e^{j\Delta p_k}. \tag{4.51}$$

Use of the Maclaurin series expansion of $e^{j\Delta p_k}$ and dropping lower order terms under the small error approximation (i.e. $\frac{\Delta p_k{}^2}{2!} << 1$) leads to an the error vector element Δ_k which retains only its first order term,

$$\Delta_k \approx d_k (j\Delta p_k). \tag{4.52}$$

In Chapter 3, it was shown that the robust constraints null all components which are phase shifted by $\frac{\pi}{2}$ radians with respect to the steering vector element. As a result, the small errors in Eq. (4.52) are eliminated. At larger values of phase error, the second order term $\frac{\Delta p_k{}^2}{2!}$ of the Maclaurin series in Eq. (3.23) becomes significant. This term does not contain a $\frac{\pi}{2}$ phase shift and therefore is not nulled by the robust constraints. The second-order term is then the portion of the error that contributes to SINR degradation, assuming higher order terms are insignificant. The value of the term is given by,

$$\Delta_{k,ROBUST} = d_k \left(\frac{-\Delta p_k{}^2}{2} \right). \tag{4.53}$$

Since the magnitude of each steering vector component is unity, Eq. (2.6), the second moment of the robust error element is,

$$E\left[|\Delta_{k,ROBUST}|^2\right] = |d_k|^2 E\left[\left(\frac{-\Delta p_k{}^2}{2}\right)^2\right], \tag{4.54}$$

$$= \frac{1}{4} E\left(\Delta p_k{}^4\right). \tag{4.55}$$

The variance for the robust error is calculated from Eq. (4.50) as,

$$\sigma^2_{\Delta,ROBUST} = E\left[|\Delta_{k,ROBUST}|^2\right] - |m_{\Delta,ROBUST}|^2, \tag{4.56}$$

$$= \frac{1}{4} E\left(\Delta p_k{}^4\right) - |m_{\Delta,ROBUST}|^2, \tag{4.57}$$

where $m_{\Delta,ROBUST}$ is the mean for the robust error. Finally, the SINR which results when robust constraints are employed is calculated by substituting the robust error variance $\sigma^2_{\Delta,ROBUST}$ for the original error variance σ^2_{Δ} in Eq. (4.48). The result is,

$$SINR_{o,ROBUST} \approx \frac{(SNR_i)\,N}{1+(SNR_i)^2\,N\,(N-1)\,\sigma^2_{\Delta,ROBUST}}. \tag{4.58}$$

In summary, the same equation can be used to measure SINR performance with and without the addition of the robust constraints provided that the error variance is modified appropriately. The robust constraints have the effect of minimizing the error variance of a phase perturbed signal by removing the first order term from the Maclaurin expansion. The higher order terms still contribute to the error thereby contributing to SINR degradation.

4.7 SINR Improvement

For the case of small phase perturbations, the robust constraints provide near optimal SINR performance. At greater error values, however, less protection is provided. It is useful to quantify the level of phase perturbation at which performance achieved using the robust constraints begins to degrade significantly from ideal performance. Traditionally, the 3 dB point is used to characterize such a limit.

The point at which the SINR degrades by 3 dB with respect to the optimal processor is determined by examining the robust SINR performance in Eq. (4.58) as a function of phase perturbation. The value which produces half the optimal

level of $(SNR_i)\,N$ is,

$$\sigma^2_{\Delta,ROBUST} = \frac{1}{(SNR_i)^2\,N\,(N-1)}. \tag{4.59}$$

When the phase errors are uniformly distributed about zero with maximum and minimum phase radian values of ψ and $-\psi$, the robust variance $\sigma^2_{\Delta,ROBUST}$ using Eq. (4.57) is equal to $\frac{\psi^4}{45}$ (Appendix D). Substitution of this value into Eq. (4.59) yields the maximum perturbation which produces 3 dB of SINR degradation,

$$\frac{\psi^4_{3dB}}{45} = \frac{1}{(SNR_i)^2\,N\,(N-1)}, \tag{4.60}$$

$$\psi_{3dB} = \sqrt[4]{\frac{45}{(SNR_i)^2\,N\,(N-1)}}, \tag{4.61}$$

$$\psi_{3dB} = \sqrt[4]{\frac{45}{\eta}}. \tag{4.62}$$

In this expression, the variable η is defined as,

$$\eta \triangleq (SNR_i)^2\,N\,(N-1)\,. \tag{4.63}$$

When the robust constraints are not used, the 3 dB point is calculated from Eq. (2.33) using an error variance of $\sigma^2_\Delta = \frac{\psi^2}{3}$ (Appendix D),

$$\sigma^2_\Delta = \frac{1}{(SNR_i)^2\,N\,(N-1)}, \tag{4.64}$$

$$\frac{\psi^2_{3dB}}{3} = \frac{1}{(SNR_i)^2\,N\,(N-1)}, \tag{4.65}$$

$$\psi_{3dB} = \sqrt{\frac{3}{\eta}}. \tag{4.66}$$

As the amount of phase error increases past the 3 dB point, it is useful to note how much SINR improvement the robust constraints provide. A performance ratio γ_{SINR} is obtained by dividing the robust performance $SINR_{o,ROBUST}$ given in

Eq. (4.58) by the unprotected performance given in Eq. (2.32),

$$\gamma_{SINR} \triangleq \frac{SINR_{o,ROBUST}}{SINR_o}, \tag{4.67}$$

$$= \frac{1+(SNR_i)^2 N(N-1)\sigma_\Delta^2}{1+(SNR_i)^2 N(N-1)\sigma_{\Delta,ROBUST}^2}, \tag{4.68}$$

$$= \frac{1+\eta\sigma_\Delta^2}{1+\eta\sigma_{\Delta,ROBUST}^2}. \tag{4.69}$$

For those values of error which are significantly beyond both 3 dB points (i.e. $\eta\sigma_{\Delta,ROBUST}^2 \gg 1$ and $\eta\sigma_\Delta^2 \gg 1$), the improvement approaches a value given by,

$$\gamma_{SINR} = \frac{\sigma_\Delta^2}{\sigma_{\Delta,ROBUST}^2}, \tag{4.70}$$

$$= \frac{15}{\psi^2}, \tag{4.71}$$

where ψ is expressed in radians. Hence, the expected SINR improvement while using the robust constraints for relatively large phase errors (beyond the 3 dB point) can be calculated as a direct function of the maximum amount of phase error. Note that the improvement is independent of the SINR of the desired signal and the number of array elements.

4.8 Partially Adaptive Beamforming

Partially adaptive beamforming is a method of adding constraints for the purpose of reducing the number of computations required in generating the optimal weight vector [25,26]. Various approaches have been suggested as the basis for adding such constraints [27,28,29]. The robust constraints derived in this dissertation can be used in such a fashion. Approximately one half of the number of degrees of freedom in an array will be removed by this processor. Since these constraints

are linear, they can be used with other partially adaptive techniques to reduce the number of degrees of freedom even further.

4.9 Summary

In this chapter, various analyses of the robust constraints have been presented. First, the steering derivative constraint was shown to be a special case of the robust constraints. Application of a derivative constraint to each individual array element output was shown to be equivalent to applying the robust constraints. It was also shown that the robust constraints can be interpreted as phase constraints on the weight vector elements. Equivalently, only the magnitude of each complex weight vector element is allowed to adapt when robust constraints are employed. The phase of each weight vector element is constrained to match the phase of the corresponding element of the steering vector for the desired signal. Performance prediction equations were developed for two types of perturbation: those produced by a single parameter (such as steering error) and those which result from multiple, uncorrelated parameters (such as placement error). The 3 dB roll-off point and subsequent improvement beyond the 3 dB point were developed from these prediction equations for the case of random uniform phase distributions.

Chapter 5

Simulations and Experimental Results

This chapter presents the results of computer simulation experiments on minimum variance beamformers in the presence of phase perturbations. Comparisons were performed between the single steering constraint method and the new robust constraint method.

The first section describes simulations performed using the closed-form solution for various types of phase error. The second section presents results relating to the number of degrees of freedom available for the robust technique. Comparisons with theoretical performances levels calculated in Chapter 4 are given. The next section illustrates adaptive convergence of the modified GSC to the closed-form solution derived for the robust system. The final section illustrates the application of the robust constraints to actual array data obtained from a real environment.

Simulations comparing the robust method to previously discussed techniques are not presented due to the fact that substantially different modelling assumptions are used for these different methods. Noise injection and weight bounding, for example, require *a priori* knowledge of the input signal power and input jammer power to determine the optimal noise injection level and weight bound, respectively (the optimal levels can be calculated for a most one jammer). The robust constraints do not use *a priori* knowledge of the signal environment. As stated previously, the method of adding eigenvector null constraints is ineffective for small phase perturbations. The simulations presented in the following sections compare the robust constraint performance to the original single steering constraint method of minimum variance beamforming.

5.1 Small Phase Errors

Simulations were performed under four types of random phase anomalies: random phase errors, array element placement errors, steering errors, and frequency errors. All simulations used one of three different array geometries for array element placement. The first was a ten element linear array with half wavelength spacing between elements. Azimuthal angles were measured in a clockwise direction from broadside of the array. The second array was a two-dimensional, thirty-six element array consisting of three concentric rings, each containing twelve array elements (see Fig. 5.1). The radii for the rings were $\frac{\lambda}{2}$, λ, and $\frac{3\lambda}{2}$. The third array was a four element square configuration with $\frac{\lambda}{2}$ element spacing on each side. As with the linear array, all azimuth directions were measured clockwise from the y-axis. Elevations were measured upward from the plane containing the array elements.

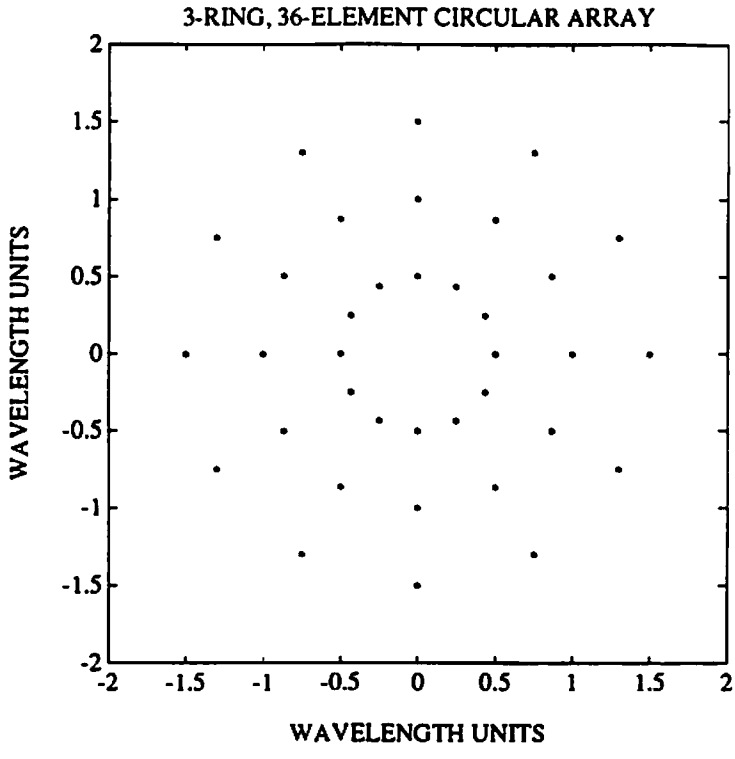

Figure 5.1: Geometry of 36 Element Circular Array

5.1.1 Channel Phase Errors

In a nonhomogeneous propagation medium, wavefront distortion of the desired signal can cause the signal's spatial propagation to deviate from that of an ideal plane wave. Calibration errors in the receiver can also cause phase errors [9]. Both types of phase errors were modeled as random phase shifts Δp_k from the nominal value at each array element. Thus,

$$\tilde{d}_k = e^{j\left(\frac{2\pi}{\lambda}\mathbf{a}_k^{\dagger}\mathbf{u}+\Delta p_k\right)}, \tag{5.1}$$

$$= e^{j\frac{2\pi}{\lambda}\mathbf{a}_k^{\dagger}\mathbf{u}}e^{j\Delta p_k}, \tag{5.2}$$

$$= d_k e^{j\Delta p_k}, \qquad k = 1, 2, \ldots, N, \tag{5.3}$$

where each random variable Δp_k had a specified probability distribution.

The output SINR results obtained for a random phase error simulation of the three-ring circular array are shown in Fig. 5.2. The probability density function for each random phase error Δp_k was uniform centered at the origin and independent from element to element. The abscissa represents the maximum value (denoted by ψ) of the uniform distribution. The signal environment consisted of a

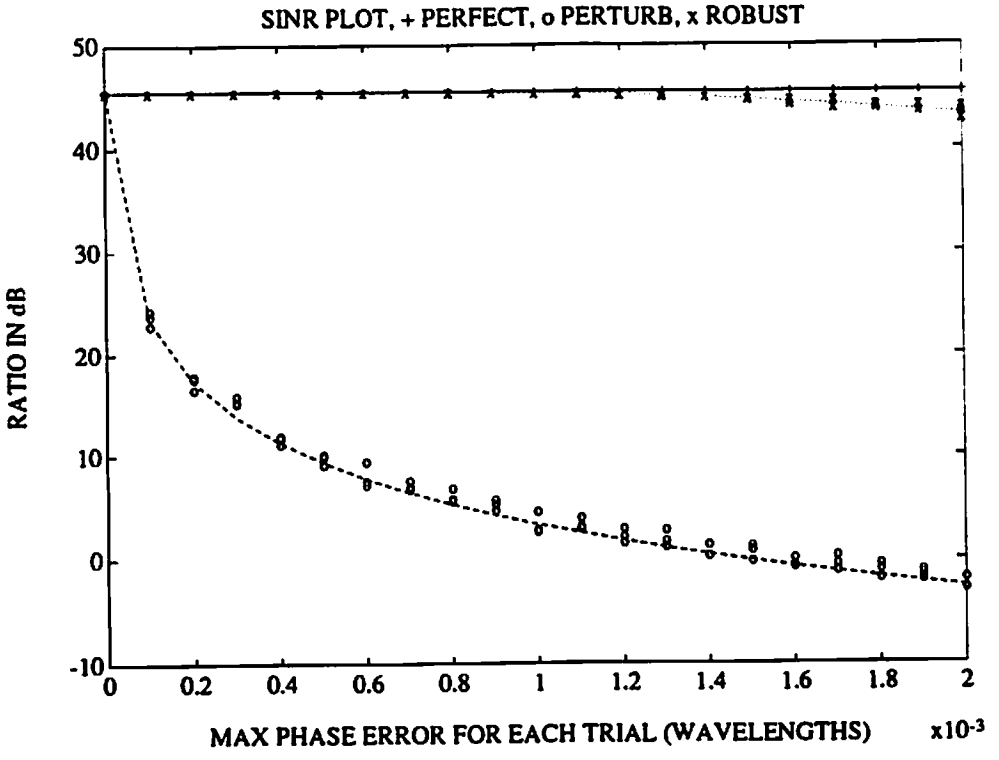

Figure 5.2: SINR Performance for Uniformly Distributed Phase Perturbations

narrowband desired signal and three narrowband jammers in a background of spatially white noise with signal parameters as shown in Table 5.1.

Jablon [16] observed that jammers do not significantly affect the output SINR performance of an array provided that enough degrees of freedom exist to null

Narrowband Signal Type	Azimuth (Degrees)	Elevation (Degrees)	Wavelength	SNR
Desired Signal	70	10	λ	30 dB
Jammer	-120	10	λ	40 dB
Jammer	0	10	λ	40 dB
Jammer	110	10	λ	40 dB

Table 5.1: Signal Parameters for Simulation in Fig. 5.2

these jammers. The experiments described here have verified that this is also the case for systems which use the robust constraints. In Fig. 5.2, the upper line indicates the ideal SINR performance of the original minimum variance beamformer with no phase perturbations. The symbol "o" shown in the figure represents SINR performance for random trials with phase perturbation. The degradation observed is consistent with that shown in Fig. 2.5. The symbol "x" represents the performance obtained from trials using the robust constraints. In all cases, three trials were performed at each perturbation value.

The dotted line that runs through the perturbed trials in Fig. 5.2 is the predicted performance from Eq. (2.32). This equation requires knowledge of the variance σ_Δ^2 of the random variables Δp_k. Since Δp_k was uniformly distributed about the origin, its variance was $\frac{\psi^2}{3}$ as shown in Appendix D.

The predicted performance for the robust technique is the line that runs through the "x" symbols in the graph. It was calculated using the robust prediction equation derived in Eq. (4.58). The robust variance $\sigma_{\Delta,ROBUST}^2$ was calculated using Eq. (4.57) to have a value of $\frac{\psi^4}{45}$ (see Appendix D).

Figure 5.2 shows that the robust method clearly outperforms the original single steering constraint technique. At small levels of perturbation, the performance

using the robust constraints was essentially equivalent to that of the unperturbed array. The performance of the original single steering constraint method degraded significantly, even for small values of phase error.

To examine the performance for relatively large phase errors, a simulation was extended to a maximum perturbation of $\psi = 0.05$ wavelengths. The desired signal and phase error had identical parameters to the previous simulation except that jammers were not present (see Table 5.2). The results, shown

Narrowband Signal Type	Azimuth (Degrees)	Elevation (Degrees)	Wavelength	SNR
Desired Signal	70	10	λ	30 dB

Table 5.2: Signal Parameters for Simulation in Fig. 5.3

in Fig. 5.3, demonstrated that robust constraints offered improved SINR performance for these cases, but that the improvement was not as dramatic as was the case for smaller errors. This reduction in performance occurs because deviations from the small phase error approximation (Fig. 3.3) cause the error vector elements Δ_k to have components which are no longer perpendicular to the desired signal steering vector elements d_k. Since only the perpendicular components are removed by using the robust constraints, the remaining non-perpendicular components contribute to SINR degradation. The dotted and dashed curves in this figure were computed using the same prediction formulas as used in Fig. 5.2. At the maximum error of 0.05λ, the ratio of SINR performance for the robust system to that for the single-constraint system was calculated to be 22 dB using Eq. (4.71). This value agrees well with the experimental results.

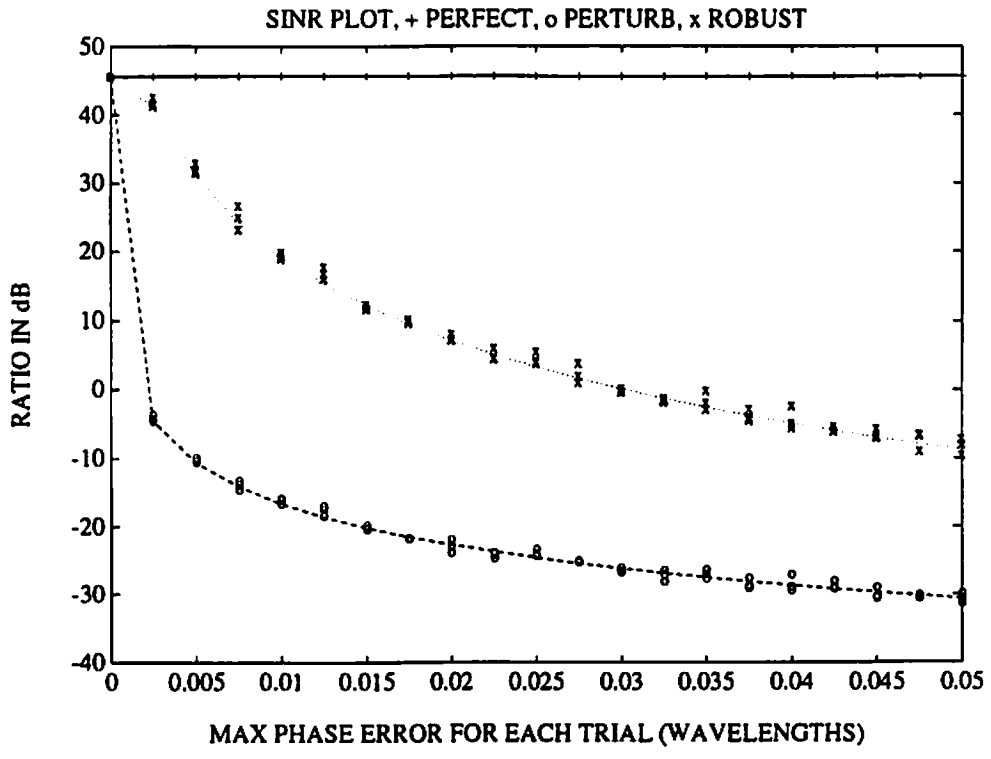

Figure 5.3: SINR Performance for Large Phase Error without Jammers Present

The second series of simulation experiments were conducted using the ten element linear array. The environment consisted of a narrowband signal in the presence of a single narrowband jammer with the parameters shown in Table 5.3. Fig. 5.4 shows the SINR degradation observed for this case. Theoretical predictions of performance also matched the simulation performance for this alternate array geometry case. At a given level of perturbation, the performance of the original and robust methods were superior to that observed in the previous simulation experiments. This difference is due to the fact that there were fewer array elements and that the input SNR was smaller. The prediction performance

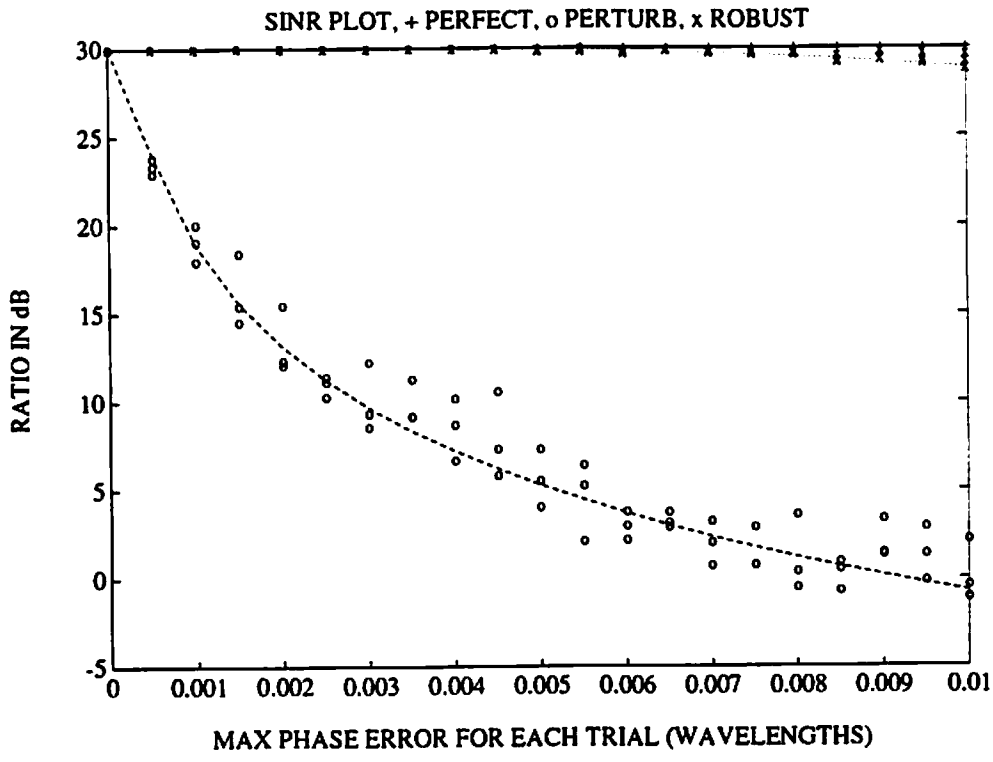

Figure 5.4: SINR Performance for the Ten Element Linear Array

results shown in Eqs. (2.32) and (4.58) indicate that a decrease of these two parameters induce in increase in output SINR.

5.1.2 Element Placement Errors

Phase errors in an array can also be caused by misplacement of the individual elements from their designed positions. The resulting altered propagation delays for the desired signal produces errors between the actual and predicted steering vectors of the desired signal. The nominal position for each array element relative to the origin was denoted by the vector $\mathbf{a}_k$ as defined in Eq. (2.1). Under conditions of array placement error, the actual perturbed location vector is denoted as

Narrowband Signal Type	Azimuth (Degrees)	Elevation (Degrees)	Wavelength	SNR
Desired Signal	30	0	λ	20 dB
Jammer	70	0	λ	20 dB

Table 5.3: Signal Parameters for Simulation in Fig. 5.4

$\bar{\mathbf{a}}_k$ and defined relative to the presumed location vector $\mathbf{a}_k$ as,

$$\bar{\mathbf{a}}_k \triangleq \mathbf{a}_k + \Delta\mathbf{a}_k, \tag{5.4}$$

where the error location vector $\Delta\mathbf{a}_k$ contains the relative Cartesian error values,

$$\Delta\mathbf{a}_k \triangleq \begin{bmatrix} \Delta a_{k,x} \\ \Delta a_{k,y} \\ \Delta a_{k,z} \end{bmatrix}, \qquad k = 1, 2, \ldots, N. \tag{5.5}$$

Substitution of Eq. (5.4) into the definition of the steering vector elements in Eq. (2.6) yields,

$$\begin{aligned} \tilde{d}_k &= e^{j\frac{2\pi}{\lambda}\bar{\mathbf{a}}_k{}^{\dagger}\mathbf{u}}, & (5.6)\\ &= e^{j\frac{2\pi}{\lambda}(\mathbf{a}_k+\Delta\mathbf{a}_k)^{\dagger}\mathbf{u}}, & (5.7)\\ &= e^{j\frac{2\pi}{\lambda}\mathbf{a}_k^{\dagger}\mathbf{u}} e^{j\frac{2\pi}{\lambda}\Delta\mathbf{a}_k^{\dagger}\mathbf{u}}, & (5.8)\\ &= d_k e^{j\frac{2\pi}{\lambda}\Delta\mathbf{a}_k^{\dagger}\mathbf{u}}. & (5.9) \end{aligned}$$

Hence, the term $e^{j\frac{2\pi}{\lambda}\Delta\mathbf{a}_k^{\dagger}\mathbf{u}}$ represents the phase shift of the predicted steering vector element d_k due to the placement error $\Delta\mathbf{a}_k$.

Simulation trials were performed in which the three error components $\Delta a_{k,x}$, $\Delta a_{k,y}$, and $\Delta a_{k,z}$ were generated as independent random variables with uniform distributions. The SINR performance for these experiments was computed as a

function of the maximum placement error of the array elements in a fashion similar to the results shown in the previous section. The thirty-six element circular array of Fig. 5.1 was used with one desired narrowband signal and one narrowband jammer with parameters shown in Table 5.4. The output SINR results

Narrowband Signal Type	Azimuth (Degrees)	Elevation (Degrees)	Wavelength	SNR
Desired Signal	45	20	λ	25 dB
Jammer	90	15	λ	30 dB

Table 5.4: Signal Parameters for Simulation in Fig. 5.5

are shown in Fig. 5.5. The predicted performance shown was computed using Eqs. (2.32) and (4.58) using the original error variance σ_Δ^2 and the robust error variance $\sigma_{\Delta,ROBUST}^2$ as calculated in Appendix D. The robust technique provided SINR performance near optimal levels for small perturbations (under 0.002 λ) and significant performance improvement at higher placement errors. Again, simulation results matched the theoretical predictions.

5.1.3 Steering Errors

The perturbed steering direction vector $\tilde{\mathbf{u}}$ is defined relative to the designed direction vector $\mathbf{u}$ in Eq. (2.2) by,

$$\tilde{\mathbf{u}} \triangleq \mathbf{u} + \Delta\mathbf{u}. \tag{5.10}$$

The perturbed steering vector element $\tilde{d}_k$ may be expressed as,

$$\tilde{d}_k = e^{j\frac{2\pi}{\lambda}\mathbf{a}_k^\dagger\tilde{\mathbf{u}}}, \tag{5.11}$$

$$= e^{j\frac{2\pi}{\lambda}\mathbf{a}_k^\dagger(\mathbf{u}+\Delta\mathbf{u})}, \tag{5.12}$$

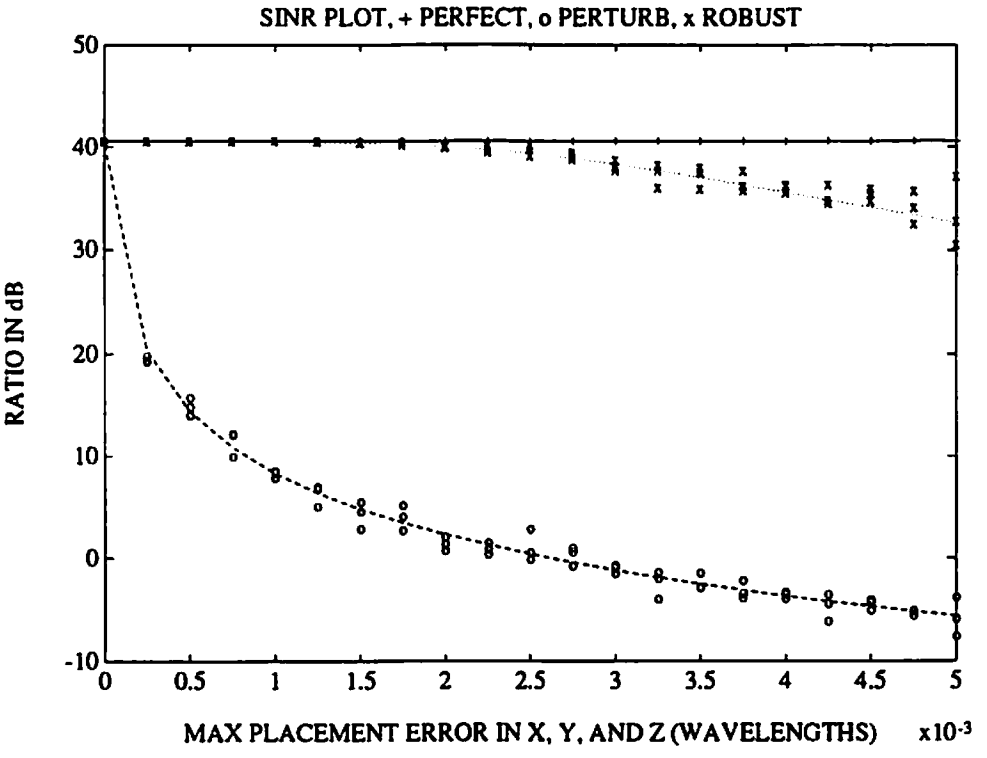

Figure 5.5: SINR Performance for Array Placement Errors

$$= e^{j\frac{2\pi}{\lambda}\mathbf{a}_k^\dagger \mathbf{u}} e^{j\frac{2\pi}{\lambda}\mathbf{a}_k^\dagger \Delta\mathbf{u}}, \tag{5.13}$$

$$= d_k e^{j\frac{2\pi}{\lambda}\mathbf{a}_k^\dagger \Delta\mathbf{u}}, \tag{5.14}$$

where the phase error in Eq. (5.14) is due to the term $e^{j\frac{2\pi}{\lambda}\mathbf{a}_k^\dagger \Delta\mathbf{u}}$.

Simulation experiments were performed with the desired narrowband signal changing arrival directions over azimuth errors as large as 0.1^o. The 36 element circular array was used with a desired narrowband signal and three narrowband jammers. The specific signal parameters used for these experiments are shown in Table 5.5. The simulations results and predicted performance curves are shown in Fig. 5.6 with the latter taken from Eqs. (2.30) and (4.46).

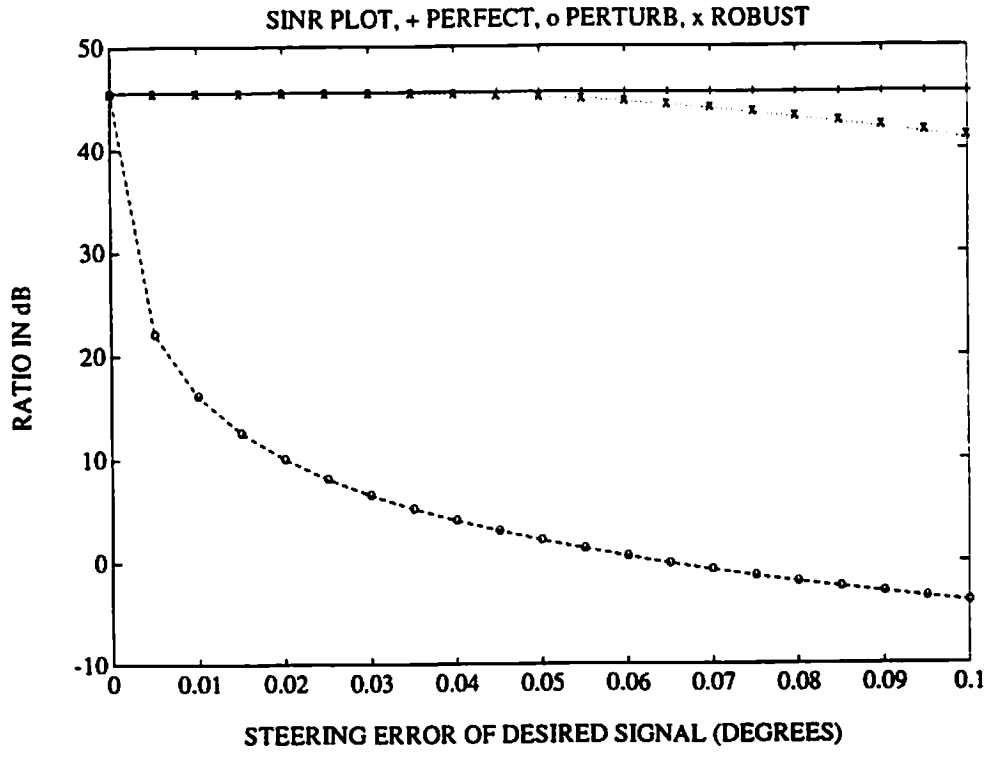

Figure 5.6: SINR Performance for Steering Errors

Although the SINR performance equation developed for the steering vector constraint system was generated for the case of a narrowband signal in spatially white noise, its predicted performance almost perfectly describes the results obtained with 3 jammers. This finding further supports the assumption that the presence of jammers does not significantly degrade SINR performance. As a result, these prediction equations can be effectively used in multiple jammer environments provided that the number of jammers is less than or equal to the number of degrees of freedom available.

For these experiments, the use of the robust constraints was observed to provide near perfect performance for steering errors less than 0.05°. In these same

Narrowband Signal Type	Azimuth (Degrees)	Elevation (Degrees)	Wavelength	SNR
Desired Signal	20	10	λ	30 dB
Jammer	-130	10	λ	40 dB
Jammer	-20	10	λ	40 dB
Jammer	70	10	λ	40 dB

Table 5.5: Signal Parameters for Simulation in Fig. 5.6

experiments, the single constraint method degraded the output SINR performance by over 40 dB. At levels greater than 0.05°, performance for the robust method degraded but was still superior to original minimum variance beamforming.

Comparisons were performed between the use of the robust constraints and the use of the steering derivative constraint in the presence of steering errors. Both methods provided similar output SINR performance. This is consistent with the analysis in Chapter 4 that shows that the steering constraint is a special case of the robust constraints.

5.1.4 Frequency Errors

An additional source of error in an array is caused by differences between the actual received desired signal frequency and that which was anticipated *a priori*. A perturbed frequency $\tilde{f}$ as a function of the nominal frequency value f,

$$\tilde{f} = f + \Delta f. \tag{5.15}$$

By noting the relationship between frequency f and wavelength λ of a signal,

$$f = \frac{c}{\lambda}, \tag{5.16}$$

where c is the speed of propagation, the steering vector element d_k for the desired signal is given by,

$$d_k = e^{j\frac{2\pi f}{c}\mathbf{a}_k^\dagger \mathbf{u}}. \tag{5.17}$$

The perturbed steering vector element $\tilde{d}_k$ due to frequency errors then becomes,

$$\begin{aligned}
\tilde{d}_k &= e^{j\frac{2\pi \tilde{f}}{c}\mathbf{a}_k^\dagger \mathbf{u}}, && (5.18)\\
&= e^{j\frac{2\pi (f+\Delta f)}{c}\mathbf{a}_k^\dagger \mathbf{u}}, && (5.19)\\
&= e^{j\frac{2\pi f}{c}\mathbf{a}_k^\dagger \mathbf{u}} e^{j\frac{2\pi \Delta f}{c}\mathbf{a}_k^\dagger \mathbf{u}}, && (5.20)\\
&= d_k e^{j\frac{2\pi \Delta f}{c}\mathbf{a}_k^\dagger \mathbf{u}}. && (5.21)
\end{aligned}$$

In this case, the phase shift error term is $e^{j\frac{2\pi \Delta f}{c}\mathbf{a}_k^\dagger \mathbf{u}}$. Eq. (5.21) can be expressed as a function of wavelength perturbation $\tilde{\lambda} \triangleq \lambda + \Delta\lambda$ by substituting wavelength values appropriately for the frequency values, i.e.,

$$\begin{aligned}
\Delta f &= \tilde{f} - f, && (5.22)\\
&= \frac{c}{\tilde{\lambda}} - \frac{c}{\lambda}, && (5.23)\\
&= \frac{c}{\lambda + \Delta\lambda} - \frac{c}{\lambda}, && (5.24)\\
&= \frac{-\Delta\lambda c}{\lambda(\lambda + \Delta\lambda)}. && (5.25)
\end{aligned}$$

A simulation was performed for a narrowband desired signal with wavelength errors of up to 1% using the signal parameters shown in Table 5.6. The 36

Narrowband Signal Type	Azimuth (Degrees)	Elevation (Degrees)	Wavelength	SNR
Desired Signal	60	10	λ	10 dB

Table 5.6: Signal Parameters for Simulation in Fig. 5.7

element circular array was used and results obtained are shown in Fig. 5.7. The

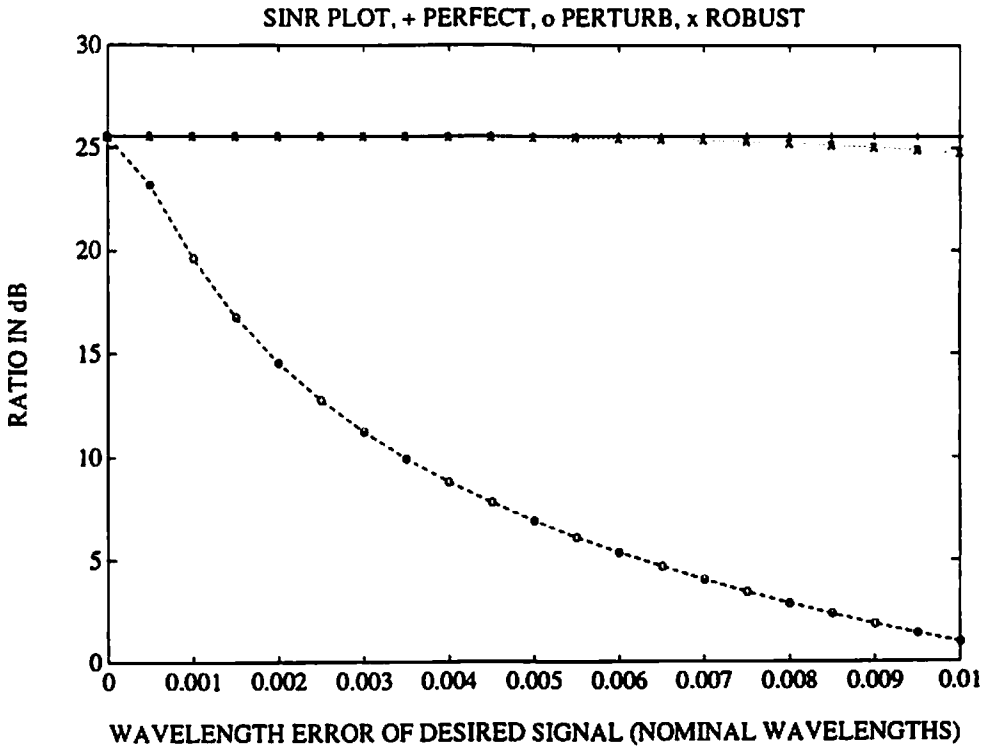

Figure 5.7: SINR Performance for Frequency Errors

robust technique provided excellent SINR protection up to an error of 0.005λ when it began to degrade. At that value, the original minimum variance beamformer had lost 20 dB in performance.

5.2 Effects of Numerous Jammers

In order to test the degrees of freedom available, the 36-element array was used with a 30 dB narrowband desired signal. In these experiments, the signal frequency was reduced by a factor of $\frac{5}{6}$ over that illustrated in Fig. 5.1. As a result, the outer radius of the array was 1.25λ rather than 1.5λ. Jammers with 40 dB

SNR were introduced from random arrival angles constrained to be outside the mainlobe of the quiescent beampattern. All signals were incident at an elevation of 10°. The array was randomly perturbed with uniform phase perturbations at each array element with a maximum perturbation of 0.025 wavelengths. Again, three types of SINR simulations were run and are shown in Fig. 5.8. The symbol "+" in the figure represents a trial in which the steering constraint was altered to match the perturbed steering vector $\tilde{\mathbf{d}}$ (i.e. the zero error case); the symbol "o" represents the performance of the perturbed array for trials with a single, unadjusted steering constraint; and the symbol "x" represents the performance of the perturbed array trials using robust constraints. The theoretical maxi-

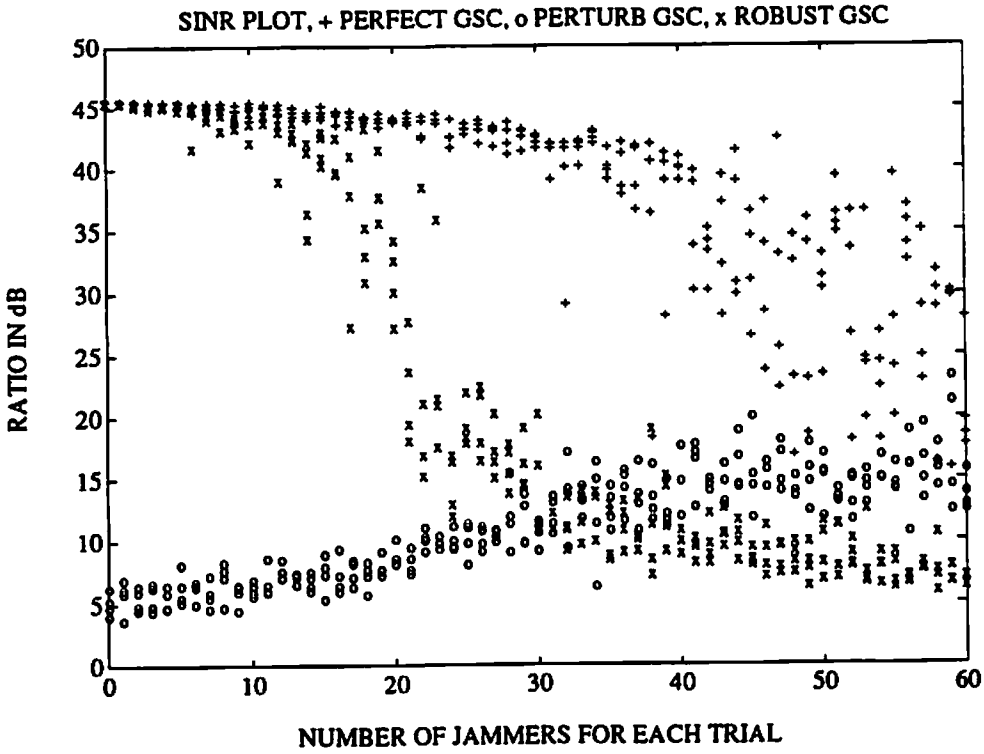

Figure 5.8: SINR as Function of Physical Element Perturbation

mum number of jammers that can be nulled by an array with a single steering constraint is $N-1$, or 35 for these experiments. Figure 5.8 shows that while some degradation in performance of the single-constraint system was observed above this number of jammers, several specific trials resulted in good performance even with more than 50 jammers present.

With the robust constraints, the maximum theoretical number of jammers is given by Eq. (4.40) as 17 jammers. The experiments indicate that the use of the robust constraints provided good performance for fewer than ten jammers and significant degradation for more than twenty jammers. This simulation confirms the theoretical findings in Chapter 4 that adding the robust constraints results in a loss of half the degrees of freedom.

This phenomena was due to linear dependencies. Since the jammers were randomly selected, some cases produced jammers which were nearly linear combinations of others. In such case, the minimum variance beamformer was still capable of nulling more than 35 jammers.

5.3 Robust Generalized Sidelobe Canceller

In this section, simulations are presented which illustrate the performance of the GSC in its original and modified robust form. The ten element linear array was used with uniform phase perturbations having a maximum deviation of 0.01λ. The normalized adaptive step size α for the iterative simulations was set to 0.001. This relatively small value for α was chosen to minimize misadjustment. The adaptive weight vectors $\mathbf{w}_a$ and $\mathbf{w}_{a,R}$ were initialized to zero values and the simulation was run for 25,000 iterations. The environment consisted of a single desired signal

with no jammers, as shown in Table 5.7. The SINR for the original and robust

Narrowband Signal Type	Azimuth (Degrees)	Elevation (Degrees)	Wavelength	SNR
Desired Signal	10	10	λ	20 dB

Table 5.7: Signal Parameters for Simulation in Fig. 5.9

methods are shown for a single experiment in Fig. 5.9. The horizontal dotted

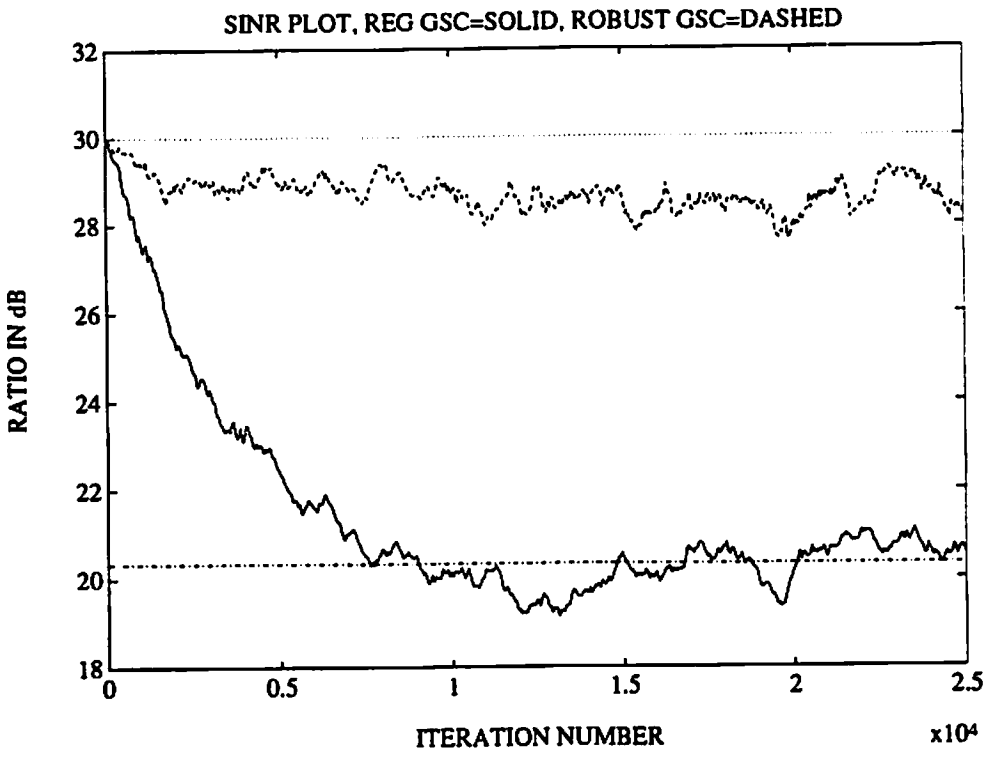

Figure 5.9: SINR Performance Comparison Between the Original GSC and the Modified GSC with Robust Constraints

line at 30 dB represents the closed-form predicted robust performance as given in Eq. (4.58). The horizontal dotted-dashed line at 20.3 dB represents the predicted performance for the single constraint system as given in Eq. (2.32).

The original GSC decayed to predicted levels after 10,000 iterations while the robust GSC stayed between 1 and 2 dB below its closed-form predicted performance mark. This latter discrepancy is due to the misadjustment within the LMS algorithm which is known to cause imperfections between ideal and actual results [13]. The misadjustment can be decreased be choosing a smaller step size α at the cost of increasing the time necessary for the GSC to adapt to a changing signal environment.

Fig. 5.10 shows the noise powers of the iterative and robust systems for the simulation in Fig. 5.9. The original complex GSC shows a significant increase in

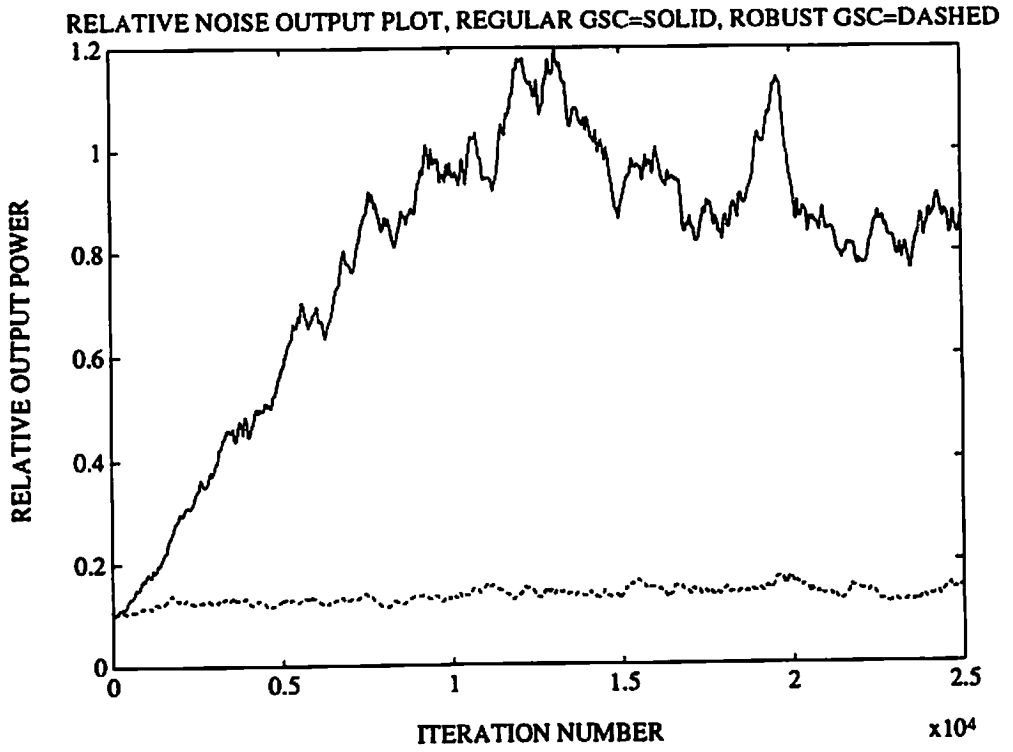

Figure 5.10: Noise Performance Comparison Between the Original GSC and the Modified GSC with Robust Constraints

noise power while the robust GSC remains relatively constant. This is consistent with the discussion presented in Chapter 3.

A second simulation was conducted to illustrate the performance for the the case of a narrowband desired signal in the presence of a narrowband jammer and spatially white noise (Table 5.8 details the signal parameters). The four element square array described earlier was used with a steering error of 5°. The SINR

Narrowband Signal Type	Azimuth (Degrees)	Elevation (Degrees)	Wavelength	SNR
Desired Signal	0	0	λ	30 dB
Jammer	30	0	λ	30 dB

Table 5.8: Signal Parameters for Simulation in Fig. 5.11

performance results obtained for 100,000 iterations with the updating factor α set to 0.0025 are shown in Fig. 5.11. The closed-form predicted performance levels are indicated by horizontal lines for the original single constraint method, robust method, and the error-free (calibrated) system. Note that the SINR for the robust method was significantly below the SINR of the calibrated method. This was due to the relatively large amount of perturbation that, in fact, violates the small phase error assumption in the robust analysis of Chapter 4. The iterations for both the robust method and the original method converged to their respective predicted values.

The poor performance of the original GSC was accompanied by a corresponding increase of the output noise power as shown in Fig. 5.12. The noise power of the robust method quickly leveled off while the noise power of the original GSC continued to increase. Both methods, however, effectively nulled the jammer.

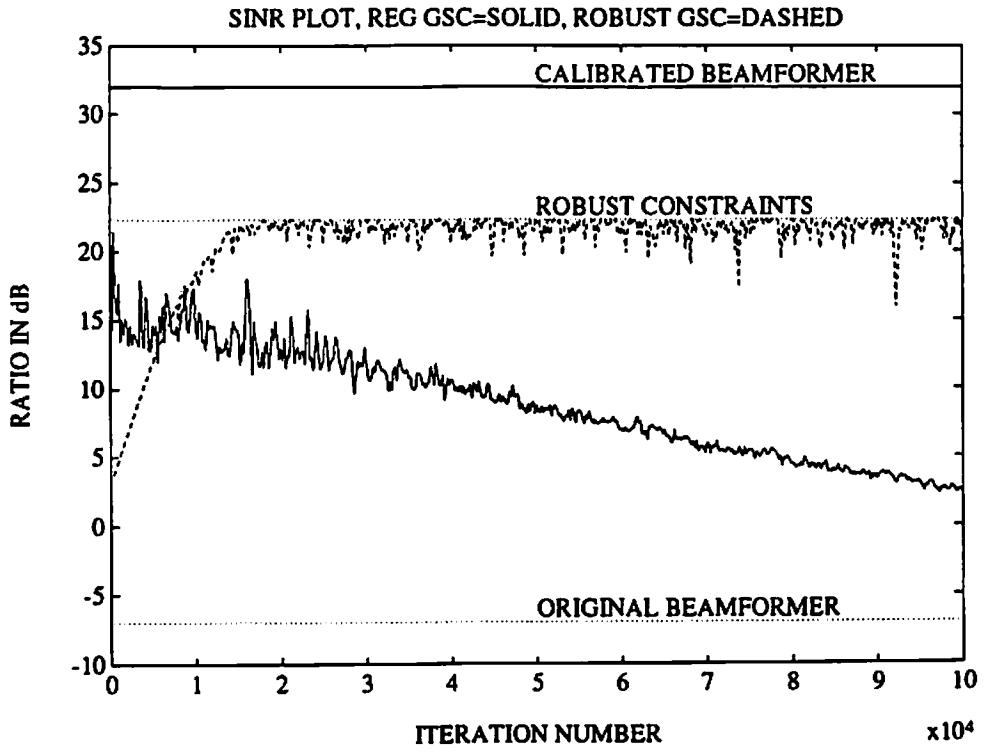

Figure 5.11: SINR Performance Comparison Between the Original GSC and the Modified GSC with Robust Constraints and One Jammer

This result is illustrated in Fig. 5.13. Although the output jammer power decreased for the original GSC, its output SINR also decreased during this interval as shown in Fig. 5.11. A decrease in the jammer output power normally results in an increase in output SINR. However, in this case, the increase in output noise power more than compensated for the decrease in jammer power.

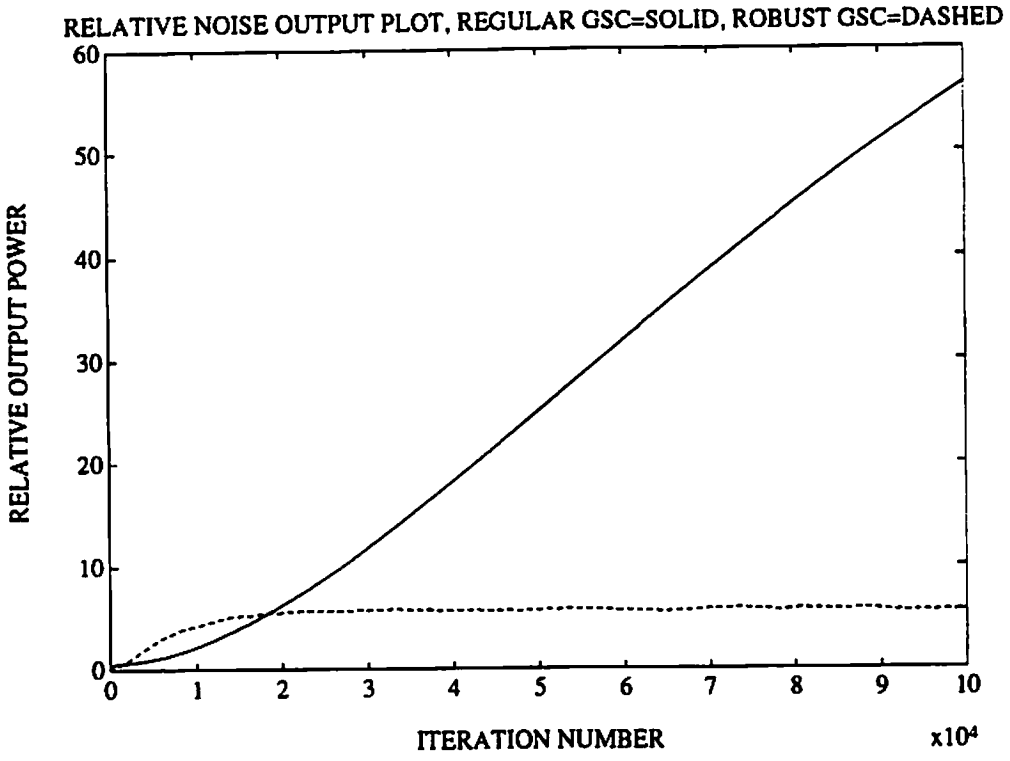

Figure 5.12: Noise Performance Comparison Between the Original GSC and the Modified GSC with Robust Constraints and One Jammer

5.4 Experimental Data Results

Experimental data from a RF linear array[1] was used to compare the original minimum variance beamformer and the new robust approach. The array consisted of thirty-six vertical whip antennas spaced at intervals of twenty meters for a total aperture of 700 meters. A narrowband signal was present at 7.335 MHz at an azimuth of $-6°$ relative to broadside. The signal was quadrature down-converted to 2 KHz and sampled at a rate of 10 KHz to generate 256 complex samples for each array element [30].

[1]Array data was generated and supplied courtesy of the Rome Air Development Center

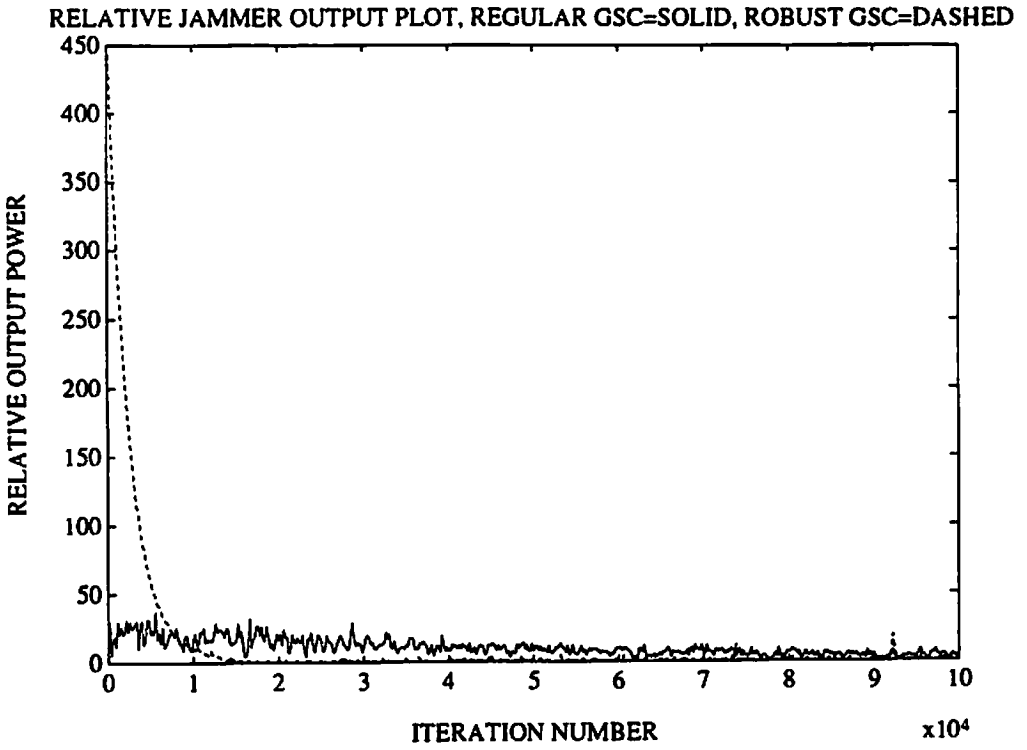

Figure 5.13: Jammer Performance Comparison Between the Original GSC and the Modified GSC with Robust Constraints

The Discrete Fourier Transform (DFT) was taken of each time series to examine the phase properties of the desired signal. Bin 52 of the DFT contained the majority of the energy for the desired signal. Since the array was linear, the phase of Bin 52 should have increased linearly for each array element. However, in the majority of the array elements, the observed phase did not closely fit this linear model, hence, their errors did not qualify as small phase anomalies. Nine of the array elements with the best linear phase properties were chosen for experimental use. The specific selections were element numbers 2, 5, 7, 8, 10, 12, 27, 34, and 35. The outputs of these nine complex data channels were individually magnitude scaled and used to form into data vectors $\mathbf{x}(n)$ for $n = 1, 2, \ldots, 256$. Constant

magnitude scaling was performed on each data stream to ensure that the diagonal elements of the estimated correlation matrix $\hat{\mathbf{R}}_{xx}$ had equal values. Scaling in this manner represents a first order attempt at minimizing the amplitude error between array elements. This matrix was formed as,

$$\hat{\mathbf{R}}_{xx} = \frac{1}{256} \sum_{n=1}^{256} \mathbf{x}(n)\, \mathbf{x}^{\dagger}(n). \tag{5.26}$$

The weights $\mathbf{w}_{opt\,ORIGINAL}$ and $\mathbf{w}_{opt\,ROBUST}$ were generated from Eqs. (2.18) and (3.61), respectively, using the estimated correlation matrix $\hat{\mathbf{R}}_{xx}$. The respective output data streams $y_{ORIGINAL}(n)$ and $y_{ROBUST}(n)$ were then generated over the same data series using the computed weight vector. Figures 5.14 and 5.15 show the magnitudes of the DFT's of the time series data $y_{ORIGINAL}(n)$ and $y_{ROBUST}(n)$.

A strong spectral peak from the narrowband signal was observed for the robust method at Bin 52, as expected. The single steering constraint method both strongly attenuated this signal peak and increased the background noise level.

A conventional beamformer that used the quiescent weight vector $\mathbf{w}_q$ to generate its output was also examined. This non-adaptive weight system provides optimal performance under conditions of a spatially white noise background and no perturbation errors. Its performance is relatively unaffected by small phase errors and it therefore offers a reasonable upper bound for SINR comparisons in a spatially white noise environment. Since the signal is approximately narrowband, its power was calculated as the square of the magnitude of the DFT of the signal at Bin 52. The noise power was calculated using an average over bins 100 to 200, inclusive, representing a spectral region well outside that of the desired signal. The output SINR was calculated as signal power divided by total noise

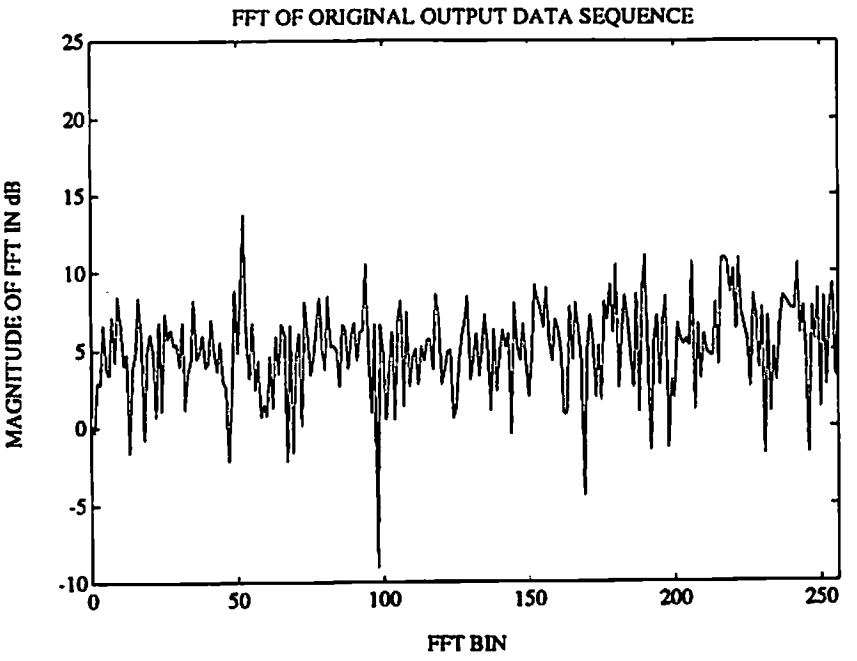

Figure 5.14: DFT of Output of Traditional Minimum Variance Beamformer with a Single Steering Constraint

power over all frequency bins. Table 5.9 shows the results obtained for the three beamformers examined in this study.

Weight Vector	Signal Power	Average Noise Power/Bin	SNR Estimate
$\mathbf{w}_q$	55,980	0.2520	29.38 dB
$\mathbf{w}_{opt,ORIGINAL}$	574.3	9.613	-6.320 dB
$\mathbf{w}_{opt,ROBUST}$	52,910	2.752	18.76 dB

Table 5.9: Comparative Performances for Different Weight Vectors

The robust constraints provided over 25 dB SINR improvement compared to the original single steering constraint system. It falls 10 dB below that of the

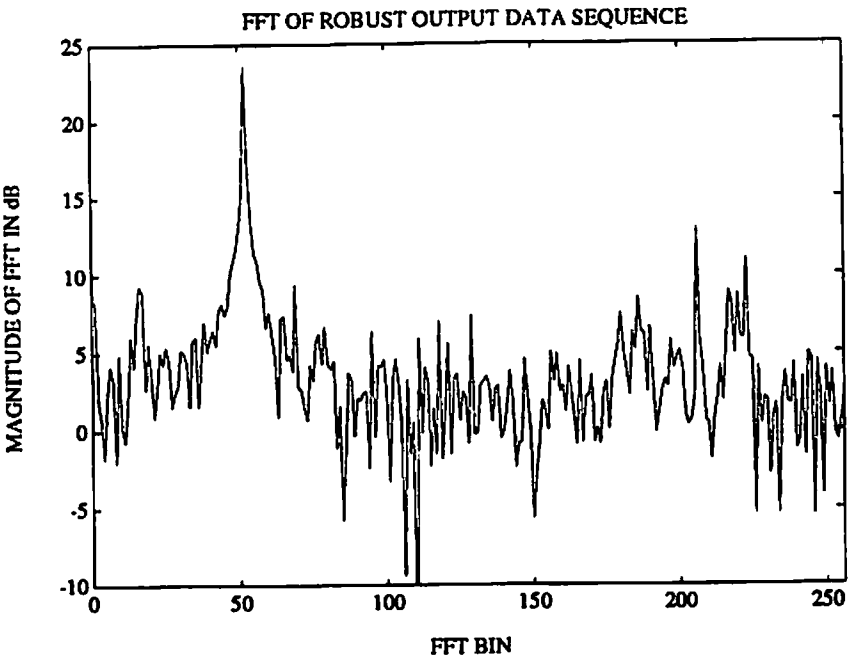

Figure 5.15: DFT of Output of Traditional Minimum Variance Beamformer with the Addition of Robust Constraints

output SINR achieved with $\mathbf{w}_q$. This is likely due to the presence of uncompensated amplitude errors and estimation errors induced by using a sample correlation matrix $\hat{\mathbf{R}}_{xx}$ instead of the the true correlation matrix $\mathbf{R}_{xx}$. It should also be noted that the presence of a strong jammer in the data would have substantially degraded the performance of the quiescent beamformer. The robust system, however, would have remained relatively unaffected.

5.5 Summary

Experimental results have been presented in which small phase errors were introduced by randomly changing the incoming phase of the signal at each array

element input, perturbing the location of each array element, applying a steering constraint that was perturbed in azimuth, and applying a steering constraint that was perturbed in frequency. In all cases studied, degraded performance was observed as the amount of perturbation increased. The performance prediction equations developed in Chapter 4 for the robust method proved accurate under all simulations. A simulation that increased the number of jammers confirmed that the number of degrees of freedom available is approximately halved when robust constraints are used. Simulations with the robust form of the Generalized Sidelobe Canceller demonstrated performance improvement over the original structure using iterative computation of the optimal weight vector from synthesized data. Actual RF array data of a narrowband signal was also used to demonstrate robust effectiveness. More than 25 dB gain in SINR over the original minimum variance approach was achieved with the addition of the robust constraints.

Chapter 6

Conclusion

6.1 Review

In unperturbed environments, linearly-constrained minimum variance beamforming provides a means of receiving a signal of interest in the presence of unwanted jammers. Unfortunately, when the input SNR is high, the existence of small phase errors seriously degrades the SINR performance of the system. The robust constraints developed in this dissertation have been definitively shown to prevent SINR degradation in such cases. This is an important contribution because precise phase calibration is more difficult than is accurate amplitude calibration in most practical applications.

The robust constraint approach was developed from two seemingly different points of view. The first involved a detailed examination of the signal output power observed in a minimum variance beamformer while the second arose from

the direct application of derivative constraints to the output of each individual array element. Both methods, however, directly constrained the adaptive processor from reducing the desired signal output power under phase perturbed conditions.

It is somewhat surprising that the technique of applying derivative constraints to each element had not previously been attempted. One possible explanation is that only complex linear constraints had been examined. Individual complex constraints would lead to an over-constrained problem with an inconsistent set of complex linear equations. This is due, in part, to that fact that the familiar complex linear form of the derivative constraint is a sufficient but not necessary condition. The new robust constraints represent both sufficient and necessary conditions and require approximately half the number of complex degrees of freedom.

In this dissertation, it was shown that the technique of applying null linear constraints to subspaces as an approach to combatting perturbations effects is ineffective for the case of small random phase errors since these errors have no preferred complex subspace. A key contribution to this thesis, however, is the definition of robust null linear constraints that are applied after the complex signal is restructured into the real domain.

Not surprisingly, closed-form and iterative techniques for deriving optimal weight vectors in the real domain (with the addition of robust constraints) have a parallel form to traditional methods derived in the complex domain. By carefully analyzing the output of the complex form of the GSC, a similar real form was implemented using the robust constraints.

It was shown that the robust constraints can also be interpreted as phase constraints on the complex weight vector elements. As a result, use of this technique

restricts the complex phase of the weight vector elements and allows only their magnitudes to adapt.

Equations were developed that predict SINR performance when the robust constraints are employed. By comparing their results with the equations for the single constraint adaptive beamformer, improvement values can be calculated for any given array environment.

The robust constraint procedure was shown to provide SINR performance improvement in both computer simulation experiments and with the use of actual RF array data. The experimental performance observed was consistent with theoretical predictions in both cases.

6.2 Areas for Future Research

Direction of Arrival Estimation

The technique of minimum variance beamforming has been used for direction of arrival (DOA) estimation. An analogous method using the addition of the robust constraints may provide DOA estimates in the presence of array phase anomalies. The cost trade-off of using such a technique can be compared to the cost of losing approximately half the degrees of freedom as described in Chapter 4. One consideration is that since the robust constraints inherently protect against steering errors, resolution will be lost in the DOA estimation of incoming signals.

Use of an Estimated Correlation Matrix

An estimated correlation matrix can be used in the closed-form solutions for the robust algorithm. The predicted performance of using such an estimate is unknown and would provide valuable information on the number of samples required for adequate performance in a perturbed environment.

Hybrid Techniques

The robust constraints developed in this dissertation protect SNR against small phase errors but do not protect against amplitude errors. Possible combinations of these constraints with previously developed robust techniques (noise injection, weight bounding, etc.) may prove fruitful under other types of perturbation.

Appendix A

Subspace Result with Small Phase Perturbations

This Appendix presents an analysis which demonstrates that the space formed from all combinations of steering vectors having small phase errors produced by independent and identically distributed (i.i.d), zero-mean, symmetrically distributed random variables has no preferred subspace.

Given $\mathbf{d}(\Theta_0, \Phi_0, \mathbf{p})$ is the steering vector for a signal from azimuth and elevation direction Θ_0, Φ_0 with an array perturbed by the vector $\mathbf{p}$ where,

$$\mathbf{p} \triangleq \begin{bmatrix} p_1 \\ p_2 \\ p_3 \\ \vdots \\ p_N \end{bmatrix}, \tag{A.1}$$

and each p_k is the phase perturbation value for element k. The probability density function of the phase errors of all N array elements is defined as $p(\mathbf{p})$. The

correlation matrix formed as an integral over all possible steering vectors due to perturbations is,

$$\mathbf{Q} = \int_{\mathbf{p}} \cdots \int p(\mathbf{p})\, \mathbf{d}(\Theta_0, \Phi_0, \mathbf{p}) \mathbf{d}^{\dagger}(\Theta_0, \Phi_0, \mathbf{p}) d\mathbf{p}. \tag{A.2}$$

Looking at the (i,j) element of the matrix $\mathbf{Q}$ yields,

$$[\mathbf{Q}]_{ij} = \int_{\mathbf{p}} \cdots \int p(\mathbf{p})\, d_i(\Theta_0, \Phi_0, p_i) d_j^*(\Theta_0, \Phi_0, p_j) d\mathbf{p}. \tag{A.3}$$

The probability densities being i.i.d. yields,

$$p(\mathbf{p}) = \prod_{k=1}^{N} p(p_k). \tag{A.4}$$

Substituting Eq. (A.4) into Eq. (A.3) for the case $i \neq j$ yields,

$$[\mathbf{Q}]_{ij} = \int p(p_i)\, d_i(\Theta_0, \Phi_0, p_i) dp_i \int p(p_j)\, d_j^*(\Theta_0, \Phi_0, p_j) dp_j \prod_{k \neq i,j} \int p(p_k)\, dp_k, \tag{A.5}$$

$$= m\left(d_i(\Theta_0, \Phi_0, p_i)\right) m\left(d_j^*(\Theta_0, \Phi_0, p_j)\right), \tag{A.6}$$

where $m(\cdot)$ represents the probability mean.

The next part will show that for small phase perturbations, the mean of the steering vector equals the unperturbed steering vector. Due to a phase error of p_i radians, the perturbed steering vector element can be represented as a phase shifted version of the unperturbed steering vector element,

$$d_i(\Theta_0, \Phi_0, p_i) = d_i(\Theta_0, \Phi_0, p_i = 0)\, e^{jp_i}, \tag{A.7}$$

where $d_i(\Theta_0, \Phi_0, p_i = 0)$ is notation for the unperturbed steering vector element. Expanding the exponential term using the Maclaurin series yields,

$$d_i(\Theta_0, \Phi_0, p_i) = d_i(\Theta_0, \Phi_0, p_i = 0) \left(1 + jp_i + \frac{(jp_i)^2}{2!} + \ldots\right). \tag{A.8}$$

For *small* errors (i.e. $|\frac{(jp_i)^2}{2!}| << 1$), the second and higher order terms are insignificant and can be ignored,

$$d_i(\Theta_0, \Phi_0, p_i) \approx d_i\left(\Theta_0, \Phi_0, p_i = 0\right)(1 + jp_i)\,. \tag{A.9}$$

Examining the mean of the steering vector element over the probability space of all possible errors and noting that $p_{i,max}$ represents maximum perturbed deviation yields,

$$m\left(d_i(\Theta_0, \Phi_0, p_i)\right) \triangleq \int_{-p_{i,max}}^{p_{i,max}} p\left(p_i\right) d_i(\Theta_0, \Phi_0, p_i) dp_i. \tag{A.10}$$

Substituting Eq. (A.9) into Eq. (A.10) yields,

$$\begin{aligned}
&m\left(d_i(\Theta_0, \Phi_0, p_i)\right) \\
&\quad = \int_{-p_{i,max}}^{p_{i,max}} p\left(p_i\right) d_i\left(\Theta_0, \Phi_0, p_i = 0\right)(1 + jp_i)\, dp_i, && \text{(A.11)} \\
&\quad = d_i\left(\Theta_0, \Phi_0, p_i = 0\right)\left(\int_{-p_{i,max}}^{p_{i,max}} p\left(p_i\right) dp_i + \int_{-p_{i,max}}^{p_{i,max}} p\left(p_i\right) jp_i dp_i\right), && \text{(A.12)} \\
&\quad = d_i\left(\Theta_0, \Phi_0, p_i = 0\right)\left(1 + \int_{-p_{i,max}}^{0} p\left(p_i\right) jp_i dp_i + \int_{0}^{p_{i,max}} p\left(p_i\right) jp_i dp_i\right). && \text{(A.13)}
\end{aligned}$$

By substituting $-p_i$ for p_i in the first integral and noting that the probability density function is symmetric (i.e. $p\left(p_i\right) = p\left(-p_i\right)$) yields,

$$\begin{aligned}
&m\left(d_i(\Theta_0, \Phi_0, p_i)\right) \\
&\quad = d_i\left(\Theta_0, \Phi_0, p_i = 0\right)\left(1 - \int_{0}^{p_{i,max}} p\left(p_i\right) jp_i dp_i + \int_{0}^{p_{i,max}} p\left(p_i\right) jp_i dp_i\right), && \text{(A.14)} \\
&\quad = d_i\left(\Theta_0, \Phi_0, p_i = 0\right)(1 - 0), && \text{(A.15)} \\
&\quad = d_i\left(\Theta_0, \Phi_0, p_i = 0\right). && \text{(A.16)}
\end{aligned}$$

Substitution into Eq. (A.6) yields the correlation matrix elements for the non-diagonal terms,

$$[\mathbf{Q}]_{ij} = d_i\left(\Theta_0, \Phi_0, p_i = 0\right) d_j^*\left(\Theta_0, \Phi_0, p_j = 0\right) \quad for \quad i \neq j. \tag{A.17}$$

For the diagonal terms of the correlation matrix $\mathbf{Q}$ (i.e. $i = j$) Eq. (A.3) becomes,

$$[\mathbf{Q}]_{ii} = \int p(p_i)\, d_i(\Theta_0, \Phi_0, p_i) d_i^*(\Theta_0, \Phi_0, p_i) dp_i \prod_{k \neq i} \int p(p_k)\, dp_k, \quad \text{(A.18)}$$

$$= E\left[|d_i(\Theta_0, \Phi_0, p_i)|^2\right], \quad \text{(A.19)}$$

$$= var\left(d_i(\Theta_0, \Phi_0, p_i)\right) + m\left(d_i(\Theta_0, \Phi_0, p_i)\right)^2, \quad \text{(A.20)}$$

$$= var\left(d_i(\Theta_0, \Phi_0, p_i)\right) + |d_i(\Theta_0, \Phi_0, p_i = 0)|^2. \quad \text{(A.21)}$$

By noting that the power to each element is equal,

$$|d_i(\Theta_0, \Phi_0, p_i = 0)|^2 = |d_j(\Theta_0, \Phi_0, p_j = 0)|^2 \quad \forall i, j, \quad \text{(A.22)}$$

and representing Eq. (A.17) and Eq. (A.21) in matrix notation yields,

$$\mathbf{Q} = \mathbf{d}(\Theta_0, \Phi_0, \mathbf{p} = 0)\, \mathbf{d}^\dagger(\Theta_0, \Phi_0, \mathbf{p} = 0) + var\left(d_i(\Theta_0, \Phi_0, p_i = 0)\right) \mathbf{I}. \quad \text{(A.23)}$$

Equation (A.23) represents the sum of the correlation matrix for the unperturbed signal with the addition of a scaled identity matrix.

Appendix B

Biasing the Error Term

One possible approach to imposing the inequality in the constraint of Eq. (3.18) is to constrain the error scalar Δp_k to be non-negative. This would have the potential benefit of producing a larger feasible solution space for the weight vector $\mathbf{w}$. This Appendix shows that attempting to enlarge the constraint region in this fashion does not achieve the desired result. However, the topic needs to be addressed to ensure that no other methods exist to enlarge the feasible solution space.

The non-negative constraint can be achieved by *biasing* the desired steering vector element to the edge of all possible perturbed steering elements. Hence,

$$\hat{\mathbf{d}} = \mathbf{d} - \boldsymbol{\Delta}_{\mathbf{max}}, \tag{B.1}$$

where $\boldsymbol{\Delta}_{\mathbf{max}}$ is a vector whose elements contain the maximum error under the small perturbation assumption. This has the effect of forcing Δp_k in Eq. (3.25) to be strictly positive. Applying algebra to Eq. (3.25) yields,

$$d_k = \frac{1}{\Delta p_k} \Delta_k e^{-j\frac{\pi}{2}}, \tag{B.2}$$

where Δ_k is the error for each element assumed under the small phase approximation. Expanding the steering vector constraint into its terms yields,

$$\sum_{k=1}^{N} d_k^* w_k = 1. \tag{B.3}$$

Substitution into Eq. (B.2) renders,

$$e^{-j\frac{\pi}{2}} \sum_{k=1}^{N} \frac{1}{\Delta p_k} \Delta_k^* w_k = 1. \tag{B.4}$$

The $\frac{\pi}{2}$ phase shift implies that the real part of the summation is zero,

$$\Re\left(\sum_{k=1}^{N} \frac{1}{\Delta p_k} \Delta_k^* w_k \right) = 0. \tag{B.5}$$

Note that each term $\Delta_k^* w_k$ is constrained to be greater than or equal to zero from Eq. (3.18). Also, each Δp_k is greater than zero due to biasing. The fact that each term is greater than or equal to zero and the sum is equal to zero implies that each term must be strictly equal to zero, hence,

$$\Re\left(\Delta_k^* w_k\right) = 0, \tag{B.6}$$

which is identical to Eq. (3.29). So even using the biased-error method to implement the inequality constraints on the weight elements still results in the same equality constraints as derived in Chapter 3.

Appendix C

Complex to Real Restructuring

This appendix justifies the complex to real transformation of the matrices used in Chapter 3. The object of the first section is to show that using transformed matrices to solve the linearly-constrained power minimization problem is equivalent to using the original complex form of the matrices. The second section shows how the GSC structure can be altered to accommodate the real transformation.

C.1 Linearly Constrained Power Minimization Equivalence

The transformation is defined as follows. Each of the matrices and vectors of interest can be broken down into their real and complex component vectors, noted with subscripts "r" and "i", respectively,

$$\mathbf{w} = \mathbf{w}_r + j\mathbf{w}_i, \tag{C.1}$$

$$\mathbf{d} = \mathbf{d}_r + j\mathbf{d}_i, \tag{C.2}$$

$$\mathbf{R}_{xx} = \mathbf{R}_{xxr} + j\mathbf{R}_{xxi}, \tag{C.3}$$

$$f = f_r + jf_i. \tag{C.4}$$

The real transformed versions of these matrices are denoted with the subscript R and defined in Eqs. (3.37) through (3.40) and repeated here,

$$\mathbf{w}_R \triangleq \begin{bmatrix} \mathbf{w}_r \\ \mathbf{w}_i \end{bmatrix}, \tag{C.5}$$

$$\mathbf{D}_R \triangleq \begin{bmatrix} \mathbf{d}_r & -\mathbf{d}_i \\ \mathbf{d}_i & \mathbf{d}_r \end{bmatrix}, \tag{C.6}$$

$$\mathbf{R}_{xxR} \triangleq \begin{bmatrix} \mathbf{R}_{xxr} & -\mathbf{R}_{xxi} \\ \mathbf{R}_{xxi} & \mathbf{R}_{xxr} \end{bmatrix}, \tag{C.7}$$

$$\mathbf{f}_R \triangleq \begin{bmatrix} f_r \\ f_i \end{bmatrix}. \tag{C.8}$$

The legitimacy of using this transformation in the minimum variance beamforming problem is verified below.

The linearly-constrained power minimization equation was given in Eq. (2.22) and is repeated here,

$$\min_{\mathbf{w}} \mathbf{w}^\dagger \mathbf{R}_{xx} \mathbf{w} \quad \textit{subject to} \quad \mathbf{d}^\dagger \mathbf{w} = f, \tag{C.9}$$

where $f = 1$. The object is to show that the problem in Eq. (C.9) is equivalent to,

$$\min_{\mathbf{w}_R} \mathbf{w}_R^T \mathbf{R}_{xxR} \mathbf{w}_R \quad \textit{such that} \quad \mathbf{D}_R^T \mathbf{w}_R = \mathbf{f}_R. \tag{C.10}$$

Expanding the output power term $\mathbf{w}^\dagger \mathbf{R}_{xx} \mathbf{w}$ in Eq. (C.9) and noting that it is in quadratic form (i.e. its imaginary part will always equal zero) yields,

$$\mathbf{w}^\dagger \mathbf{R}_{xx} \mathbf{w} = (\mathbf{w}_r + j\mathbf{w}_i)^\dagger (\mathbf{R}_{xxr} + j\mathbf{R}_{xxi}) (\mathbf{w}_r + j\mathbf{w}_i), \tag{C.11}$$

$$= \mathbf{w}_r^T \mathbf{R}_{xxr} \mathbf{w}_r - \mathbf{w}_r^T \mathbf{R}_{xxi} \mathbf{w}_i + \mathbf{w}_i^T \mathbf{R}_{xxr} \mathbf{w}_i + \mathbf{w}_i^T \mathbf{R}_{xxi} \mathbf{w}_r. \tag{C.12}$$

Expanding the real transformed power version $\mathbf{w}_R^T \mathbf{R}_{xxR} \mathbf{w}_R$ yields,

$$\mathbf{w}_R^T \mathbf{R}_{xxR} \mathbf{w}_R = \begin{bmatrix} \mathbf{w}_r \\ \mathbf{w}_i \end{bmatrix}^T \begin{bmatrix} \mathbf{R}_{xxr} & -\mathbf{R}_{xxi} \\ \mathbf{R}_{xxi} & \mathbf{R}_{xxr} \end{bmatrix} \begin{bmatrix} \mathbf{w}_r \\ \mathbf{w}_i \end{bmatrix}, \tag{C.13}$$

$$= \mathbf{w}_r^T \mathbf{R}_{xxr} \mathbf{w}_r - \mathbf{w}_r^T \mathbf{R}_{xxi} \mathbf{w}_i + \mathbf{w}_i^T \mathbf{R}_{xxr} \mathbf{w}_i + \mathbf{w}_i^T \mathbf{R}_{xxi} \mathbf{w}_r. \tag{C.14}$$

The right side of Eq. (C.14) matches the right side of Eq. (C.12), implying that both forms of the output power are equivalent,

$$\mathbf{w}^\dagger \mathbf{R}_{xx} \mathbf{w} = \mathbf{w}_R^T \mathbf{R}_{xxR} \mathbf{w}_R. \tag{C.15}$$

The equivalence between the complex and real transformed linear constraints in Eqs. (C.9) and (C.10) will be demonstrated. Starting with the complex linear constraint $\mathbf{d}^\dagger \mathbf{w} = f$ and expanding yields,

$$\mathbf{d}^\dagger \mathbf{w} = f, \tag{C.16}$$

$$(\mathbf{d}_r + j\mathbf{d}_i)^\dagger (\mathbf{w}_r + j\mathbf{w}_i) = f_r + jf_i, \tag{C.17}$$

$$\left(\mathbf{d}_r^T \mathbf{w}_r + \mathbf{d}_i^T \mathbf{w}_i\right) + j\left(\mathbf{d}_r^T \mathbf{w}_i - \mathbf{d}_i^T \mathbf{w}_r\right) = f_r + jf_i. \tag{C.18}$$

Pairing the real and imaginary terms in Eq. (C.18) as two separate real constraints yields two equations:

$$\mathbf{d}_r^T \mathbf{w}_r + \mathbf{d}_i^T \mathbf{w}_i = f_r, \tag{C.19}$$

$$\mathbf{d}_r^T \mathbf{w}_i - \mathbf{d}_i^T \mathbf{w}_r = f_i, \tag{C.20}$$

which can be written in matrix form,

$$\begin{bmatrix} \mathbf{d}_r & -\mathbf{d}_i \\ \mathbf{d}_i & \mathbf{d}_r \end{bmatrix}^T \begin{bmatrix} \mathbf{w}_r \\ \mathbf{w}_i \end{bmatrix} = \begin{bmatrix} \mathbf{w}_r \\ \mathbf{w}_i \end{bmatrix}, \tag{C.21}$$

$$\mathbf{D}_R^T \mathbf{w}_R = \mathbf{f}_R. \tag{C.22}$$

Hence, $\mathbf{d}^{\dagger}\mathbf{w} = f$ is an equivalent constraint to $\mathbf{D}_R^T\mathbf{w}_R = \mathbf{f}_R$. Consequently, the constrained problem in complex form in Eq. (C.9) is equivalent to the real version in Eq. (C.10). Therefore, using either form to solve for the optimal weight vector $\mathbf{w}_{opt}$ in Eq. (2.18) will yield the same real and imaginary components for $\mathbf{w}_{opt}$.

C.2 Transformed GSC

The last section showed how a closed-form solution could be found for use with the robust constraints. This section develops an altered form of the original GSC that can iteratively compute the optimal weights. Part of the derivation parallels Widrow, McCool, and Ball's [31] derivation for the complex form of the LMS algorithm. All "r" and "i" subscripts designate real and imaginary parts, respectively.

The analogous outputs to y, y_a, and y_q of the original GSC in Fig. 2.3 are defined below for the new real structure in Fig. 3.4,

$$\mathbf{y}_R \triangleq [y_r, -y_i] \triangleq [y_{R1}, y_{R2}], \tag{C.23}$$

$$\mathbf{y}_{a,R} \triangleq [y_{ar}, -y_{ai}] \triangleq [y_{a,R1}, y_{a,R2}], \tag{C.24}$$

$$\mathbf{y}_{q,R} \triangleq [y_{qr}, -y_{qi}] \triangleq [y_{q,R1}, y_{q,R2}]. \tag{C.25}$$

The matrix $\mathbf{W}_{s,R}$ is constructed by generating its columns to span the orthogonal space of the constraint matrix $\mathbf{C}_R$,

$$\mathbf{W}_{s,R}^T\mathbf{C}_R = \mathbf{0}, \tag{C.26}$$

where $\mathbf{0}$ is a matrix containing all zero entries. Examining the complex output y of an linear array processor yields,

$$y = y_r + jy_i, \tag{C.27}$$

$$= \mathbf{w}^{\dagger}\mathbf{x}, \tag{C.28}$$

$$= (\mathbf{w}_r - j\mathbf{w}_i)^T (\mathbf{x}_r + j\mathbf{x}_i), \tag{C.29}$$

$$= \left(\mathbf{w}_r^T\mathbf{x}_r + \mathbf{w}_i^T\mathbf{x}_i\right) + j\left(\mathbf{w}_r^T\mathbf{x}_i - \mathbf{w}_i^T\mathbf{x}_r\right). \tag{C.30}$$

The real weight vector $\mathbf{w}_R$ is defined in Eq. (C.5) and the real data matrix $\mathbf{X}_R$ is defined as,

$$\mathbf{X}_R \triangleq \begin{bmatrix} \mathbf{x}_r & -\mathbf{x}_i \\ \mathbf{x}_i & \mathbf{x}_r \end{bmatrix} \triangleq \begin{bmatrix} | & | \\ \mathbf{x}_{R1} & \mathbf{x}_{R2} \\ | & | \end{bmatrix}. \tag{C.31}$$

The lower path data matrix $\mathbf{X}_{a,R}$ contains two column vectors $\mathbf{x}_{a,R1}$ and $\mathbf{x}_{a,R2}$ generated as,

$$\mathbf{x}_{a,R1} = \mathbf{W}_{s,R}^T\mathbf{x}_{R1}, \tag{C.32}$$

$$\mathbf{x}_{a,R2} = \mathbf{W}_{s,R}^T\mathbf{x}_{R2}. \tag{C.33}$$

This can be written in matrix notation as,

$$\mathbf{X}_{a,R} = \mathbf{W}_{s,R}^T\mathbf{X}_R. \tag{C.34}$$

By noting from Fig. 3.4 that $\mathbf{w}_R = \mathbf{w}_{q,R} - \mathbf{W}_{s,R}\mathbf{w}_{a,R}$, the real and imaginary parts of the output y from Eq. (C.30) can be written as,

$$y_r \triangleq y_{R1} = \mathbf{w}_R^T\mathbf{x}_{R1} = \mathbf{w}_{q,R}^T\mathbf{x}_{R1} - \mathbf{w}_{a,R}^T\mathbf{x}_{a,R1}, \tag{C.35}$$

$$y_i \triangleq -y_{R2} = -\mathbf{w}_R^T\mathbf{x}_{R2} = -\mathbf{w}_{q,R}^T\mathbf{x}_{R2} + \mathbf{w}_{a,R}^T\mathbf{x}_{a,R2}. \tag{C.36}$$

The criterion used in deriving an update vector is minimizing the output power of the processor is,

$$\min_{\mathbf{w}_{a,R}} E|y|^2 \Leftrightarrow \min_{\mathbf{w}_{a,R}} E\left(y_r^2 + y_i^2\right). \tag{C.37}$$

The instantaneous gradient (i.e. the gradient taken while ignoring the expectation) is given as,

$$\nabla_{\mathbf{w}_{a,R}}\left(y_r^2+y_i^2\right) = 2y_r\nabla_{\mathbf{w}_{a,R}}(y_r)+2y_i\nabla_{\mathbf{w}_{a,R}}(y_i), \tag{C.38}$$

$$= 2y_r(-\mathbf{x}_{a,R1})+2y_i(\mathbf{x}_{a,R2}). \tag{C.39}$$

The adaptive weight vector update is (note that time sample notation is added),

$$\mathbf{w}_{a,R}(n+1) = \mathbf{w}_{a,R}(n)-\mu\nabla_{\mathbf{w}_{a,R}}\left(y_r^2(n)+y_i^2(n)\right), \tag{C.40}$$

$$= \mathbf{w}_{a,R}(n)+2\mu\left(y_r(n)\mathbf{x}_{a,R1}(n)-y_i(n)\mathbf{x}_{a,R2}(n)\right), \tag{C.41}$$

$$= \mathbf{w}_{a,R}(n)+2\mu\mathbf{X}_{a,R}(n)\mathbf{y}_R^T(n). \tag{C.42}$$

Appendix D

Error Variance Expressions

D.1 Uniform Phase Perturbation

D.1.1 Variance without Robust Constraints

The error variance σ_Δ^2 for the case of uniform phase errors can be calculated in a straight forward manner. Since Δp_k is uniformly distributed about the origin (thus has a mean of zero) and the error is only in phase (i.e. $\Delta_k = \Delta p_k$), and noting that ψ represents the maximum value of the uniform probability density function, the variance is calculated as,

$$\begin{aligned}
\sigma_\Delta^2 &= E\left[|\Delta_k|^2\right] - |m_\Delta|^2, && \text{(D.1)}\\
&= E\left[|\Delta p_k|^2\right] - 0, && \text{(D.2)}\\
&= \int_{-\infty}^{\infty} {\Delta p_k}^2 p\left(\Delta p_k\right) d\Delta p_k, && \text{(D.3)}\\
&= \int_{-\psi}^{\psi} {\Delta p_k}^2 \left(\frac{1}{2\psi}\right) d\Delta p_k, && \text{(D.4)}\\
&= \frac{1}{2\psi}\left(\frac{{\Delta p_k}^3}{3}\right]_{-\psi}^{\psi}, && \text{(D.5)}
\end{aligned}$$

$$= \frac{1}{2\psi}\left(\frac{\psi^3}{3} - \left(-\frac{\psi^3}{3}\right)\right), \tag{D.6}$$

$$= \frac{\psi^2}{3}. \tag{D.7}$$

D.1.2 Variance with Robust Constraints

The variance of the error with robust constraints is calculated for the case of uniformly distributed phase errors at each element. From Eq. (4.57), the robust variance for a general probability density can be calculated as,

$$\sigma^2_{\Delta,ROBUST} = E\left[|\Delta_{k,ROBUST}|^2\right] - |m_{\Delta,ROBUST}|^2, \tag{D.8}$$

$$= \frac{1}{4}E\left[{\Delta p_k}^4\right] - |m_{\Delta,ROBUST}|^2. \tag{D.9}$$

The uniform density distribution for the original phase error at each element Δp_k is assumed to have mean zero and have maximum and minimum values of ψ and $-\psi$, thus having a uniform density value of $\frac{1}{2\psi}$ over that range. Solving Eq. (D.9) first requires finding the fourth moment [32] of the phase error random variable Δp_k,

$$E\left[{\Delta p_k}^4\right] = \int_{-\infty}^{\infty} {\Delta p_k}^4 p\left(\Delta p_k\right) d\Delta p_k, \tag{D.10}$$

$$= \frac{1}{2\psi}\int_{-\psi}^{\psi} {\Delta p_k}^4 d\Delta p_k, \tag{D.11}$$

$$= \frac{1}{2\psi}\left(\frac{{\Delta p_k}^5}{5}\right]_{-\psi}^{\psi}, \tag{D.12}$$

$$= \frac{1}{2\psi}\left(\frac{\psi^5}{5} - \left(-\frac{\psi^5}{5}\right)\right), \tag{D.13}$$

$$= \frac{\psi^4}{5}. \tag{D.14}$$

The mean of the uniform phase error with the robust constraints $m_{\Delta,ROBUST}$ is calculated by taking the expectation of the error approximation in Eq. (4.53),

$$
\begin{aligned}
m_{\Delta,ROBUST} &= E\left[\Delta_k\right], && \text{(D.15)}\\
&= E\left[d_k\left(\frac{-\Delta {p_k}^2}{2}\right)\right], && \text{(D.16)}\\
&= -\frac{d_k}{2}E\left[\Delta {p_k}^2\right], && \text{(D.17)}\\
&= -\frac{d_k}{2}\int_{-\infty}^{\infty}\Delta {p_k}^2 p\left(\Delta p_k\right)d\Delta p_k, && \text{(D.18)}\\
&= -\frac{d_k}{2}\int_{-\psi}^{\psi}\Delta {p_k}^2\left(\frac{1}{2\psi}\right)d\Delta p_k, && \text{(D.19)}\\
&= -\frac{d_k}{4\psi}\left(\frac{\Delta {p_k}^3}{3}\right]_{-\psi}^{\psi}, && \text{(D.20)}\\
&= -\frac{d_k}{4\psi}\left(\frac{\psi^3}{3}-\left(-\frac{\psi^3}{3}\right)\right), && \text{(D.21)}\\
&= -\frac{d_k\psi^2}{6}. && \text{(D.22)}
\end{aligned}
$$

The robust variance is calculated by inserting Eq. (D.14) and Eq. (D.22) into Eq. (D.9) and noting that $|d_k| = 1$ from Eq. (2.6) yields,

$$
\begin{aligned}
\sigma^2_{\Delta,ROBUST} &= \frac{1}{4}E\left[\Delta {p_k}^4\right] - \left|m_{\Delta,ROBUST}\right|^2, && \text{(D.23)}\\
&= \frac{1}{4}\left(\frac{\psi^4}{5}\right) - |d_k|^2\left(\frac{\psi^2}{6}\right)^2, && \text{(D.24)}\\
&= \frac{\psi^4}{20} - \frac{\psi^4}{36}, && \text{(D.25)}\\
&= \frac{\psi^4}{45}. && \text{(D.26)}
\end{aligned}
$$

D.2 Array Placement Errors

D.2.1 Variance without Robust Constraints

Array placement errors cause phase errors in the resulting steering vector $\tilde{\mathbf{d}}$. The placement is assumed to be uniformly random with zero mean in the x, y, and z Cartesian coordinate directions. The placement variance for each direction equals $\frac{\psi^2}{3}$ as was calculated earlier in the appendix for a uniform density where ψ and $-\psi$ are the maximum and minimum values, respectfully, for the density function. The variance is calculated as a direct result of the error phase shift implied in Eq. (5.9),

$$\Delta p_k = \frac{2\pi}{\lambda} \Delta \mathbf{a}_k^\dagger \mathbf{u}. \tag{D.27}$$

Using the definitions for $\mathbf{u}$ and $\Delta \mathbf{a}_k$ in Eqs. (2.2) and (5.5) yields,

$$\Delta p_k = \frac{-2\pi}{\lambda} \left(\Delta a_{k,x} \sin(\Theta)\cos(\Phi) + \Delta a_{k,y} \cos(\Theta)\cos(\Phi) + \Delta a_{k,z} \sin(\Phi) \right). \tag{D.28}$$

Since each error value $\Delta a_{k,x}$,$\Delta a_{k,y}$, and $\Delta a_{k,z}$ are all zero mean, the mean of the phase error $E[\Delta p_k]$ is zero.

Since the random variable Δp_k is zero mean, the variance of the error σ_Δ^2 equals the second moment of the phase error $E\left[{\Delta p_k}^2\right]$,

$$\sigma_\Delta^2 = E\left[{\Delta p_k}^2\right], \tag{D.29}$$

$$\begin{aligned} = & \left(\frac{-2\pi}{\lambda}\right)^2 \left[E\left[\Delta a_{k,x}^2\right] \sin^2(\Theta)\cos^2(\Phi) + E\left[\Delta a_{k,y}^2\right] \cos^2(\Theta)\cos^2(\Phi) \right. \\ & + E\left[\Delta a_{k,z}^2\right] \sin^2(\Phi) + 2E\left[\Delta a_{k,x}\right] E\left[\Delta a_{k,y}\right] \sin(\Theta)\cos(\Theta)\cos^2(\Phi) \\ & + 2E\left[\Delta a_{k,x}\right] E\left[\Delta a_{k,z}\right] \sin(\Theta)\cos(\Phi)\sin(\Phi) \\ & \left. + 2E\left[\Delta a_{k,y}\right] E\left[\Delta a_{k,z}\right] \cos(\Theta)\cos(\Phi)\sin(\Phi) \right], \end{aligned} \tag{D.30}$$

where the independence between the x, y, and z coordinate errors has been used. By noting that $E[\Delta a_{k,x}] = E[\Delta a_{k,y}] = E[\Delta a_{k,z}] = 0$ and also $E\left[\Delta a_{k,x}^2\right] = E\left[\Delta a_{k,y}^2\right] = E\left[\Delta a_{k,z}^2\right] = \frac{\psi^2}{3}$ yields,

$$\sigma_\Delta^2 = \left(\frac{-2\pi}{\lambda}\right)^2 \left(\frac{\psi^2}{3}\right) \left(\sin^2(\Theta)\cos^2(\Phi) + \cos^2(\Theta)\cos^2(\Phi) + \sin^2(\Phi)\right) \quad \text{(D.31)}$$

$$= \left(\frac{-2\pi}{\lambda}\right)^2 \left(\frac{\psi^2}{3}\right) \left(\left(\sin^2(\Theta) + \cos^2(\Theta)\right)\cos^2(\Phi) + \sin^2(\Phi)\right), \quad \text{(D.32)}$$

$$= \left(\frac{-2\pi}{\lambda}\right)^2 \left(\frac{\psi^2}{3}\right) \left(\cos^2(\Phi) + \sin^2(\Phi)\right), \quad \text{(D.33)}$$

$$= \left(\frac{-2\pi}{\lambda}\right)^2 \left(\frac{\psi^2}{3}\right). \quad \text{(D.34)}$$

Note that the variance is independent of the direction of the desired signal.

D.2.2 Variance with Robust Constraints

To calculate the effective variance using the robust constraints, the fourth moment of the phase error $E\left[{\Delta p_k}^2\right]$ needs to be computed: By taking the fourth power of $\Delta p_k$and applying the expectation operator to each term, all first power terms of $\Delta a_{k,x}$,$\Delta a_{k,y}$, and $\Delta a_{k,z}$ will be zero since they are all zero mean. By examining the remaining terms and noting that $E\left[\Delta a_{k,x}^4\right] = E\left[\Delta a_{k,y}^4\right] = E\left[\Delta a_{k,z}^4\right] = \frac{\psi^4}{5}$ yields,

$$\begin{aligned} E\left[{\Delta p_k}^4\right] &= \left(\frac{-2\pi}{\lambda}\right)^4 \left[E\left[\Delta a_{k,x}^4\right]\sin^4(\Theta)\cos^4(\Phi)\right. \\ &\quad + E\left[\Delta a_{k,y}^4\right]\cos^4(\Theta)\cos^4(\Phi) + E\left[\Delta a_{k,z}^4\right]\sin^4(\Phi) \\ &\quad + 6E\left[\Delta a_{k,x}^2\right]E\left[\Delta a_{k,y}^2\right]\sin^2(\Theta)\cos^2(\Theta)\cos^4(\Phi) \\ &\quad + 6E\left[\Delta a_{k,x}^2\right]E\left[\Delta a_{k,z}^4\right]\sin^2(\Theta)\sin^2(\Phi)\cos^2(\Phi) \\ &\quad \left. + 6E\left[\Delta a_{k,y}^2\right]E\left[\Delta a_{k,z}^4\right]\cos^2(\Theta)\sin^2(\Phi)\cos^2(\Phi)\right], \quad \text{(D.35)} \\ &= \left(\frac{2\pi}{\lambda}\right)^4 \left[\frac{\psi^4}{5}\left(\sin^4(\Theta)\cos^4(\Phi)\right.\right. \end{aligned}$$

$$
\begin{aligned}
&+\cos^4(\Theta)\cos^4(\Phi)+\sin^4(\Phi)\Big) \\
&+6\left(\frac{\psi^2}{3}\right)\left(\frac{\psi^2}{3}\right)\Big(\sin^2(\Theta)\cos^2(\Theta)\cos^4(\Phi) \\
&+\cos^2(\Theta)\sin^2(\Phi)\cos^2(\Phi)\Big)\Big], \qquad \text{(D.36)} \\
= &\left(\frac{2\pi}{\lambda}\right)^4\left[\frac{\psi^4}{5}\Big(\Big(\sin^4(\Theta)+\cos^4(\Theta)\Big)\cos^4(\Phi)+\sin^4(\Phi)\Big)\right. \\
&+\frac{2\psi^4}{3}\cos^2(\Phi)\Big(\sin^2(\Theta)\cos^2(\Theta)\cos^2(\Phi) \\
&\left.+\sin^2(\Theta)\sin^2(\Phi)+\cos^2(\Theta)\sin^2(\Phi)\Big)\right], \qquad \text{(D.37)} \\
= &\left(\frac{2\pi}{\lambda}\right)^4\left[\frac{\psi^4}{5}\Big(\Big(\sin^4(\Theta)+\cos^4(\Theta)\Big)\cos^4(\Phi)+\sin^4(\Phi)\Big)\right. \\
&\left.+\frac{2\psi^4}{3}\cos^2(\Phi)\Big(\sin^2(\Theta)\cos^2(\Theta)\cos^2(\Phi)+\sin^2(\Phi)\Big)\right]. \qquad \text{(D.38)}
\end{aligned}
$$

The final robust variance equation uses the second and fourth moments,

$$
\begin{aligned}
\sigma^2_{\Delta,ROBUST} &= \frac{1}{4}E\left[{\Delta p_k}^4\right]-\left|m_{\Delta,ROBUST}\right|^2, \qquad \text{(D.39)} \\
&= \frac{1}{4}E\left[{\Delta p_k}^4\right]-\left|E\left[d_k\frac{-{\Delta p_k}^2}{2}\right]\right|^2, \qquad \text{(D.40)} \\
&= \frac{1}{4}E\left[{\Delta p_k}^4\right]-|d_k|^2\frac{\left(E\left[{\Delta p_k}^2\right]\right)^2}{4}, \qquad \text{(D.41)} \\
&= \frac{1}{4}\left[E\left[{\Delta p_k}^4\right]-\left(E\left[{\Delta p_k}^2\right]\right)^2\right], \qquad \text{(D.42)}
\end{aligned}
$$

where $E\left[{\Delta p_k}^4\right]$ and $E\left[{\Delta p_k}^2\right]$ are given by Eqs. (D.38) and (D.34).

References

[1] W. F. Gabriel. "Adaptive arrays — An introduction". *Proceedings, IEEE*, 64:239–272, Feb. 1976.

[2] S. P. Applebaum and D. J. Chapman. "Adaptive arrays with main beam constraints". *IEEE Trans. on Antennas and Propagation*, AP-24:650–662, Sept. 1976.

[3] Cox *et al.* "Resolving power and sensitivity to mismatch of optimum array processors". *The Journal of the Acoustical Society of America*, 54:771–785, Sept. 1983.

[4] A. M. Vural. "Effects of perturbations on the performance of optimum / adaptive arrays". *IEEE Trans. Aerosp. Electron. Syst.*, AES-15:76–87, Jan. 1979.

[5] C. L. Zahm. "Application of adaptive arrays to suppress strong jammers in the presence of weak signals". *IEEE Trans. Aerosp. Electron. Syst.*, AES-9:260–271, Mar. 1973.

[6] N. K. Jablon. "Adaptive beamforming with the generalized sidelobe canceller in the presence of array imperfections". *IEEE Trans. on Antennas and Propagation*, AP-34:996–1012, Aug. 1986.

[7] N. K. Jablon. "Effect of element errors on half-power beamwidth of the Capon adaptive beamformer". *IEEE Trans. on Circuits and Systems*, CAS-34:743–752, July 1987.

[8] Cox *et al.* "Robust adaptive beamforming". *IEEE Trans. on Acoustics, Speech, and Signal Processing*, ASSP-35:1365–1376, Oct. 1987.

[9] M. H. Er and A. Cantoni. "A unified approach to the design of robust narrow-band antenna array processors". *IEEE Trans. on Antennas and Propagation*, AP-38:17–23, Jan. 1990.

[10] M. W. Hoffman and K. M. Buckley. "A simple adaptive implementation for linearly and nonlinearly constrained optimization". In *European Signal Processing Conference*, pages 741–744, Barcelona, Spain, Sept. 1990.

[11] R. A. Monzingo and T. W. Miller. *Introduction to Adaptive Arrays*. Wiley-Interscience, 1980.

[12] L. J. Griffiths and K. M. Buckley. "Quiescent pattern control in linearly constrained adaptive array". *IEEE Trans. on Acoustics, Speech, and Signal Processing*, ASSP-35:917–926, July 1987.

[13] B. Widrow and S. D. Stearns. *Adaptive Signal Processing.* Prentice-Hall, 1985.

[14] L.J. Griffiths and C.W. Jim. "An alternative approach to linearly constrained adaptive beamforming". *IEEE Trans. on Antennas and Propagation*, AP-30:27–34, Jan. 1982.

[15] C. Y. Tseng. *Adaptive Linearly-Constrainted Filtering: Principles and Implementations.* Ph.D. dissertation, University of Southern California, 1990.

[16] N. K. Jablon. *Adaptive Beamforming with Imperfect Arrays.* Ph.D. dissertation, Stanford University, 1985.

[17] R. T. Compton Jr. "The effect of random steering vector errors in the applebaum adaptive array". *IEEE Trans. Aerosp. Electron. Syst.*, AES-18:392–400, Sept. 1982.

[18] J. E. Hudson. *Adaptive Array Principles.* Peter Peregrinus and The Institute of Electrical Engineers, 1981.

[19] M. H. Er and A. Cantoni. "Derivative constraints for broad-band element space antenna array processors,". *IEEE Trans. on Acoustics, Speech, and Signal Processing*, ASSP-31:1378–1393, Dec 1983.

[20] K. M. Buckley and L. J. Griffiths. "An adaptive generalized sidelobe canceller with derivative constraints". *IEEE Trans. on Antennas and Propagation*, AP-34:311–319, Mar. 1986.

[21] K. M. Buckley. *A Source Representation Space Approach to Digital Array Processing.* Ph.D. dissertation, University of Southern California, 1986.

[22] C. Y. Tseng. "Minimum variance beamforming with phase independent derivative constraints". Submitted to *IEEE Trans. on Antennas and Propagation.*

[23] H. S. C. Wang. "Interference rejection by amplitude shading of sonar transducer arrays". *The Journal of the Acoustical Society of America*, 61:1251–1259, May 1977.

[24] R. T. Compton Jr. *Adaptive Arrays - Concepts and Performance.* Prentice-Hall, 1988.

[25] D. J. Chapman. "Partial adaptivity for the large array". *IEEE Trans. on Antennas and Propagation*, AP-24:685–696, Sept. 1976.

[26] D. R. Morgan. "Partially adaptive array techniques". *IEEE Trans. on Antennas and Propagation*, AP-26:823–833, Nov. 1978.

[27] B. D. Van Veen and R. A. Roberts. "Partially adaptive beamformer design via output power minimization". *IEEE Trans. on Acoustics, Speech, and Signal Processing*, ASSP-35:1524–1532, Nov. 1987.

[28] B. D. Van Veen. "Eigenstructure based partially adaptive array design". *IEEE Trans. on Antennas and Propagation*, AP-36:357–362, Mar. 1988.

[29] T. T. Ma and L. J. Griffiths. "A solution space approach to achieving partially adaptive arrays". In *Proc. of the Int'l. Conference on Acoustics, Speech, and Signal Processing*, pages 2869–2872, New York, NY, Apr. 1988.

[30] A. J. Gould. *A High Resolution HF Digital Radar to Measure Ionospheric Conditions of the High Latitudes.* Master's thesis, University of Lowell, 1990.

[31] B. Widrow, J. M. McCool, and M. Ball. "The complex LMS algorithm". *Proceedings, IEEE*, 63:719–720, April 1975.

[32] A. Papoulis. *Probability, Random Variables, and Stochastic Processes.* McGraw-Hill, 1984.